Department of Precision and Microsystems Engineering

Lung-on-a-chip: Design and Manufacture of a Resealable Device for Recreating the Alveolar-Capillary Barrier In Vitro

Zabreen Nissar

Report no	: MNE-2021.068
Coach	: Prof. dr. U. Staufer
Professor	: Prof. dr. U. Staufer
Specialisation	: Micro and Nano Engineering
Type of report	: Master Thesis
Date	: 14 September 2021

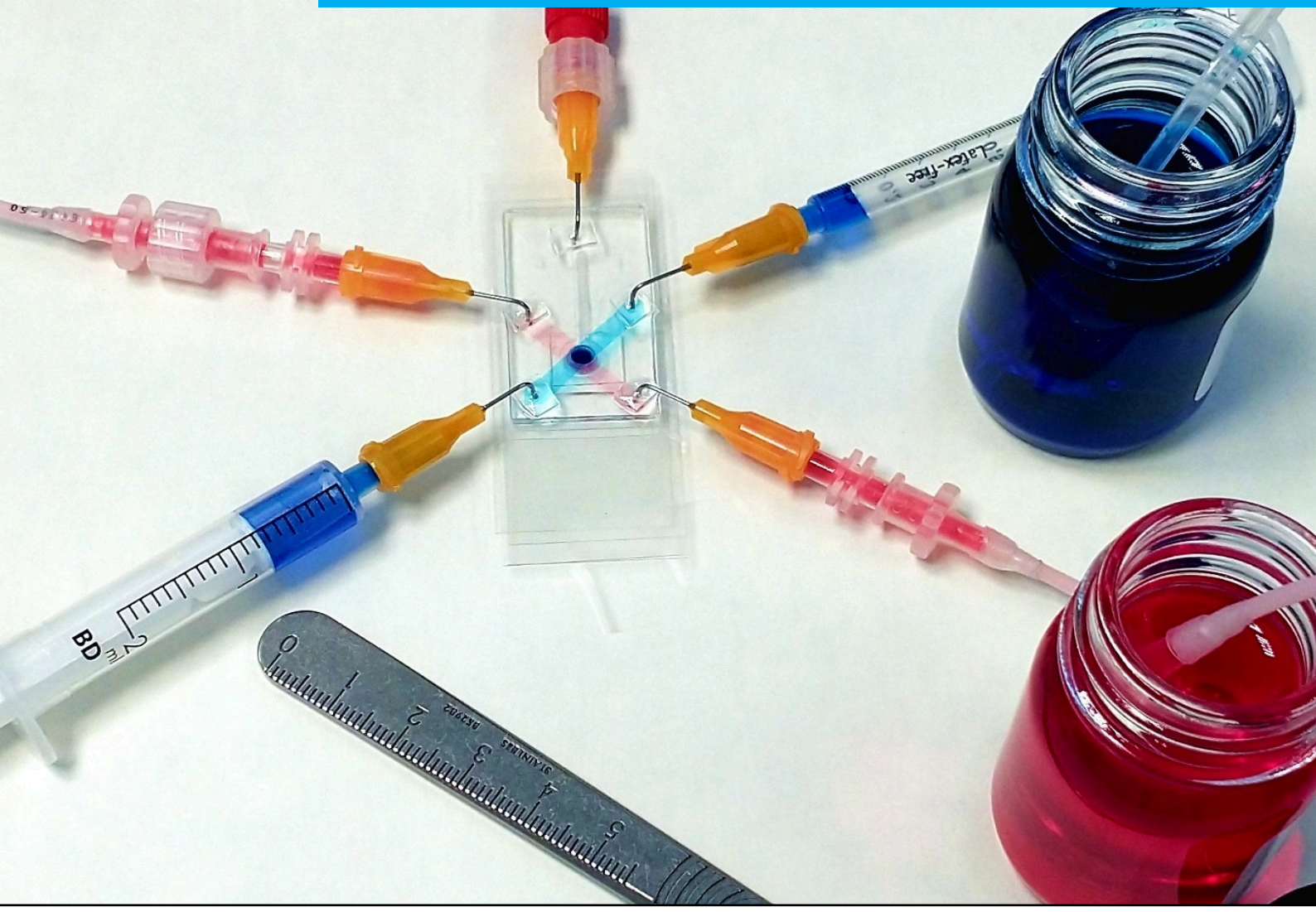

TU Delft Delft University of Technology

Challenge the future

Lung-on-a-chip

Design and Manufacture of a Resealable Device for Recreating the Alveolar-Capillary Barrier In Vitro

by

Zabreen Nissar

in partial fulfilment of the requirements for the degree of

Master of Science
in Mechanical Engineering

at the Delft University of Technology

to be defended publicly on Tuesday, September 14, 2021 at 02:00 PM.

Student number:	5046475	
Project duration:	July 20, 2020 – September 14, 2021	
Supervisors:	Prof. dr. U. Staufer	TU Delft
	Dr. R. Rottier	Erasmus MC
Thesis committee:	Prof. dr. U. Staufer	TU Delft
	Dr. R. Rottier	Erasmus MC
	Dr. S. Iskander-Rizk	TU Delft
	Dr. Massimo Mastrangeli	TU Delft

TU Delft

Contents

Acknowledgements

I would like to thank my supervisors, Dr. U Staufer and Dr. R. Rottier, for guiding me throughout this project and for readily providing support when needed. Their motivating words helped me stay positive in times when thing weren't going as planned. I am thankful to Dr. B.J. Scholte for sharing his vision of the Lung-on-a-chip device, this was extremely helpful in forming the design goal for my thesis project. I would like to thank my colleagues Damla Yengül, Matthijs van Reeuwijk and Qais Akolawala for their useful inputs and suggestions. I would like to especially thank Sarah Aalbers for taking out the time to describe the working of the hot embossing press made by her and for sharing the reports of previous students that used the plasma system in the department for bonding PDMS. I would like to thank Ahmed Sharaf for providing the substrates with pillars, which were essential for the manufacture of porous membranes. I would like to thank Gideon Emmaneel for providing the 3D printed moulds that were used for initial stages of development of the device. I would like to thank Dr. Andres Hunt for providing the laser cut glass layers in early stages of the project. I would like to thank Dr. Hanieh Bazyar for demonstrating the phase separation method for making porous polymer membranes.

I would like to thank M.C. Iriondo Martinez for demonstrating the basics of cell culture and for giving an insight into the environment in which the final product will be used. I would like to thank Dr. K.F. Skarp and M.C. Iriondo Martinez for setting up the samples for cell culture. I would like to thank M.C. Iriondo Martinez and Anne de Munck for their help with using the confocal microscope. I would also like to thank the staff at PME for their support during the experiments and their invaluable inputs and suggestions.

I would like to thank my parents and my sisters for not allowing physical distance to prevent them from being supportive and encouraging throughout the project.

List of Figures

List of Tables

Acronyms

ALI	Air-liquid interface 5, 19, 25, 44, 47, 48
APTES	(3-Aminopropyl)triethoxysilane 7, 41, 42
BEGM	Bronchial epithelial cell growth medium 8, 41–43
BPE	Bovine pituitary extract 8, 41, 42
BSA	Bovine serum albumin 41
COC	Cyclo-olefin copolymer 8, 29, 48, 60, 74, 87
COP	Cyclo-olefin polymer 60, 74
COPD	Chronic obstructive pulmonary disease 1, 56
DAPI	4′,6-diamidino-2-phenylindole 41
DLS	Digital Light Synthesis 59
DMEM	Dulbecco's Modified Eagle Medium 42, 43
ECM	Extracellular matrix 40, 51, 53
EGF	Epidermal growth factor 41, 42
FBS	Fetal bovine serum 42, 43
HMDS	Hexamethyldisilazane 7, 26
HUVECs	Human umbilical vein endothelial cells 14
IPA	Isopropyl alcohol 21, 23, 31
iPS	Induced pluripotent stem cells 54, 57
KSFM	Keratinocyte serum-free medium 8, 41, 42
LOC	Lung-on-a-chip v, 1, 2, 4, 5, 8, 19, 21, 31, 37, 39, 40, 45, 47, 48, 55
OOC	Organ-on-a-chip 1, 2, 8, 20, 31, 35, 47, 64
PBECs	Primary bronchial epithelial cells iv, 8, 41–43, 46
PBS	Phosphate-buffered saline 7, 40–42
PC	Polycarbonate 29, 48, 53, 61, 87
PDMS	Polydimethylsiloxane 6, 8, 11, 19, 20, 24, 47, 48, 59, 60
PEGDA	Poly(ethylene glycol) diacrylate 61, 68
PET	Polyethylene terephthalate 53
PGLA	Poly(lactic-co-glycolic acid) 61
PMMA	Poly(methyl methacrylate) 60
PS	Polystyrene 7, 32, 53, 60
PTFE	Polytetrafluoroethylene 34, 53, 61
SEBS	Styrene-ethylene-butylene-styrene 8, 11, 20, 24, 48
SLA	Stereolithography 59
TEER	Transepithelial/transendothelial electrical resistance 3, 5, 8, 48, 64
TLC	Total lung capacity 52

1

Introduction

In vitro models are essential for getting an insight into the physiological function of the organs and to study how disease and changes in cell environment affect organ structure and function. Traditional in vitro models, set up using cell culture dishes, flasks, wells and inserts, lack dynamic mechanical cues that play an important role in organ behaviour [29, 47, 62]. In animal models, physiological complexity of the organ is present, however, variation between human and animal physiology is significant and these models often fail to predict the response to drugs and diseases [61, 82]. With the use of **organ-on-a-chip (OOC) devices** it is possible to mimic the in vivo environment in a 3D structure with cellular co-culture. The cultured cells are provided with mechanical cues, that they would encounter in vivo. This makes OOCs one the most sophisticated in vitro models.

Lungs are responsible for gas exchange in the human body and their disease-free function is essential for a good quality of human life. Using LOC to study the functioning of lungs and further for disease modelling and drug testing can be useful in improving the available treatments for lung diseases. LOCs have been used to study the inflammatory response to nanoparticles [47] , cigarette smoke [66] and particulate matter with diameter equal or less than 2.5 μm [121]. Drug responses for chronic obstructive pulmonary disease (COPD) [34] and cancer [71, 122] have also been studied using LOCs. These studies have demonstrated the advantages of using LOCs over traditional in vitro models, with the cell behaviour in LOCs being closer to the in vivo behaviour [47, 107].

The advances in the field of micromanufacturing have made the fabrication of microfluidic devices for cell culture possible. One of the first OOC devices was developed back in 2010, a LOC device that was used to recreate the blood-gas barrier with breathing cues and blood flow [47]. Since then, many devices have been made for personal use of researchers and for commercial use. Many of the available devices are not easy to use or lack some of the important features such as cyclic strain, media flow and co-culture of different types of cells. There is still a need for improving the fabrication techniques to allow for use of more suitable materials and to scale up production. This project aimed to contribute to such improvements.

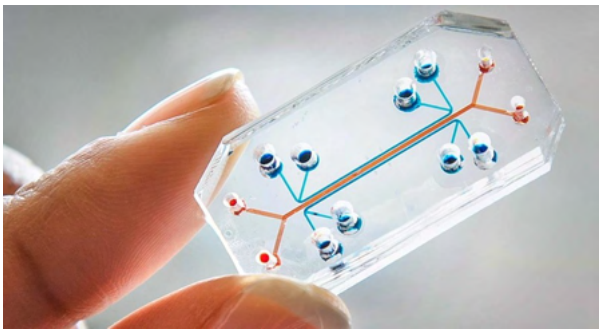

Figure 1.1: Organ-on-a-chip [9]

1.1. Need for a New Design

The devices made by researchers for a study are often designed to satisfy the specific needs of the experiments that they are being used for and may not be ideal for a broad range of experiments. The devices made by Janna Tenenbaum-Katan et al. focused on recreating dimensionally correct models of the ductal airways and the alveoli to study the respiratory flow patterns, but did not recreate the cyclic stretching involved with breathing as it was not a focus of their research [110]. For similar reasons, many LOC devices made over the years by researchers for personal use do not incorporate all the features that would make the device suited for a **broad range of experiments**. In comparison, commercially available devices are often **not organ specific** and offer the same platform for recreating OOC models of various organs [10, 17, 18, 20–22]. The ones that are specifically made for LOC models do not recreate the in vivo environment as accurately as would be desired and are often not easy to set up [16, 19, 23].

Most of the existing LOC devices do not satisfy the criteria of cyclically stretching the epithelial cells along with satisfying the criteria of applying the required shear stress to the endothelial cells. The device from Emulate [19] satisfies both the criteria, but it imparts uniaxial strain to the epithelial cells which does not replicate the in vivo strain type. Moreover, it causes the epithelial cells to align perpendicular to the stretching direction, which is something that is not observed in vivo [47]. The device from AlveoliX [16] imparts tri-axial strain to the epithelial cells, which is closest to the in vivo strain type, however, it does not provide shear stress to the endothelial cells [107]. The OOC platform from Bi/ond [10] imparts tri-axial strain and satisfies the shear stress criterion as well, however, it is difficult for the user to set up the chip as it requires seeding cells using microfluidic channels. The OOC device from Micronit [21] allows for direct seeding of the cells without the use of microfluidic channels but does not have a mechanism to impart cyclic stretching to mimic breathing.

For this thesis project it was decided to come up with a LOC device that imparts **cyclic strain to the epithelial cells and shear stress to the endothelial cells in a way that replicates the in vivo mechanical cues as closely as possible and at the same time is easy to use for medical researchers**.

1.2. Device Requirements

The aim of this project was to come up with a device for the purpose of cell culture to form a lung-on-a-chip. The LOC device has to provide an environment for co-culturing of cells to recreate the **alveolar-capillary barrier** in vitro. The chip environment should replicate the in vivo environment as closely as possible. The device must have a **thin porous membrane** on which the lung epithelial cells will be cultured on one side and endothelial cells will be cultured on the other side, to form the blood-gas barrier. The membrane must be at least 2.5mm in diameter. This is essential to ensure that a confluent cell layer is obtained and that enough cells are in the device for post experiment analysis. There have to be two chambers, one on either side of the membrane, each connected to an inlet and an outlet. There should be a mechanism to stretch the membrane to mimic breathing.

Using microfluidic channels to deliver the cells to the membrane results in loss of cells in the fluid channels. It is also tougher to achieve a confluent layer in this manner, as it provides lesser control to the user, and this method differs significantly from the steps used to culture cells in the culture well inserts, the current popular devices for in vitro models of the lung. The device must allow for **seeding cells on the membrane** directly by pipetting cells on the membrane, just as for seeding cells on a culture insert. In this way, first confluent cell layers will be achieved by a method that is familiar to most end users and then the membrane will be integrated into the device environment. The shear stress provided by blood flow in the capillaries and cyclic stretching of the alveoli due to breathing are two of the major factors that need to be replicated to recreate the in vivo alveolar environment. It must be possible to vary flow and strain parameters in the biologically relevant range. The membrane has to be cyclically stretched to **mimic breathing strains**. The frequency for cyclic stretching must be ~ 0.2 Hz and one dimensional strain up to 20% must be possible to replicate breathing strains.

There needs to be continuous flow of media in the basal chamber to **mimic blood flow**. The flow speed needs to be customised according to the device design so that the shear experienced by the endothelial cells is comparable to the in vivo shear 0.28-9.55 N/m^2 [75]. The flow must be free from fluctuations to recreate capillary blood flow that is smooth and continuous. The apical chamber needs to be provided with gas flow. The composition of that gas should be the same as gas in the alveoli. Gas cyclically pumped in and out of the apical chamber is needed to **replicate air flow** in the lungs. There must also be a provision to fill up the apical chamber with liquid. This could be required to achieve a complete epithelial cell monolayer, before replacing the culture media with gas to form the air-liquid barrier. transepithelial/transendothelial electrical resistance (TEER) measurement also requires a conducting liquid to be present in the apical chamber. Controlling the gas composition, to adjust for the levels of O_2, CO_2, humidity and aerosols, should be possible with the use of the pumping system. The culture environment must recreate the environment shown in Figure 1.2.

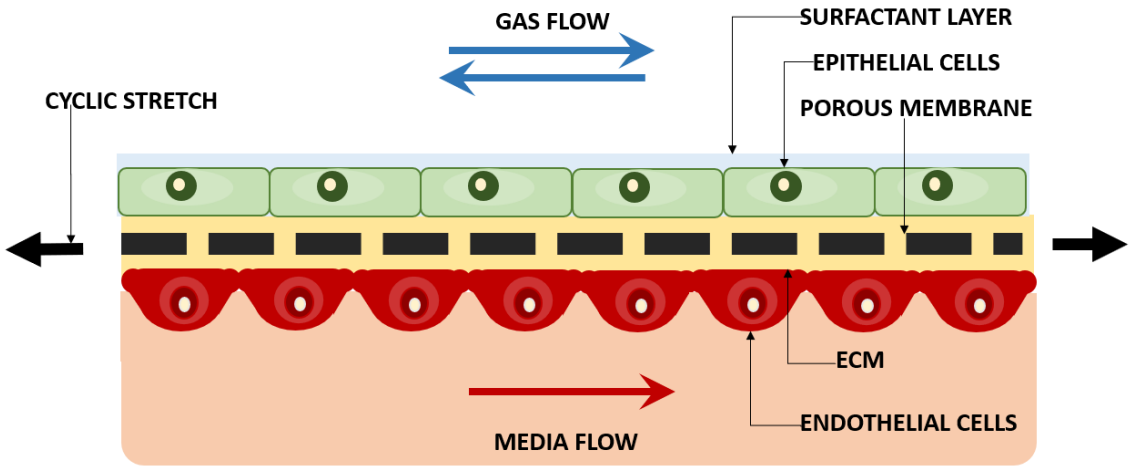

Figure 1.2: How the designed alveolar-capillary barrier should look like

The device does not aim to recreate the dimensions of the alveolus and the capillaries. It does, however, aim to replicate the flow properties of gas and blood as present in vivo so that the cells behave as they do inside the body.

It must be possible to sterilize the device before use by autoclave, 70% ethanol or 5% H_2O_2. The device **material** must be **biocompatible** to allow for cell culture. It must not absorb molecules from or shed molecules into the culture media as this can alter the results of the biological experiments being carried out. The material on both sides of the membrane must be **optically transparent** for microscopic observation of the cells and it should not interfere with luminescent and fluorescent assays. The membrane itself must be biocompatible and hydrophilic to sustain the long term cell culture. The device must sustain a number of cycles ($\sim 5x10^5$) of stretching for long-term culture of at least two weeks and up to four weeks.

The **device structure** should be thin enough to be compatible with the confocal microscope, the cells must be at max 1.8 mm below the device-window's outer surface. It must be portable to allow for easy transport between incubator and microscope. After conducting an experiment it must be possible to **retrieve the membrane** along with the cultured cells. For this it must be possible to dismantle the device without disturbing the cultured cells. The collection of fluids for analysis, post interaction with the cells, should also be possible. It must be possible to integrate sensors in the device to measure temperature, TEER, pH, O_2 and CO_2. It must also be possible to manufacture an array of such devices in a culture well plate like format.

1.3. Report Structure

This report documents the design stage, the manufacturing stage and the testing stage for the made LOC device. Chapter 2 presents the LOC device and the main achievements of the project.

Chapter 3 explains the design method followed and presents in detail the design of the device. The **layout design and the dimensional design** for the device are discussed. The design is discussed with regards to the criteria set for cyclic stretching and required shear stress on the endothelial cells. Chapter 4 begins with explaining the choice of materials for the device. The development of the **manufacturing procedure** for the different layers is discussed. The bonding, assembly and alignment of the different layers to form the device is also discussed.

Chapter 5 gives the results of the **tests done on the manufactured device**. The test procedures are described and the results are discussed. The tests show how well the device satisfies the criteria set for membrane stretching, culture media flow and suitability for cell culture. It is explained how the test results are used to fine tune the manufacturing procedure. Some suggestions regarding the **usage of the device** are also provided.

Chapter 6 provides a summary of what has been achieved in this project and where the future scope of this project lies. Some improvements have been suggested with regards to the design of the device and the manufacturing materials, to make it more suited for cell culture experiments.

The **literature review** done for this project can be found in Appendix A. It begins with a short description of the lungs and the blood-gas barrier in vivo. After which the available in vitro models of the lungs are described and compared with each other. The need for LOC devices is justified and the **state-of-the-art of the LOC microfluidic** devices is described in detail. The devices are discussed on the basis of their layout, material, manufacturing methods, and breathing strain mimicking method. The drawbacks of the devices are pointed out. A short section on the types of sensors that are to be used to study the cells in the chip follows.

2

The Lung-on-a-Chip Device

The LOC device described in this report provides an environment to recreate the alveolar-capillary barrier in vitro. It provides dynamic mechanical cues to the cells cultured on the Air-liquid interface (ALI). These cues mimic the breathing strain in the alveoli and blood flow in the capillaries. It has been proven that such mechanical cues are essential in recreating the function of the alveolar-capillary barrier accurately [34, 47].

The device is designed to cyclically stretch the cell culture membrane bi-axially to impart strain to the epithelial cells and to provide appropriate levels of shear stress to the endothelial cells with the set flow rate of the culture media. The resealable LOC device allows for direct pipetting of the cells on the membrane and it is possible to retrieve the cells after the experiment for further analysis. The materials used for the device are cell culture compatible and transparent. It is compatible with confocal microscopy and optical sensors for measuring O_2 concentration, CO_2 concentration and pH. It is possible to incorporate TEER sensors and temperature sensors in this device during the manufacturing.

2.1. Membrane Stretching Mechanism and Device Layout

A pneumatic actuator was designed to stretch the membrane bi-axially to impart up to 20% linear strain to the membrane. The actuator layout can be seen in Figure 3.3. When negative pressure is applied through the channel, in black, the elastomer wall connected to the porous membrane bends inward, into the donut shaped hollow around it. This causes the membrane attached to the wall to increase in diameter, and hence expand.

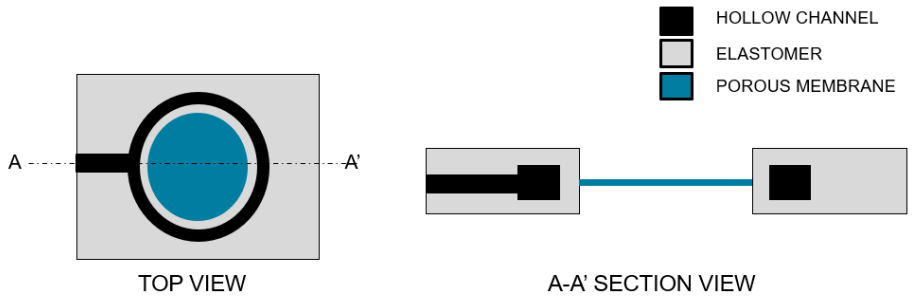

Figure 2.1: Actuator Layout (not to scale)

The dimensions for the actuator wall height (1.4 mm), wall thickness (0.4 mm) and membrane thickness (10 μm) were set to get the desired performance of the actuator while ensuring that it is manufacturable using replica moulding.

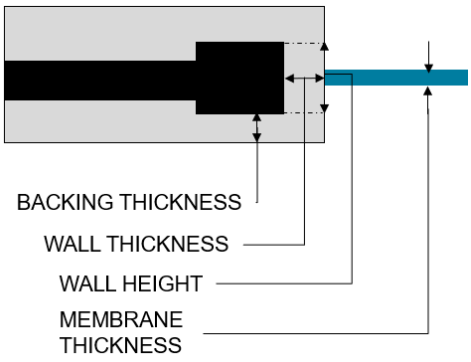

Figure 2.2: Terminology for actuator parts

Channels were added on the top and bottom of the membrane for gas and culture media flow. The lower channel was designed with a step below the cultured membrane, which allows for controlling the channel height, and thus, the shear stress that the endothelial cells will be subjected to for a selected flow rate. The step also prevents most of the culture media from flowing straight through the channel, which would happen in absence of the step, and deflects it towards the membrane to give a streamlined flow below the membrane which is ideal for imparting constant shear stress to the endothelial cells.

2.2. Device Fabrication

The device is made out of polydimethylsiloxane (PDMS) and glass. In total five PDMS layers and four glass layers were bonded together to make the device. The individual layers can be seen in 2.3.

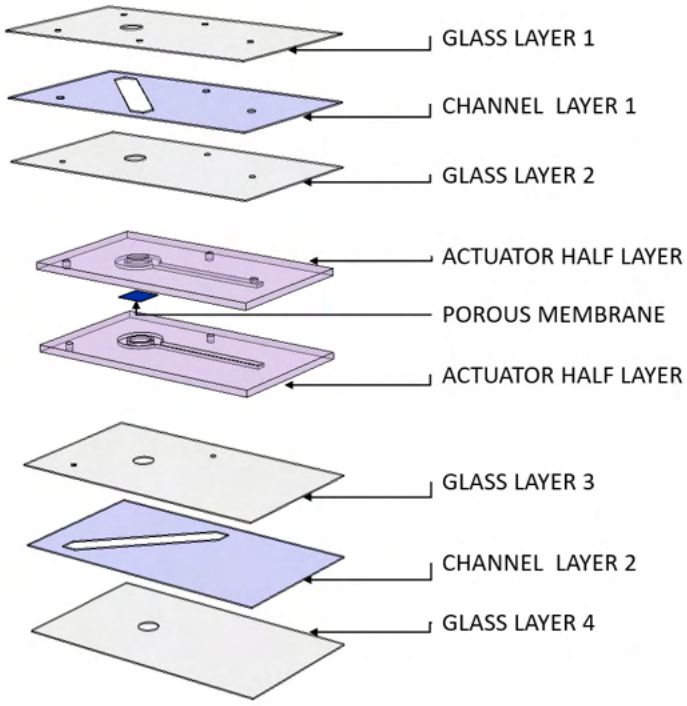

Figure 2.3: Exploded view of the device showing all the different glass and PDMS layers

The actuator consists of two actuator half layers and the porous membrane for cell culture . For making the actuator half layers, SYLGARD™ 184 Silicone Elastomer kit was used to prepare the PDMS prepolymer by mixing the base polymer and the curing resin in the ratio 10:1. The prepolymer was put

in a desiccator for 10 minutes to remove all trapped air bubbles before use. For making the **actuator half layer** the prepolymer was poured into 3D printed moulds. The moulds were printed using Envisontec Micro Hi-res Plus 3D printer using HTM140 resin. The moulds with the poured prepolymer were again placed in a desiccator to remove any bubbles trapped during pouring. A glass slide coated with Pluronic® F-127 was brought gradually in contact with the mould to close it while taking care that no bubbles are trapped inside. Rubber bands were used to hold the glass slide in tight contact with the mould and the arrangement was left for 48 hrs at room temperature to allow the PDMS to cure. The cured actuator half layers were removed from the moulds using a sharp blade and acetone.

The **porous membrane** was made by spin coating a 10 μm layer of PDMS prepolymer on a substrate with 3D printed pillars with a diameter of 8 μm. The pillars were arranged in a square array with the pitch distance 48 μm to give a membrane with 2.1% porosity. To make it easy to peel off the membrane and to reduce the pillar detachment from the substrate a layer of hexamethyldisilazane (HMDS) was deposited and a layer of Pluronic® F-127 was coated on top. The spin coated layer was cured at 150°C for 5 minutes.

To **assemble the actuator** uncured PDMS bonding method was used to bond the half actuator layers and the porous membrane [51]. A 25 μm layer of PDMS prepolymer was spin coated on a polystyrene (PS) petri dish. The actuator half layer was placed on it to coat it with a thin layer of prepolymer and then lifted and placed on the cured membrane, still attached to the substrate it was spin coated on. The thin layer was then cured at 50°C for one hour after which the membrane was peeled off the pillar substrate with the help of the bonded half actuator layer. The membrane areas covering the vacuum channel were manually cut out and removed. A biopsy punch was used to punch out an access hole for the vacuum channel. The second actuator layer was then coated with a thin layer of prepolymer, aligned correctly over the other actuator half layer, with the porous membrane bonded to it, and cured as before.

The **channels** were made by sandwiching a PDMS channel layer, with a recess in place of the channel, between glass layers. For the top channel, channel layer 1 was sandwiched between glass layer 1 and glass layer 2. For the bottom channel, channel layer 2 was sandwiched between glass layer 3 and glass layer 4. The 1.5 H coverslips (24 mm x 60 mm x 170 μm) were used for making the four glass layers. The central hole (diameter = 3.1 mm) for access to the porous membrane and holes (diameter = 1 mm) for making connections to the top and bottom channel were laser cut into the layers. A 200 μm layer of PDMS prepolymer was spin coated on a PS petri dish and cured at room temperature. It was covered with scotch tape to cut the channel layers 1 and 2 out of it, without damaging the thin PDMS layer. The cut out channel layers were transferred to the glass layer using scotch tape. The tape was then removed and another glass layer was placed on top to complete the channel.

These top and bottom channels were plasma bonded to the actuator. Syringe tips were attached to the inlets and outlets of the channels to make connections for the culture media flow and vacuum. The coverslips to seal the channels were made by cutting out squares from the coverslip. These were plasma bonded to a 40 μm layer of PDMS. A cylindrical cut out of PDMS with height 0.8 mm, with the two ends trimmed for letting the liquid pass through, was bonded on the lower cover slip to control the channel height.

2.3. Device Characterization

A maximum in plane deflection of 302 μm for the actuator wall was obtained for an applied pressure of -700 mbar. This corresponds to 20% linear strain in the membrane. The membrane was cyclically stretched at 0.2 Hz using a triangular pressure wave with the minimum pressure of -900 mbar and maximum pressure of 0 mbar. The out of plane deflection of the membrane when the fluid was withdrawn from the channel using a syringe pump, for a flow rate of 2.6 ml/min, was found to be 0.443 mm. However, if the liquid is flown using pressure driven flow controllers the out of plane deflection of the membrane can be minimized. Use of peristaltic pumps for recirculating liquid in the basal chamber was found to cause fluctuating out of plane deflection of the membrane.

2.4. Cell Culture

PDMS, being hydrophobic, is not suited for long term cell culture without pre-treatment to change its surface properties. To make the cells attach to the membrane for long term culture, type 1 rat tail collagen was covalently bonded to the PDMS surface. For this, the surface of the porous PDMS membrane was activated using air plasma for 3 minutes at a pressure of 4 mbar. The activated membrane was put in 10% (3-Aminopropyl)triethoxysilane (APTES) solution in ethanol for 5 minutes and washed twice with phosphate-buffered saline (PBS). This was followed by a 1 hour incubation in ascorbic acid at room temperature. Lastly, 50 $\mu g/ml$ type 1 collagen diluted in 0.1 M acetic acid was put on the membrane for 1 hour at room temperature. After this, the membrane was directly used or stored in the fridge at 4°C for further use. The device was sterilized using 70% ethanol prior to use.

Human PBECs were seeded on the membrane, 1.38 $\times 10^3$ cells/mm2, to test out the suitability of the membrane for long term cell culture.The cells were cultured in keratinocyte serum-free medium (KSFM) (Thermofisher 17005-034) + P/S (Penicillin/Streptomycin) + EGF (Thermofisher 17005-075) + bovine pituitary extract (BPE) (Thermofisher 17005-075) for 5 days after which they were found to fully cover the porous membrane. After 5 days the culture media was changed to bronchial epithelial cell growth medium (BEGM) to stop the cells from dividing further and to allow them to start differentiating. The cells were found to be alive after 16 days in culture, confirming that the membrane is suitable for long term cell culture.

2.5. Conclusion

The LOC device provides a cell culture friendly environment to recreate the alveolar-capillary barrier. It satisfies the requirements set for the cyclic strain that it can provide to the lung epithelial cells and the shear stress that it can provide to the endothelial cells. The device is made of cell culture compatible materials, PDMS and glass. Live confocal imaging of the cells cultured in the device is possible and the cells can be retrieved post an experiment for analyses.

Although the device satisfies the set requirements, there is still room for improvement. Future scope for this project includes replacing PDMS with a polymer more suited for OOC application, such as styrene-ethylene-butylene-styrene (SEBS). Materials such as cyclo-olefin copolymer (COC) and SEBS can be used to replace glass and PDMS respectively to make the device suitable for large scale production. An array of the unit LOC can be designed, on the lines of a culture well plate, to allow for setting up multiple LOCs simultaneously. There is also a need to integrate sensors in the device for measuring TEER, temperature, pH, O_2 concentration and CO_2 concentration.

3

Design

In order to make a device, that satisfies the set requirements well, a good design is crucial. This design has to be suitable for manufacturing and must pass the set tests to ensure that it performs according to the requirements. To obtain such a design an iterative design approach was selected. The design process was set up in a way that subsequent iterations would use the same design principles and design models that were set up for the initial design. This reduces the time required for iterations. Figure 3.1 shows the iterative plan for making the device and the device design stages are marked in blue. In this chapter the design will be described with reference to the initial dimensional design. Appropriate discussion is included to explain layout and dimension choices.

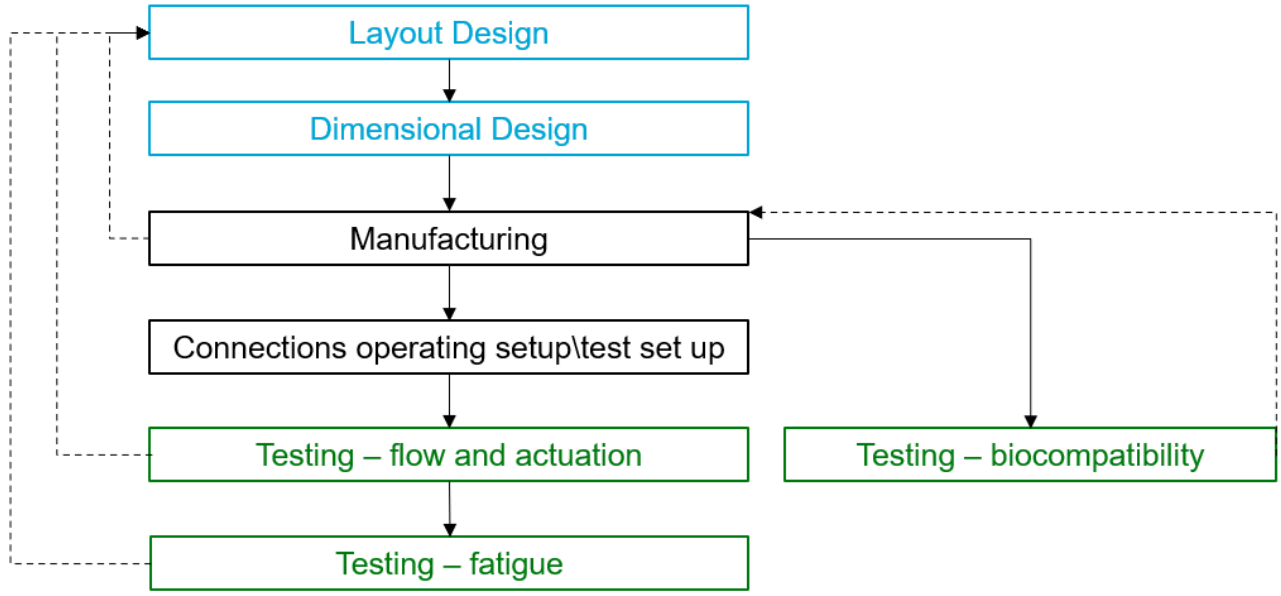

Key: Blue - Design Stage, Black - Manufacturing Stage, Green - Testing Stage.

Figure 3.1: Project Plan

3.1. Design Method

A step wise, iterative approach was undertaken to design the device. The first step was to come up with a **layout for the device**. A suitable method for actuation was chosen and the actuator layout was decided. After that the layout of the full device was designed around that.

The second step was the **dimensional design** of device. The dimensions were set to fulfill the requirements set for the device. The shear stress on the endothelial cells, the cyclic strain of the membrane and the compatibility with the confocal microscope were the main criteria that determined the dimensions. At this step, any layout that did not satisfy the requirements well was discarded and the first step was repeated to come up with a new suitable layout.

The third step was the **simulation of the device in COMSOL**. This gave the approximate operating parameters for the device. If the parameters were not suitable, step two was repeated to get new dimensions that resulted in desired operating parameters.

Further iterations were also made for making the design compatible with the manufacturing procedure. Any design flaws that came into notice during testing were corrected by making appropriate changes in the design and dimensions. To make any changes in the dimensions, step two and three were repeated to ensure that the conformity to device requirements was maintained.

3.2. Actuator Design

The actuator has to cyclically stretch the membrane to mimic breathing strains. Linear strain has to go up to 20% and the frequency for the strain has to be around 0.2 Hz.

3.2.1. Strain Direction

The strain direction can be uni-axial, bi-axial or tri-axial, as shown in Figure 3.2. The strain profile has an affect on the functioning of the cells [62]. For the alveolus, tri-axial strain mimics the in vivo strain most accurately and is thus presumed to be the most suitable strain direction to elicit functioning of the lung cells that is closest to the in vivo functioning [107].

Type of mechanical strain (illustration of a stretched cell)	Type of mechanical strain	Linear strain (num. example)	Surface area strain
	Uniaxial strain (x)	10%	10%
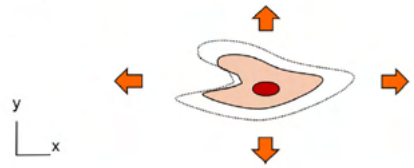	Bi-axial strain (xy)	10%	21%
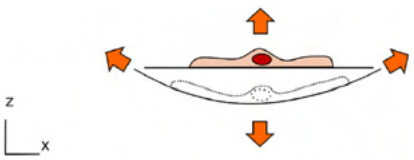	Bi-axial strain (xz)	10%	≈10%
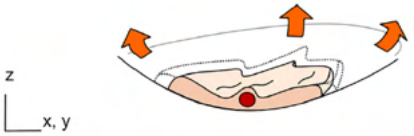	Tri-axial strain (xyz)	10%	≈21%

Figure 3.2: Mechanical strain in membranes in microfluidic devices [62]

The diameter for the membrane, on which the cells are to be cultured, has to be 3 mm. In comparison, the diameter of an alveolus is about 10 ×smaller, ranges from 100 μm to 300 μm, and the diameter of a type 1 lung epithelial cell is about 40 μm [98, 118]. Thus, due to comparable diameters of the lung cell and alveolus, tri-axial strain in the alveolus imparts a tri-axial strain to the lung epithelial cells, with considerable out of plane strain. For the cell culture membrane, due to the large difference in the scale of the two, tri-axial strain in the membrane will impart a tri-axial strain to each cell for which the out of plane component will be negligible.

Thus, tri-axial strain in a membrane, with a surface area as large as that present in this device, would almost be perceived by a single cell as bi-axial strain. The surface area strain for bi-axial strain (xy) is comparable to that of tri-axial strain and thus bi-axial strain (xy) should elicit similar functionality as tri-axial strain. However, due to a lack of studies comparing the effects of bi-axial strain and tri-axial strain on the functionality of lung cells, this can not be assumed for sure.

For **out of plane actuation** and to impart tri-axial strain up to 20% , the membrane with 3 mm diameter will have an out of plane displacement of 0.845 mm. This means that the chamber, apical or basal, in which the membrane will expand has to have a height greater than 0.845 mm. This would result in varying cross sections of the media channel, placed on the endothelial cell layer side of the membrane. At a given flow rate, the shear stress due to media flow experienced by endothelial cells on the membrane will show high variance for this style of actuation.

For **in plane actuation**, to impart a bi-axial strain, the shear force will be uniform for the majority of the endothelial cells on the membrane as the variance of the media channel cross section is much lower than that in case of out of plane actuation. Thus an **in plane actuator is selected for the LOC device**.

3.2.2. Pneumatic Actuators

Pneumatic actuators have been the most popular type of actuators used in LOC devices [47, 50, 66, 78, 107, 110]. The reason for this is that the incorporation into the chip is low cost as no additional material, apart from the elastomer from which the device is being made, needs to be included in the chip. The actuation pressure is applied using pumps and pressure controllers. Pneumatic actuators can be operated with positive pressure or negative pressure.

A **negative pressure operated actuator** was selected for the device. Negative pressure was selected over positive pressure for operation as it was more suited for the actuator layout. It also reduces the chances of failure of the connections and the bonds inside the device. Direct application of pressure on the membrane, negative or positive, was avoided. This was done as for a membrane thickness of 10 μm and higher the pressure required to actuate the membrane could lead to cell death [78]. For less than 10% linear strain in the membrane, this method could also be suitable and would greatly reduce the device complexity.

The actuator and the membrane were designed to be made out of PDMS using soft lithography but can also be made out of other elastomers like SEBS [46]. (see subsection 4.1.1 and subsection G.1.1)

3.2.3. Layout

The layout of the actuator is shown in Figure 3.3. When negative pressure is applied through the channel, in black, the elastomer wall connected to the porous membrane bends inward, into the donut shaped hollow around it. This causes the membrane attached to the wall to increase in diameter, and hence expand.

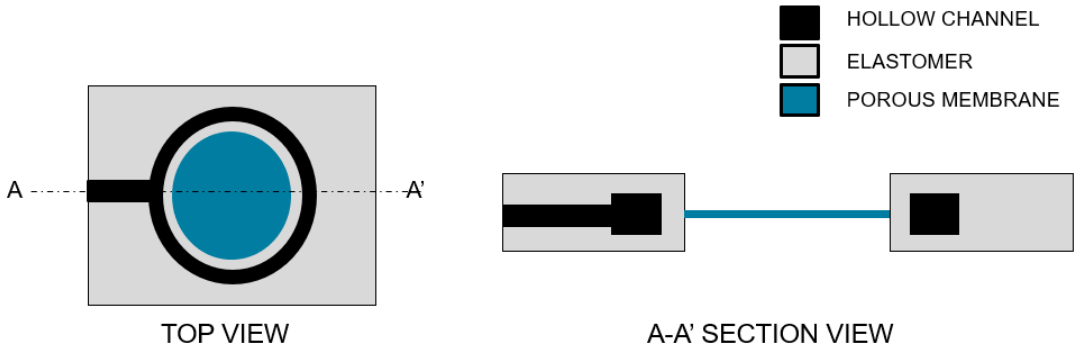

Figure 3.3: Actuator Layout (not to scale)

3.2.4. Dimensional Design

The pressure required for actuation depends on the actuator wall thickness, wall height and the thickness of the membrane, as marked in the Figure 3.4. The pressure also depends on the material properties of PDMS which in turn depend up on the preparation process parameters (see subsection 4.1.1). To make sure that the actuator was compatible with most commercially available vacuum pumps and pressure controllers, the actuator has to be designed to work within a pressure range of 0 mbar to -800 mbar [12, 13].

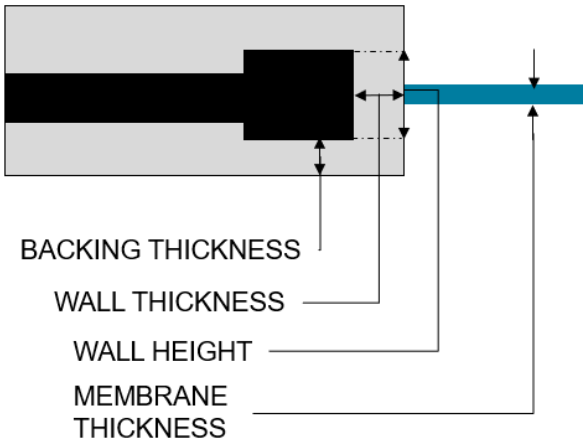

Figure 3.4: Terminology for actuator parts

The dimensions were set after simulating the actuator in COMSOL. The **material properties** found by Kim et. al [73], through testing, were used to define the hyperelastic material in COMSOL. The Mooney-Rivlin model was selected and the material constants were used to set up the material model. Although these properties will vary from the properties of the PDMS used to make the actuator, as the process parameters and manufacturing methods differ, it was considered a good approximation to get plausible dimensions for the device.

A COMSOL model was used to estimate the **actuating pressure** required for the obtaining 20% linear strain, which corresponds to a 300 μm displacement of the actuator wall. The symmetric layout of the actuator allowed for the use of a 2D axisymmetric model. The top and bottom surfaces of the actuator were fixed and negative pressure was applied to the inner side of the actuator wall. The pressure estimation was in turn used to tune the actuator dimensions so that it would be deformed to the required extent using pressure over -800 mbar.

The actuator wall needs to be thick enough for providing enough surface area for bonding to the membrane. Therefore, even though reducing the actuator **wall thickness** will lead to reduction in the actuation pressure magnitude, it is not desired to make the wall too thin. Increasing the **actuator wall height** will lead to a reduction of actuation pressure magnitude, however, the wall height also needs to be appropriate for the device to satisfy the criteria for compatibility with the confocal microscope. Decreasing the **membrane thickness** will lead to a reduction of actuation pressure magnitude, however, the membrane thickness selection also depends on other factors such as ease of manufacture, ease of handling and behaviour of the membrane with media flow.

Table 3.1 shows the effect of change in different dimensions, within their possible maximum and minimum limits, on the actuation pressure. It was observed that increasing the PDMS base polymer to resin ratio leads to reduction of actuation pressure. The dimensions were set so that they satisfied the criteria mentioned above and thus are all suitable for manufacturing. Change in membrane thickness, with a minimum of 10 μm and a maximum of 40 μm varied the actuation pressure by 50 mbar. Changing the wall thickness and wall height had a more pronounced effect with the change in wall height resulting in a 300 mbar change in actuation pressure.

Table 3.1: Effect of actuator parameters on actuation pressure

Base polymer:Resin	Wall Height	Wall Thickness	Membrane Thickness	Actuation Pressure
5:1	1 mm	0.4 mm	10 μm	-1000 mbar
15:1	1 mm	0.4 mm	10 μm	-700 mbar
15:1	1.4 mm	0.4 mm	10 μm	-400 mbar
15:1	1 mm	0.4 mm	40 μm	-750 mbar
15:1	1 mm	0.3 mm	10 μm	-500 mbar

The observations made using the COMSOL model were used to select the following dimensions for initial manufacturing:

- Actuator Wall Height = 1 mm
- Actuator Wall Thickness = 0.4 mm
- Membrane Thickness = 10 μm

Figure 3.5 shows the strain distribution for these dimensions for 20% liner strain in the membrane. The actuation pressure required for 20% linear strain was -700 mbar, which is within the set level of -800 mbar. Figure 3.6 shows the radial section in the 3D actuator. See files `Actuator Strain.gif` and `Actuator Strain 3D.gif` in supplementary files for a video of the actuator strain.

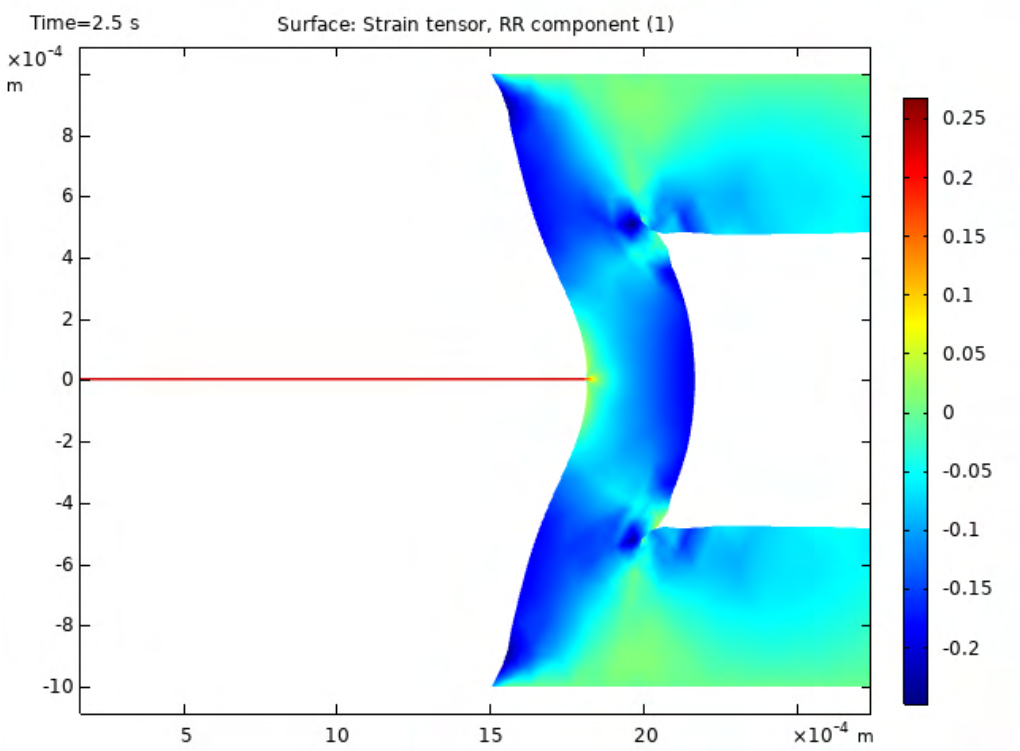

Figure 3.5: Strain distribution for the actuator made of PDMS 15:1

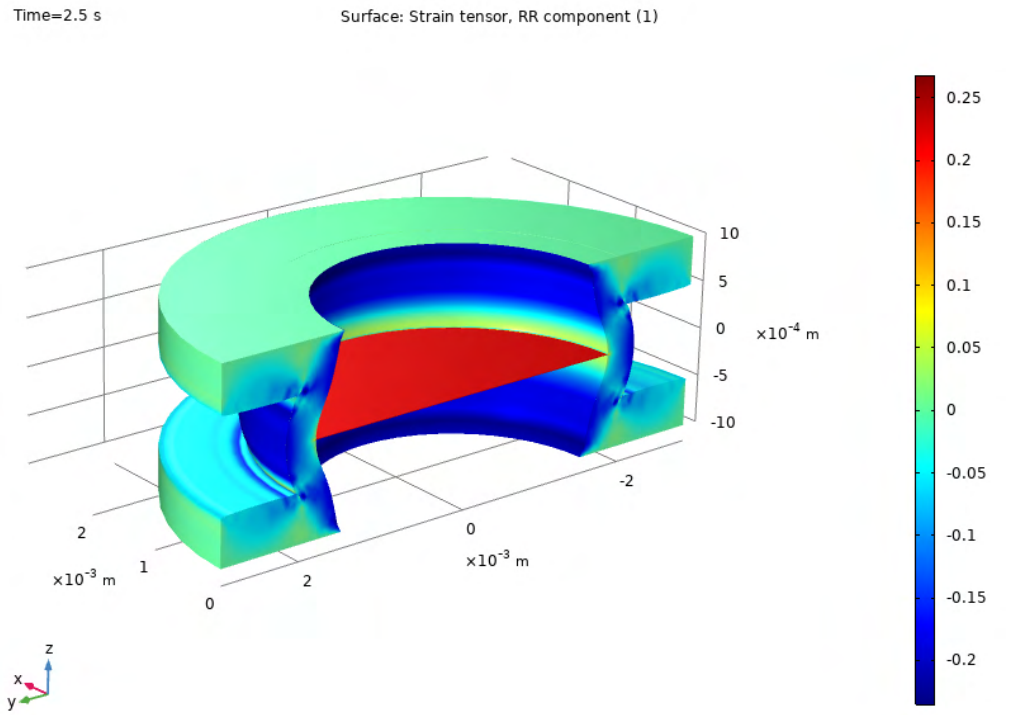

Figure 3.6: Section view of strain distribution for the actuator made of PDMS 15:1

3.3. Channel Design

The shear stress that the endothelial cells experience under culture media flow depends upon the dimensions of the flow channel, the flow rate and the viscosity of the culture media. An approximation for this shear force is given by the equation for **Hele-Shaw flow** (Equation 3.1), which assumes an incompressible Newtonian fluid in a steady-state laminar flow in a rectangular channel with height much lower than the width [104]. The value of shear stress (τ) on the top and bottom channel surfaces is:

$$\tau = \frac{6\eta Q}{wh^2} \tag{3.1}$$

Here, η is the dynamic viscosity of the fluid, Q is the flow rate, w is the width of the channel and h is the height of the channel.

The in vivo range for **shear stress (τ)** on endothelial cells ranges from 0.28 Pa to 9.55 Pa [75]. In previous in vitro models the lower limit for the shear stress was found to be inadequate for having the desired effect on the endothelial cells and a minimum shear stress of 0.55 Pa was suggested [78]. The source of the endothelial cells also determines the magnitude of shear for which the cells show desired characteristics in response to the shear, for human umbilical vein endothelial cells (HUVECs) shear stress up to 1.5-2 Pa could be required [44]. For the design, the required value of the shear stress was set as **0.55 Pa**. If experiments with endothelial cells under flow suggest an increase or decrease in the shear stress is required that will be done by varying the flow rate (Q).

The **dynamic viscosity (η)** of the culture media depends upon the composition of culture media used [89]. As the cells are sensitive to the exact composition of the culture media, the composition varies for different types of cells. The viscosity of the culture media is about four times lower than that of human blood, thus recreating the shear observed in vivo requires increasing the flow rate or decreasing the cross-section area of the channel. Use of additives such as dextran, xanthan gum and alginate to

increase the viscosity of the culture media allows replicating the shear stress at physiological flow rates [38]. These additives also help in replicating the non-Newtonian behaviour of blood.

For the purpose of this project the use of additives is not considered as they can also affect cell function, which is not desired [96]. For the initial design, the dynamic viscosity of the culture media was approximated to be equal to that of water at 37°C, $0.6913x10^{-}3$ kg/ms. This is slightly lower than the actual dynamic viscosity of the culture medium, but it is still close enough to get an initial channel design. The shear stress can be fine tuned after setting the channel dimensions by making changes in the culture media flow rate.

The channels needs to be wide enough to cover the cell culture membrane, thus the width (w) was set as 3.2 mm. The height (h) of the channel was set as 300 μm. The channel length (L) was set as 2 cm.

3.3.1. Flow Rate

The flow rate for the culture media was found by using Equation 3.1. The values mentioned above were used to get the flow rate for those channel dimensions and culture media properties, which is **137.5 ml/hr**. As the cost of culture media is high ($\sim$ 200 Euros/500ml [78]), at such high flow rates the cost of running the chip for four weeks will be huge. Thus, **recirculation of culture media** is needed to run the chip. Using recirculation of culture media also gives more freedom to adjust the channel dimensions to suit the manufacturing and usage without running into high culture media consumption.

3.3.2. Shear Stress Distribution

The assumption of Hele-Shaw flow ignores the variations of shear stress that will be present across the channel wall surface. To get an idea of that variation, Poiseuille flow is assumed in a channel of rectangular cross-section with the above set dimensions. Even though this assumption is only valid for channels with a fixed cross sections throughout the length, it gives a good assumption for the variation of shear stress.

The **velocity field** for the Poiseuille flow in a channel with rectangular cross-section is given by the equation [39]:

$$V_x(y,z) = \frac{4h^2\Delta p}{\pi^3 \eta L} \sum_{n,odd}^{\infty} \frac{1}{n^3} \left[1 - \frac{\cosh\left(n\pi \frac{y}{h}\right)}{\cosh\left(n\pi \frac{w}{2h}\right)} \right] \sin\left(n\pi \frac{z}{h}\right) \tag{3.2}$$

Here, Δp is the pressure drop across the channel and can be calculated from the flow rate Q as $\Delta p = Q/R_{hyd}$ and R_{hyd} is the hydraulic resistance of the rectangular channel. This is then used to find the local shear rate ($\dot{\gamma}$) as [53]:

$$\dot{\gamma}_{local}(y,z) = \sqrt{\left(\frac{\partial V_x}{\partial y}(y,z)\right)^2 + \left(\frac{\partial V_x}{\partial z}(y,z)\right)^2} \tag{3.3}$$

This equation can then be used to get the **shear distribution on the top wall** of the channel. Figure 3.7 shows the effect of channel height on the shear distribution. It can be seen that for a higher channel height the shear stress distribution is less uniform and that for a channel height of 300 μm the shear stress for the top wall is close to the desired value of 0.55 Pa for most of the wall surface.

Appendix D gives the equations and MATLAB code used to calculate this. The normalized velocity profile and normalized shear rate profile is also included.

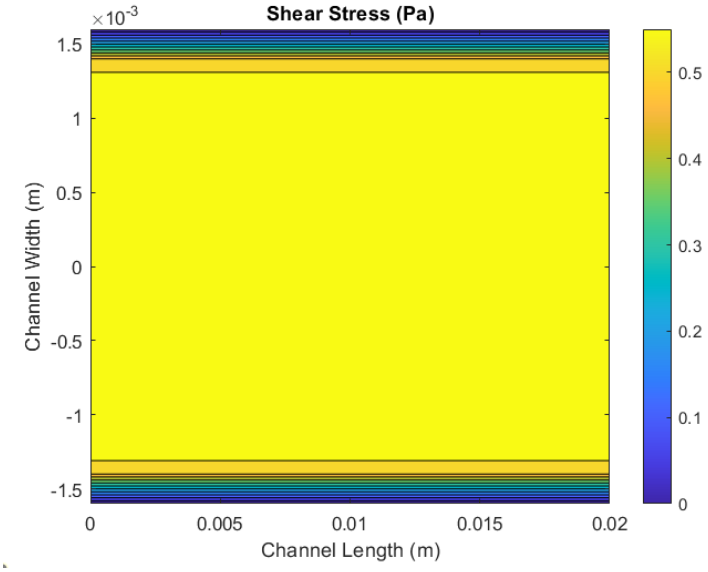

(a) Channel Height (h) = 300μm

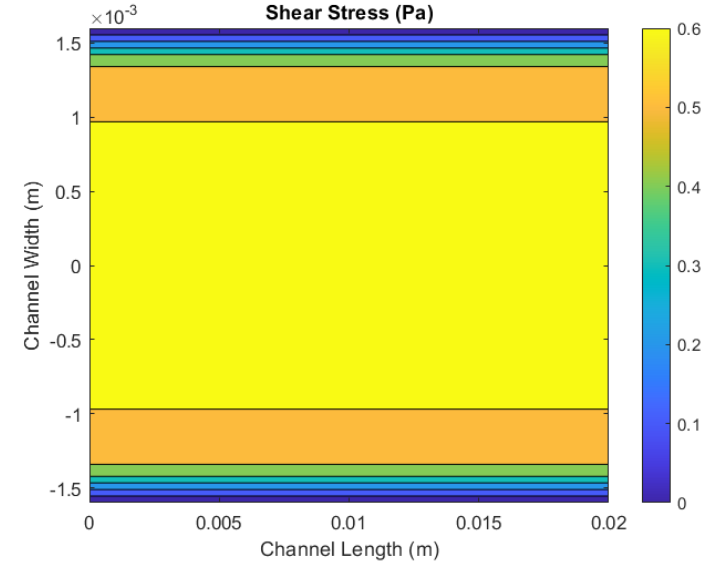

(b) Channel Height (h) = 500μm

Figure 3.7: Shear Distribution on the channel top wall

3.4. Device Design

The device was designed around the actuator, channels were include above and below the membrane. The device is made of multiple layers bonded together, permanently or temporarily, to get a structure with desired thickness and level of strength.

3.4.1. Layout

The actuator layer is sandwiched between two glass layers to provide support to the actuator wall form top and below. A PDMS layer, with a recess at the place of the channel, is bonded to that. Over that another glass layer, with a hole at the place of the membrane, is bonded to close the channel. A removable glass cover slip is added on top to seal the channel. The lower channel has a similar layout as well. The layout can be seen in Figure 3.8.

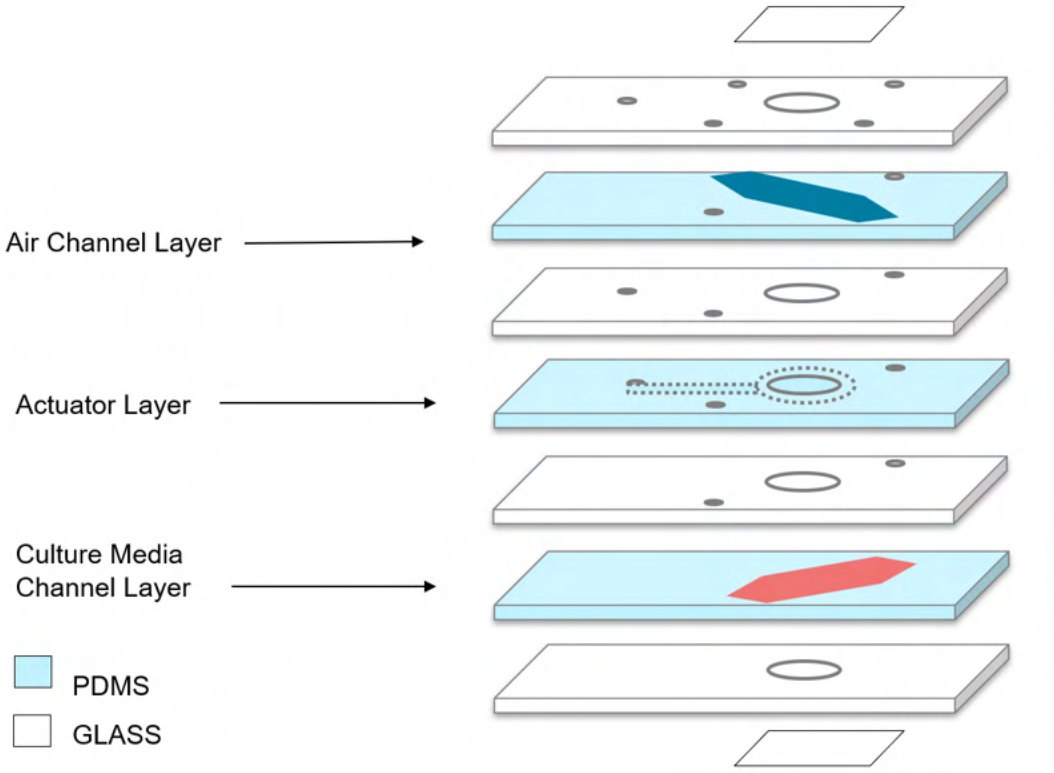

Figure 3.8: Device Layout

Holes are made in the layers to allow for connections for cyclic vacuum, gas and culture media flow to be made to the layers below. To make sure that the cover slip seals the channels completely a thin layer of PDMS is added to it. To the bottom cover slip a step made of PDMS is also added to allow for control over the channel height at the place of the membrane, as shown in Figure 3.9. The PDMS step is transparent and compatible with imaging techniques, however, the image quality will be lower in comparison to a glass coverslip.

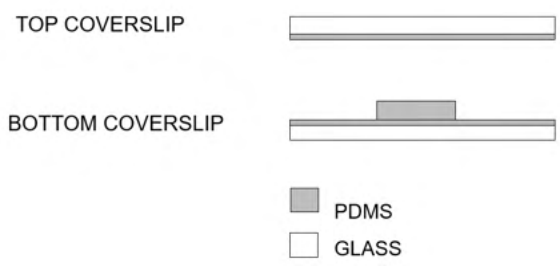

Figure 3.9: Coverslips

3.4.2. Dimensional Design

The dimensions of the different layers are limited by the criteria for confocal microscopy, manufacturing and also the actuator and channel design. There are in total nine layers, four layers on either side of the central actuator layer. The distance between the membrane and the outer most layer is given by:

$$\begin{aligned} 0.5\text{x Actuator Layer} &= 1mm \\ +\text{Glass Layer 2} &= 0.17mm \\ +\text{Channel Layer} &= 0.2mm \\ +\text{Glass Layer 1} &= 0.17mm \\ +\text{Coverslip} &= 0.21mm \\ \text{Total} &= 1.75mm \end{aligned}$$

As required, this distance is less than 2 mm, the working distance of the confocal microscope.

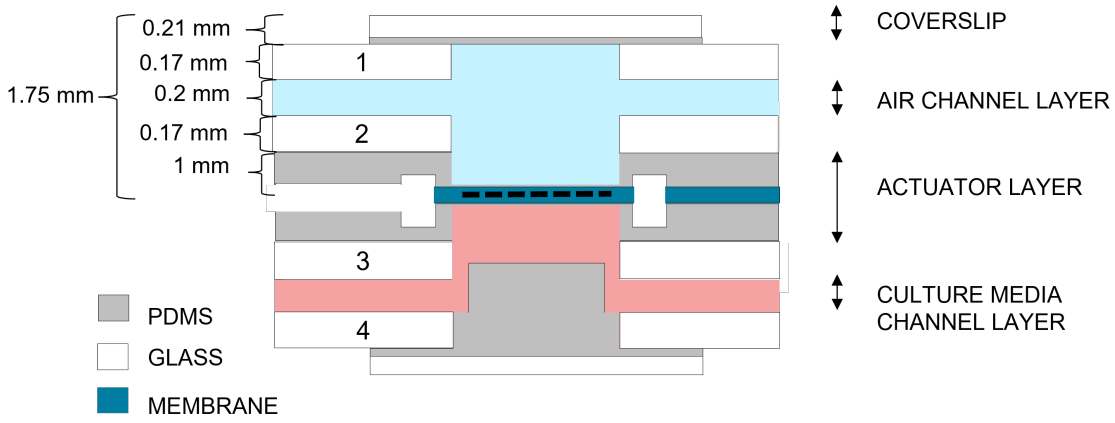

Figure 3.10: Cross-section of the device layout

3.4.3. Shear and Strain in the Device

The stretching of the membrane has an affect on the channel flow and in turn the liquid flow in the channel affects the membrane strain. To check how well the device design satisfies the criteria of shear stress and strain for the membrane the device was modelled in COMSOL. Cyclic vacuum was applied to the actuator wall and the culture media flow rate, obtained from the Equation 3.1, was set. The model had the same dimensions as the initial device design. The material selected was 10:1 PDMS and the membrane thickness was set as 10 μm.

In the absence of a step on the lower coverslip most of the culture media will flow straight across, this results in lower shear stress on the endothelial cells even at a high flow rate. Thus, a step needs to be incorporated on the lower coverslip to deflect the culture media, from its straight path, into the basal chamber.

It was observed that the membrane has an out of plane deformation due to the pressure applied by the flowing media, making the strain tri-axial. For this case, it was considered that the culture media would be injected into the channel at the desired flow rate. This causes the shear on the membrane to vary during the stretching cycle, as shown in `Membrane Shear Stress.gif`. Reducing the out of plane deformation of the membrane will lead to a more uniform shear stress on the membrane. This can be achieved by making the membrane of a stiffer material or/and by making the membrane thicker or by reducing the pressure difference between the two sides of the membrane.

The out of plane deformation of the membrane also results in making the linear strain due to 300 μm inward deflection of the actuator wall to be greater than 20%. In case the out of plane deformation is not completely eliminated by changing the membrane properties, the actuator wall deflection will have to be reduced to get a total of 20% linear strain while stretching the membrane.

The velocity flow is visualized in the files `Device - Velocity Flow (Top View).gif` and `Device - Velocity Flow (Side View).gif`. It can be seen that the flow is always directed from the channel inlet to the outlet. The changes in channel cross-section due to the actuation are at a frequency that is much lower than the culture media velocity and do not change the flow direction.

3.5. Chapter Summary

An iterative approach was selected to design the LOC device. The design includes a **pneumatic actuator made of PDMS** that can apply 20% cyclic strain at 0.2 Hz to the cell culture membrane. A channel for gas flow is included above the membrane and a channel for culture media flow is included below the membrane to allow culture of lung cells at ALI. The **dimensions of the channel are set to ensure that the culture media flow provides the desired shear stress to the endothelial cells** cultured on the lower side of the membrane. The device was designed to be made out of PDMS and glass layers. COMSOL models were used ensure that the dimensions for design of the actuator satisfied the operating parameters. A COMSOL model for the **fluid-structure interaction of the flow in the channel with the moving actuator** was used to visualize the flow and the resulting shear stress on the membrane in the full device design. The outcome of the design stage was not only the initial dimensional design of the device but also the methodology of design and models which were used to ensure that the design satisfied the requirements while making subsequent iterations of the design.

4

Device Manufacture

The device is made up of a central actuator layer with a porous membrane, four glass layers, two channel layers, a top and a bottom cover slip. In this chapter, the procedure for manufacturing of these layers and assembly of the device will be discussed. For each layer, the development of the manufacturing procedure is discussed and learnings from that process are incorporated into the final recommended manufacturing procedure.

4.1. Materials

The materials used to make the device need to satisfy the requirements set in section 1.1. **Glass and PDMS** were selected to make the device. Having been among the standard materials used to make devices for in vitro models, OOC and lab-on-a-chip, these two materials have been extensively studied for application in OOC devices. The manufacturing techniques for these materials are well documented and they are easily available at a low cost.

4.1.1. PDMS

A SYLGARD™ 184 Silicone Elastomer kit was used to prepare the PDMS prepolymer by mixing the base polymer and the curing resin in the desired ratio. The prepolymer has to be heat cured to get the PDMS elastomer. The **mechanical properties** of the obtained PDMS structure depend on the ratio of base polymer to the curing resin, the time and temperature used for curing and the method used to make the structure [72, 73, 80, 90]. After a method for making the required actuator structure is obtained, the curing time and temperature and the base polymer to curing resin ratio can be adjusted to fine tune the mechanical propertied of the actuator structure.

A major disadvantage of using PDMS for an OOC device is that it **absorbs small molecules** and thus alters the result of the experiments [113]. It was still decided to use PDMS as it is easily available and suited for making on chip pneumatic actuators. Moreover, improvement of PDMS properties to make it more suited for OOC applications is an active research field and methods for reducing small molecule absorption by PDMS have already been demonstrated [114]. Another elastomer, SEBS, has been demonstrated to be suitable to replace PDMS in pneumatic actuators for OOC application. This elastomer not only shows reduced absorption of small molecules but is also suited for large scale production using injection moulding [46]. Thus actuator structures that are made using PDMS in this project can later be made by injection moulding using SEBS.

4.1.2. Glass

For manufacturing the first version of the device all glass layers will be made of 1.5 H cover slips (24mm x 60mm). The reason for this is their easy availability in the lab. The thickness is also suited for keeping the device thickness below the desired maximum level. These cover slips are delicate due to low thickness, 0.17mm, and break easily.

4.2. Actuator

The actuator is made up of two identical PDMS layers, consisting of the actuator wall and the channel for vacuum, with a porous PDMS membrane sandwiched between the two layers. The half actuator layers are made by curing PDMS in the 3D printed mould covered with a glass slide. After that bonding of the two parts and the membrane is done. The manufacturing process can be divided into **four parts**- mould manufacture, surface treatment, PDMS layer manufacture and assembly.

4.2.1. Mould Manufacture

Mould design for the PDMS layer was made using Solidworks, as shown in Figure 4.1. See section E.1 for detailed drawing. The mould has two alignment markers for proper alignment of the two half actuator layers. It was 3D printed using Envisontec Micro Hi-res Plus 3D printer. HTM140 high temperature mold material was used for printing. The printer exposes the resin layer by layer to UV light in the pattern of the required layer, the layer height can be set as low as 25 μm. The step wise procedure is mentioned as follows:

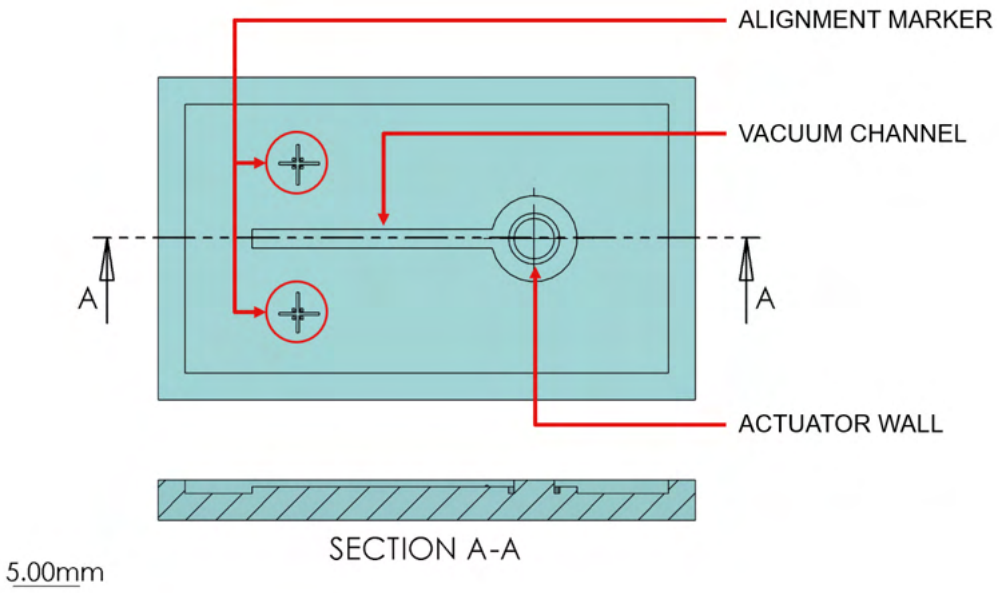

Figure 4.1: Actuator half layer mould design

Part A: Mould Manufacture

1. Draw the 3D CAD model of the mould in Solidworks.
2. Import the drawing into the Perfactory RP software for converting it in to a layer by layer format compatible with the printer.
3. Print the mould out of HTM140 using Envisontec.
4. Clean the excess resin from the printed mould with isopropyl alcohol (IPA), in an ultrasonic bath, in two sessions of 5 minutes each.
5. Cure the mould in Photopol Curing Unit for 3 minutes. Flip the mould and cure again to ensure uniform curing.

There were some undulations in the printed mould, as shown in Figure 4.2. The scratches and other defects on the membrane at the bottom of the resin tub of the 3D printer, through which the light enters to cure the resin, were found to be the reason for this.

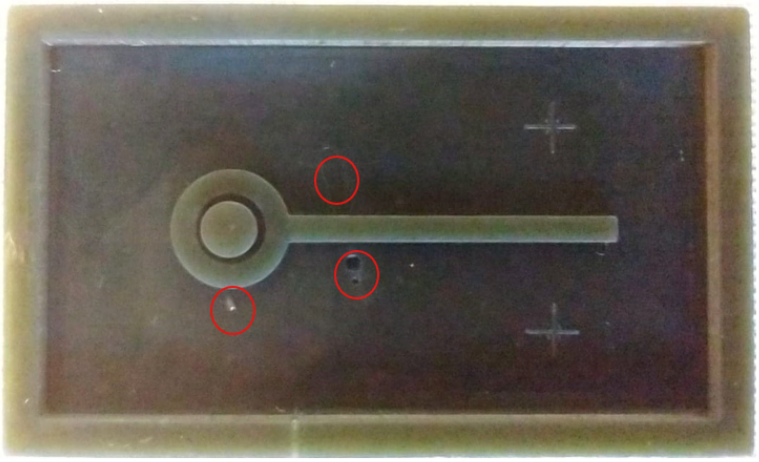

Figure 4.2: 3D printed mould with the surface undulations circled in red.

4.2.2. Surface Treatment

To ensure that the PDMS does not stick to the mould, surface treatment was needed. This makes the mould surface hydrophobic and aids in easy removal of the PDMS layer after curing. Pluronic® F-127 and DW-40 were tried out for this purpose. It was decided to select Pluronic® F-127, being a product used in cell culture, for the LOC application of the device [4]. It is suitable for mammalian cell culture and thus any traces entrapped in the actuator half layer will not have a harmful impact on the cultured cells. The step wise procedure is as follows:

Part B: Surface treatment

1. Mix 2% by weight Pluronic® F-127 powder in water. Ensure that the powder mixes well and there are no lumps in the solution.
2. Cover the mould and glass slide with the solution and let it stand for 5 minutes.
3. Blow dry the mould and glass slide with the help of an air gun.

4.2.3. PDMS Layer Manufacture

The actuator half layer was made by curing PDMS prepolymer in the mould covered by a glass slide. The ratio of PDMS base polymer to curing resin, curing time and temperature can only be fine tuned after testing. The following working recipes were used for the initial manufacturing :

- PDMS 5:1 Curing: 2 hrs at 75°C
- PDMS 10:1 Curing: 2:40 hrs at 75°C

The undulations on the mould surface cause undulations on the actuator half layer as well. To mitigate the effect of such undulations they are shaved off using a blade to make the surface smoother. The step wise procedure is as follows:

Part C: PDMS Layer Manufacture

1. Mix the PDMS base polymer and curing resin thoroughly, in the desired ratio, for 5 minutes.
2. Degas the PDMS prepolymer in the desiccator for 15 minutes or till the time when no bubbles are visible, whichever is longer.
3. Pour the PDMS prepolymer into the mould.
4. Degas the PDMS in the mould by placing in the desiccator for 15 minutes or till the time when no bubbles are visible, whichever is longer.

5. Cover the PDMS filled mould with the glass slide by bringing the glass slide gradually into contact with the PDMS surface to ensure no bubbles are trapped between them.
6. Use rubber bands or tape to keep the glass slide in full contact with the mould top surface.
7. Put the mould into an oven for to cure the PDMS. Set the time and temperature according to the selected recipe.
8. After curing, remove the mould from the oven and keep it at room temperature to cool down for 5 minutes .
9. Remove the glass side gently, ensuring the the PDMS structure is not damaged.
10. With a sharp blade make cuts along the rectangular boundary of the PDMS layer.
11. Put the mould with PDMS in a petridish with IPA for 10 minutes. This swells up the PDMS and aids in its removal from the mould.
12. Peel off the PDMS layer from the mould and clean it with IPA and then with deionized water to remove any sticky PDMS debris.
13. Let the PDMS layer dry at room temperature.

4.2.4. Actuator Assembly

The steps for the assembly of the actuator are shown in Figure 4.3. To assemble the actuator the half actuator PDMS layer is bonded to the membrane (1). The membrane is then peeled off from the substrate and the membrane parts covering the vacuum channel are removed using a sharp blade (2). Holes for connections punched into the layer. Then the other half actuator PDMS layer is bonded on top to give the actuator structure (3). To this a glass layer is bonded on either side to provide support (4).

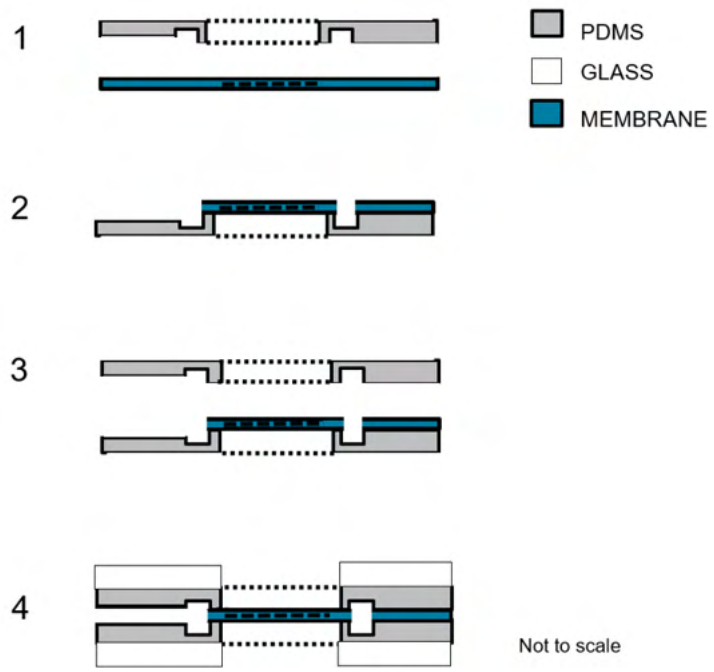

Figure 4.3: Steps for assembling the actuator.
(1) Bond the actuator half layer to the PDMS membrane. (2) Remove membrane layer areas covering the vacuum channel. (3) Bond the other actuator half layer on top. (4) Sandwich the actuator layer between glass layers to provide support to the actuator walls.

The PDMS to PDMS bonding can be done using several methods [51]. To bond the PDMS layers plasma bonding and bonding using uncured PDMS were tried. The **plasma bonding** procedure described in Appendix F was followed. For the **uncured PDMS method** a 25 μm thin layer of PDMS was spin coated on to a plastic petri dish. The cured actuator half layer was placed on top of that to cover it with a thin layer of uncured PDMS, with the side to be bonded facing the uncured PDMS. Then the actuator half layer was lifted and placed on the membrane, still on the substrate.

After curing this thin layer, at 50°C for 1 hour, the membrane bonds to the actuator half layer. Then, the membrane is peeled off from the substrate and excess membrane covering the vacuum channels removed using a sharp blade. Another actuator half layer is bonded on top using another layer of uncured PDMS in the same way as before. Before curing the thin PDMS bonding layer, the actuator layers are placed under a microscope and the **alignment** markers in the two half actuator layers are made to overlap. This results in accurate alignment of the two actuator half layers.

The strength of this bond is really important as any leaks would allow the culture media, present in the basal chamber, to leak into the vacuum channel. This will cause device failure, as well as, damage the vacuum pumps. The uncured PDMS method was found to result in a better bond and thus was chosen for manufacturing. The actuator layers made using this bonding method had no leaks up to a pressure of -900 mbar applied to the actuator wall. The glass layers were plasma bonded on either side of the actuator layer using the method described in Appendix F. The step wise procedure for assembly is as follows:

Part D: Assembly

1. Clean the PDMS surfaces with IPA or an air gun to remove any dust particles.
2. Bond one PDMS layer to the PDMS membrane, with the wall side facing the membrane.
3. Peel off the membrane from the substrate.
4. Remove the membrane covering any part of the channel and chamber for vacuum.
5. Use a 0.75mm diameter biopsy punch to make a hole in the layer for connections.
6. Bond another PDMS layer to this, again with the wall facing the membrane. This will result in a hollow donut structure with the membrane in the middle. Punch out holes in the actuator layers for connections to the basal chamber.
7. Plasma bond the assembled channels (4.4) on either side of the actuator using the procedure described in Appendix F.

It was found that the **uneven surface** of some of the actuator half layers hampered their bonding to the membrane and to each other. Even after manually shaving off the undulations, the surface was not completely smooth. This resulted in areas which were not in contact during curing of the thin PDMS bonding layer. A method was developed to use the PDMS layers with uneven surfaces. To reduce such areas the total surface to be bonded was reduced by bonding the membrane to just the actuator walls and not the whole half actuator layer. The membrane on the substrate is cut into a rough circle with the diameter greater than the 3.8mm but smaller than 6mm. The half actuator layer is covered with a thin layer of PDMS, manually, just at the actuator walls. It is then placed on the cut membrane area and the thin PDMS layer is cured to bond the actuator wall to the membrane. The membrane is peeled off and the other half actuator layer is bonded on top using a thin layer of uncured PDMS, using the process described before.

This method eliminates the need for removing the membrane covering the vacuum channels. The only drawback is the manual application of PDMS at the actuator wall, due to which this method is **not scalable**. This alternative method for manufacturing, is summarised in subsection G.1.2. A combination of the two methods was found to be the most **practical approach** for solving the problem of uneven surfaces. After step 4, the membrane covering any place except the actuator walls was removed from the actuator half layer using forceps. This leaves the membrane layer just covering the area between and on the actuator walls, similar to the alternative method.

As PDMS has several drawbacks, it was decided to try out manufacturing the actuator by hot embossing SEBS sheets using the same mould that was used for the PDMS actuator half layers, see subsection G.1.1 for more. The moulds and the available setup did not prove to be up to the mark to emboss, and, more importantly, bond the SEBS actuator half layers. Further development of material specific manufacturing techniques is required to make the actuator out of SEBS.

4.3. Porous Membrane

The porous membrane for cell culture was made of PDMS. PDMS prepolymer was spin coated on a silicon substrate with 3D printed pillars. The pillars were prepared by Ahmed Sharaf by using the method given in section H.2.The standard method for making such pillars is lithography [47, 79, 93, 107]. As that method needs more resources than that were easily available, it was decided to 3D print the pillars. The IP-S resin from Nanoscribe, which is biocompatible and non-cytotoxic, was used to print the pillars [2].

For the purpose of a ALI the pores need to cover 3-3.5% of the surface area. The pores must be small enough to not let cells (type 1 lung epithelial cells diameter 40 μm [98, 118]) on one side pass on to the other side and at the same time allow cells like neutrophils (diameter 12-14 μm [88]) to squeeze through. The pillar diameter determines the membrane pore diameter and the pillar height must be tall enough not to be covered by the prepolymer while spin coating, as that will result in blocked pores.

To determine the suitable pillar diameter and height, pillars with four combinations of dimensions were made with diameter 8 μm and 15 μm and height 30 μm and 50 μm. The pillars were printed an a square array, with a side of 3 mm, and the pitch of the pillars was set as 41 μm for the 8 μm diameter pillars and 77 μm for the 15 μm diameter pillars to ensure that the pores covered 3-3.5% of the area. The pillar height was chosen to be more than the desired membrane thickness to get pores all the way through the membrane.

A 25 μm layer of PDMS prepolymer was spin coated and cured. The membrane was then peeled off and observed under a microscope. Some of the pillars also detached from the substrate with the membrane. Figure 4.4 shows the effect of pillar parameters on the detachment of pillars and Figure 4.5 shows the detached pillars stuck in the membrane pores. The detachment decreased with the increasing pillar diameter and with decreasing pillar height, thus with the aspect ratio of the pillars, as shown in Table 4.1.

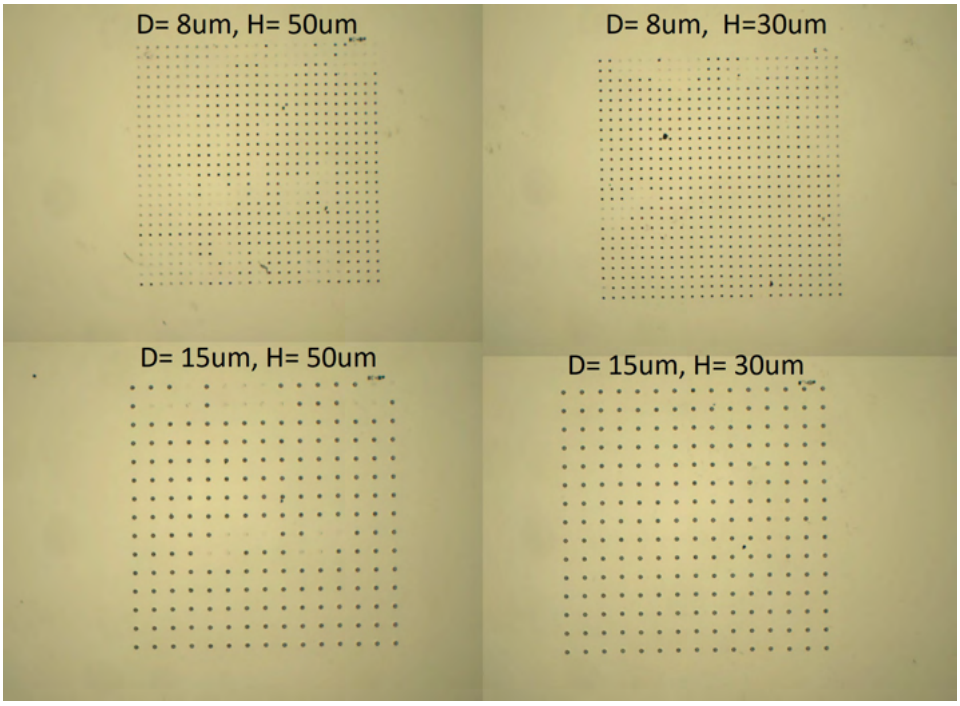

Figure 4.4: Trial pillar mould after peeling off the PDMS membrane

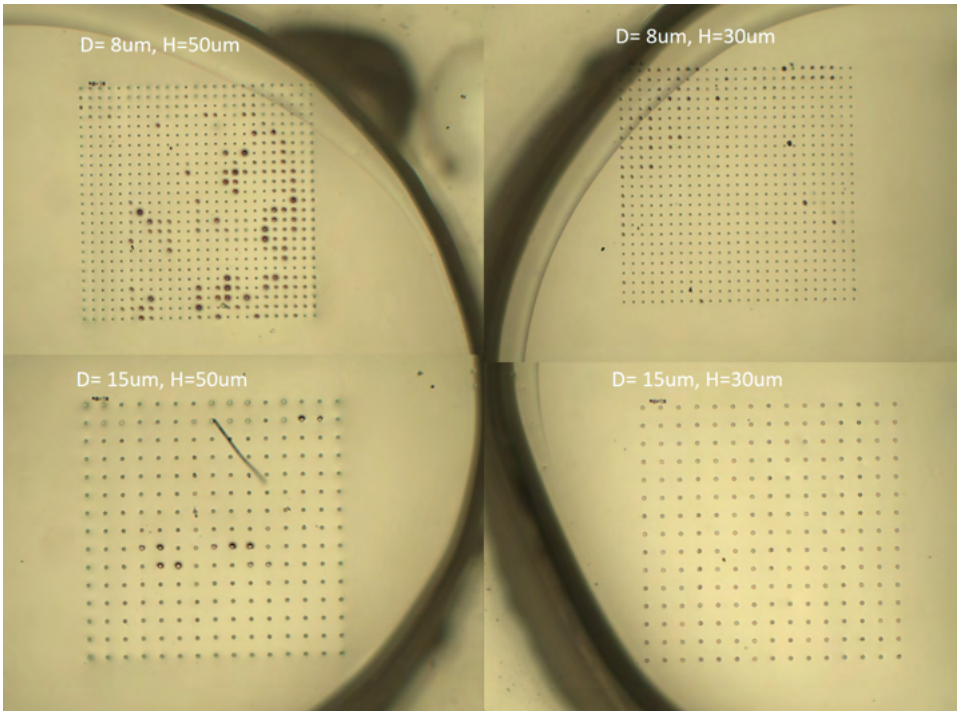

Figure 4.5: Porous PDMS membrane for trial pillar mould

Table 4.1: Mould pillar detachment with varying parameters

	H = 50 μm	**H = 30** μm
D = 8 μm	Maximum pillar detachment	Some pillar detachment
D = 15 μm	Some pillar detachment	Negligible pillar detachment

It was not possible to remove the pillars stuck in the membrane pores by putting them in an acetone in an ultrasonic bath sonicator for 30 minutes. As the pillar are made of a polymer resin as well, it was also not possible to dissolve them using chemicals as that would also damage the porous membrane. Thus, any detached pillars are permanently stuck in the membrane pores.

The trial membrane was found to be porous. A drop of coloured liquid was placed on the top of the membrane and it passed to the lower side within minutes. As the four arrays were made on the same sample it was not possible to determine if pores made by pillars of both the heights made pores all the way through. For that pillar moulds with array of pillars with a diameter of 10 μm and heights 30 μm and 50 μm were made of different samples. The resulting membranes obtained showed that, for the pillars of height 30 μm, a 25 μm PDMS membrane covers the pillars and is not porous and a 10 μm membrane does not cover the pillars and is porous.

Considering the results from the trials it was decided that **a substrate with pillars of diameter of 10** μm **and height of 30** μm **would be used for making a porous membrane of thickness 10** μm. It is also possible to use a pillar with height 50 μm to get a 25 μm thick porous membrane, however, this option was not chosen due to higher pillar detachment. There was also a significant decrease in the detachment of pillars if the pillar moulds were silanized using HMDS. Using Pluronic® F-127 allowed for peeling of the membrane from the substrate with ease and without any tears. The reason for this is that HMDS chemically bond to the silicon surface, forming a single molecule thin layer over it which does not allow PDMS to bond to the glass surface. Pluronic® F-127 particles are left behind on the surface as the water evaporates. These particles ensure that the PDMS does not clasp the pillars so that they are not peeled off along with the membrane.

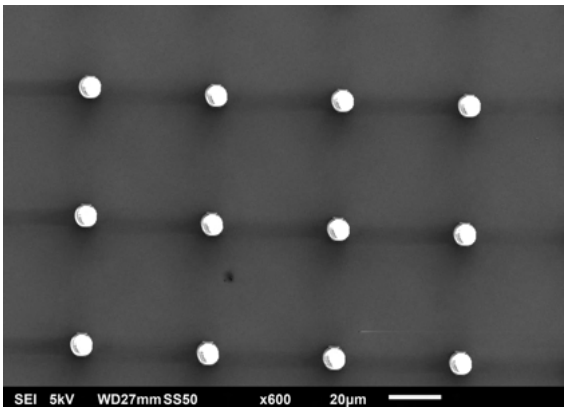

Figure 4.6: SEM image of the printed pillars. The pillar diameter is 8 μm and the pitch is 48 μm.

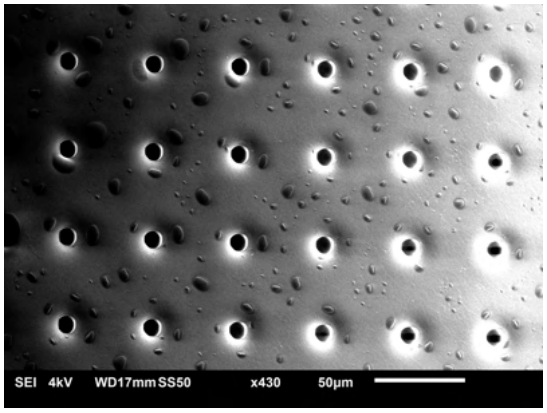

Figure 4.7: SEM image of the obtained porous PDMS membrane.

The SEM images of the pillar mould revealed that the 10 μm printed pillars were 8 μm in reality and the pitch was found to be 48 μm instead of the intended pitch of 51 μm, as seen in Figure 4.6. The membrane obtained using this pillar array can be seen in Figure 4.7. To correct for this the intended 10 μm pillars have to be printed with a pitch of 37 - 40 μm the pores to cover 3-3.5% of the membrane. This will result in a membrane with pores of diameter 8 μm covering 3-3.5% of the surface.

4.3.1. Procedure for manufacturing the porous membrane

1. Keep the silicon substrate with pillars on a hot plate at 100°C for 20 minutes to prepare it for silanization.
2. Put the pillar mould into a desiccator along with 1-2 drops of HMDS in a glass petri dish for 2 hours.
3. Keep the pillar mould on a hot plate at 100°C for 20 minutes to activate the HMDS coating.
4. Let the pillar mould cool down to room temperature.
5. Put the pillar mould in a 1% solution of Pluronic® F-127 in DI (Deionized) water for 5 minutes.
6. Remove the mould from the solution and keep it in the fume hood for drying out. Do not use an air gun to blow dry the mould.
7. Spin coat a 10 μm layer of PDMS prepolymer and cure it at the desired temperature.
8. Attach a holder (or the actuator half layer) to the membrane to aid the removal, and subsequent handling, of the cured porous membrane.

For making membrane samples for cell culture tests (section 5.4) a holder made of PDMS was bonded to the membrane before peeling it off. The holder was made by cutting out a rectangular piece from a slab of cured PDMS and a 3.5 mm hole was punched out from its center. This hole would be covered by the porous part of the membrane. For making the full device, an actuator half layer were bonded to the membrane before peeling it off. The 3 mm hole in the layer was placed above the porous part of the membrane.

Alternatively, it was attempted to laser cut the pores into the PDMS membrane, see section G.2 for more. The method did not prove to be suitable for this application as the laser spot size of 20 μm resulted in pores of diameter 40 ±5 μm, which was much bigger than the required pore diameter of 10 μm. This resulted in lung cells passing through the pores, instead of staying on the membrane, when seeding them on this membrane was attempted.

4.4. Channels

The channels were made by sandwiching a PDMS channel layer between two glass layers. The glass layers were made by laser cutting the required holes for connections and access to the membrane into coverslips (# 1.5). The drawing for different glass layers is shown in section E.2. The OPTEC Laser Cutter was used for this with the laser parameters set as follows:

Table 4.2: Laser Parameters for cutting # 1.5 Glass Coverslips

Parameter	Value
Diode Current	7.25 A
Speed	150 mm/s
Jump Speed	200 mm/s
Laser Firing Rate	75 KHz
Laser Power	100%
Repetitions:	
Connection Holes	40
Membrane Access Hole	80

Damage of mirrors in the laser cutter and lack of regular maintenance can cause the laser cut to be weak and the repetitions need to increased to mitigate that. The glass layers can be seen in Figure 4.8

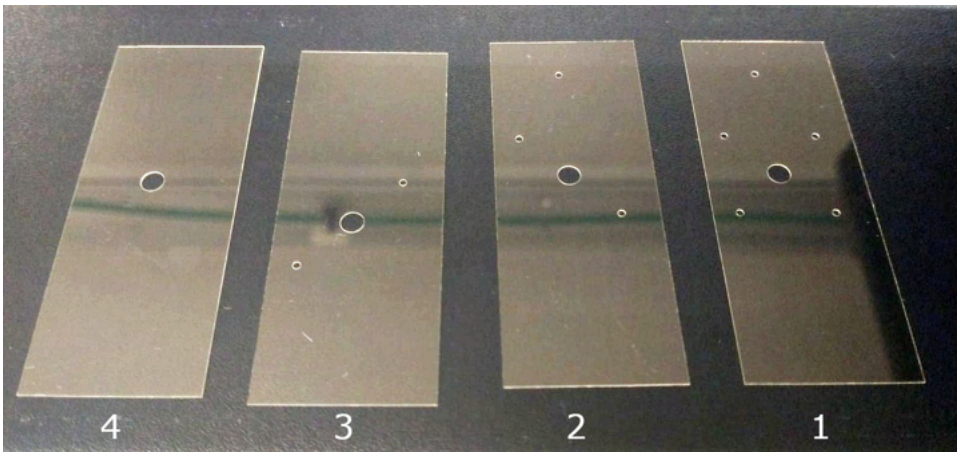

Figure 4.8: Glass Layers

The **channel layer** was cut out of a 200 μm layer of PDMS. To make that a 100 μm layer of PDMS was spin coated and cured on a glass slide, see section H.1. Then another 100 μm layer of PDMS was spin coated and cured on top of the first PDMS layer. The glass slide was coated with Pluronic® F-127, as described in subsection 4.2.2. The channel was then cut out in the PDMS layer by tracing a printout of the channel drawing placed below the glass slide. The drawing for the channels is shown in Figure 4.9.

Due to surface tension the spin coated PDMS prepolymer layer rounded at the edges of the glass slide before it could be cured. This resulted in non uniform contact of the PDMS layer with the glass layer resulting in improper sealing of the channel. To prevent that, it was decided to cut the channel layers from a 200 μm layer of PDMS spin coated on to a **polystyrene petri dish**. Scotch tape was used to cover the PDMS layer and then the channel layer was cut out and peeled off from the petri dish using the tape as a support for the thin PDMS layer. The peeled off PDMS layer was then brought gradually into contact with a glass layer ensuring that no air bubbles are trapped in between. The Figure 4.10 shows a glass layer with a PDMS channel layer transferred onto it using a scotch tape.

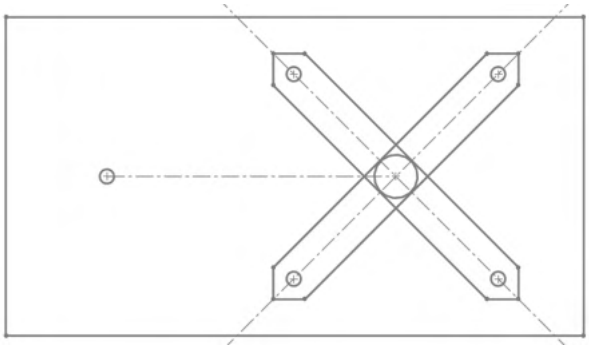

Figure 4.9: Drawing for tracing out channels

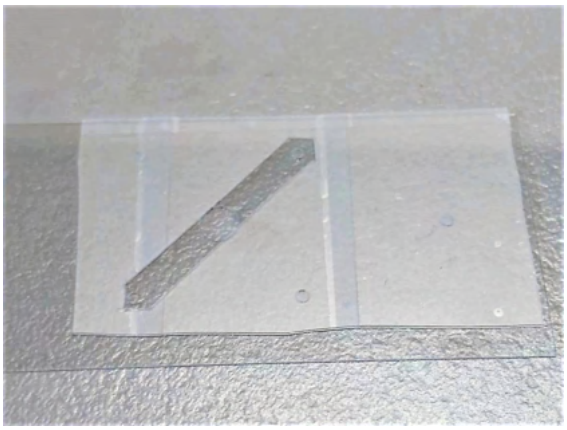

Figure 4.10: PDMS channel layer transferred onto a glass layer using scotch tape.

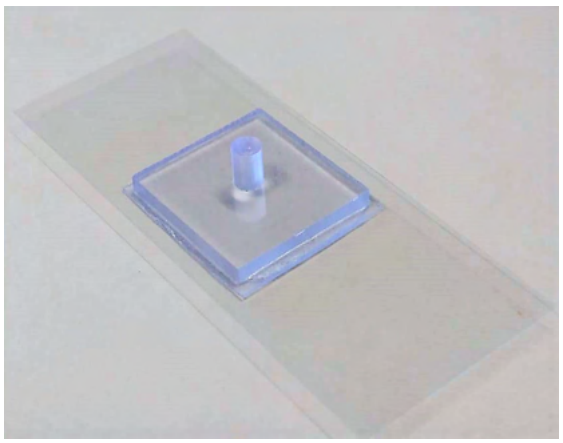

Figure 4.11: Alignments stage for assembling the channels.

The PDMS layer was pressed to make it stick well to the glass layer and then the tape was peeled off. The second glass layer was then brought into contact with the PDMS layer to form the channel. An **alignment stage** was used to make sure that the central hole for access to the membrane and the holes for connections are properly aligned. The alignment stage with a glass layer is shown in Figure 4.11. This method was used to make the top and bottom channels. The channels were then kept for 2 hours at 80°C to ensure good bonding of the glass layers with the PDMS layer.

4.4.1. Procedure for manufacturing the channel layers

1. Spin coat a 200 μm layer of PDMS prepolymer on a polystyrene perti dish.
2. Cover the petri dish and let the PDMS cure at room temperature for two days. Curing at higher temperatures can cause the polystyrene petri dish to warp.
3. Cover the cured PDMS layer with scotch tape. This layer ensures that the blade cuts the PDMS layer without causing any undesired damage and prevents foreign particles from sticking to the PDMS surface.
4. Attach the channel drawing to the bottom of the petri dish and trace out the channels using a sharp blade.
5. Remove the cut outs and cover the channel with another layer of scotch tape to ensure that the channel shape does not get distorted while transferring it to the glass layer.
6. Peel off the PDMS layer with the help of the tape.
7. Place the PDMS layer on the glass layer with the help of the tape. It is possible to reposition the layer several times to ensure that the placement is correct.
8. Remove the tape.
9. Place the glass layer with the PDMS layer attached to it on the alignment stage with the PDMS side facing upwards.
10. Bring the other glass layer into contact with the PDMS layer using the alignment stage.

Alternatively, it was attempted to make the channels by hot embossing COC and polycarbonate (PC). This method was not chosen as the technique for bonding PDMS to COC/PC was not perfected. See G.3 for more.

4.5. Device Assembly

The actuator layer and the channels were plasma bonded together to form the full device, as shown in Figure 4.12. See Appendix F for the full plasma bonding method. The central hole for access to the 3 mm diameter porous membrane was made a bit larger (3.1 mm) in diameter to ensure that even while manually aligning the actuator layers with the channel, the glass does not end up covering any part of the membrane.

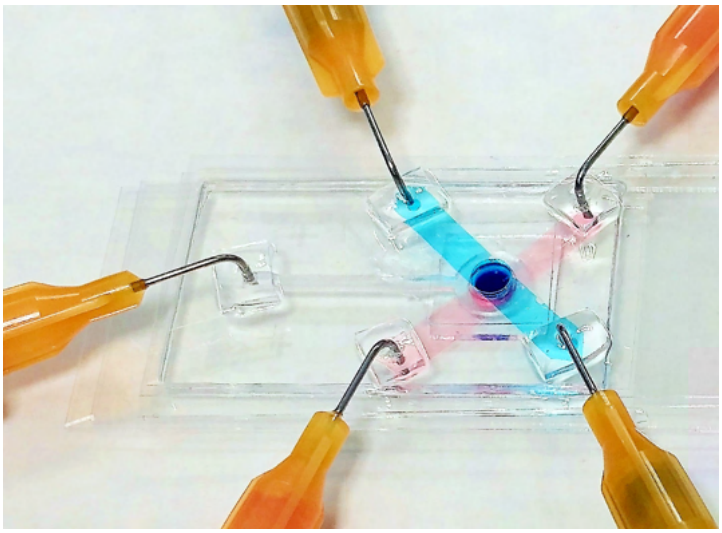

Figure 4.12: The assembled lung-on-a-chip device. The top and bottom channels are filled with coloured water to show the overlap at the membrane.

4.5.1. Device Connections

The connections for applying cyclic vacuum, gas flow and culture media flow were made using **90° bent needle tips**. These tips are compatible with male luer lock tips and luer slip tips and can be used with standard microfluidic connectors available with the pressure controllers. To connect the needle tip to the chip, a PDMS patch is attached at the channel inlet/outlet hole on the top glass layer. The needle tip is pushed through this patch, sealed off with more uncured PDMS and left at room temperature to cure.

4.5.2. Coverslips

The coverslips are laser cut to the required size (9 mm x 9 mm), by the method mentioned in section 4.4. Then they are plasma bonded to a 40 μm layer of PDMS spin coated on a glass slide. A sharp blade is used to cut the boundary of PDMS along the coverslip edge before peeling it off the glass substrate. For making the PDMS step, for the culture media channel layer, a cylinder is punched out from a PDMS slab of desired thickness and then the sides are cut out with a sharp blade. This step is then plasma bonded to the PDMS layer bonded to the glass coverslip.

The coverslips could be reversibly bonded to the device to seal the channels while using negative pressure for culture media flow. If positive pressure has to be used for culture media flow then there is a need of a holder that will provide continuous external pressure to hold the cover slip tight against the glass surface of the device for a proper seal.

4.6. Chapter Summary

The LOC device was made out of glass and PDMS, two materials widely used for OOC application. The pneumatic actuator was made out of two PDMS actuator half layers and a porous PDMS membrane. The PDMS actuator half layer was made by curing the PDMS prepolymer in a 3D printed mould and the porous membrane was made by spin coating a 10 μm layer of PDMS prepolymer on a silicon substrate with 3D printed pillars of diameter 10 μm and height 30 μm. The step wise manufacturing procedure for the actuator half layer and the porous membrane is shown in Figure 4.13 and Figure 4.14 respectively.

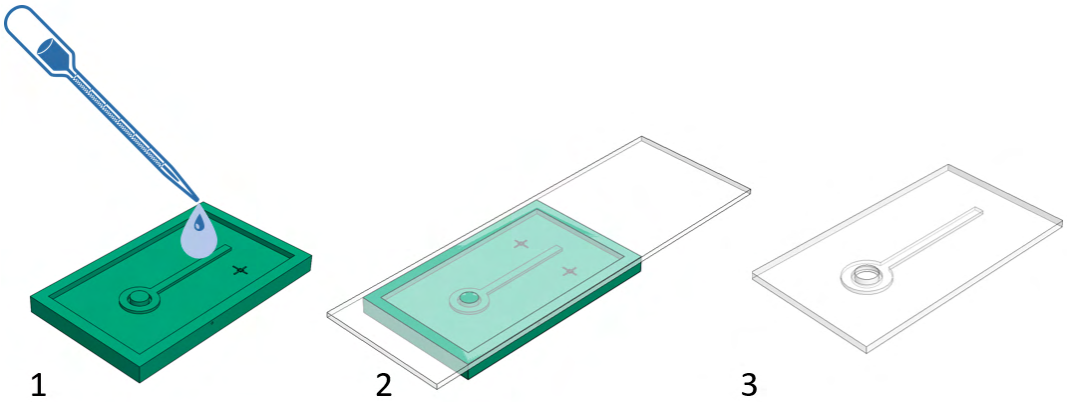

(1) PDMS prepolymer with base to resin ration 10:1 was poured in a 3D printed mould for the actuator half layer.
(2) The prepolymer was degassed in a desiccator and then the mould was covered with a glass slide, which was held in place with the help of rubber bands. The prepolymer was left at room temperature for 48 hours to cure.
(3) The cured PDMS actuator half layer was removed from the mould with the help of a blade and IPA .

Figure 4.13: Manufacturing procedure for the actuator half layer

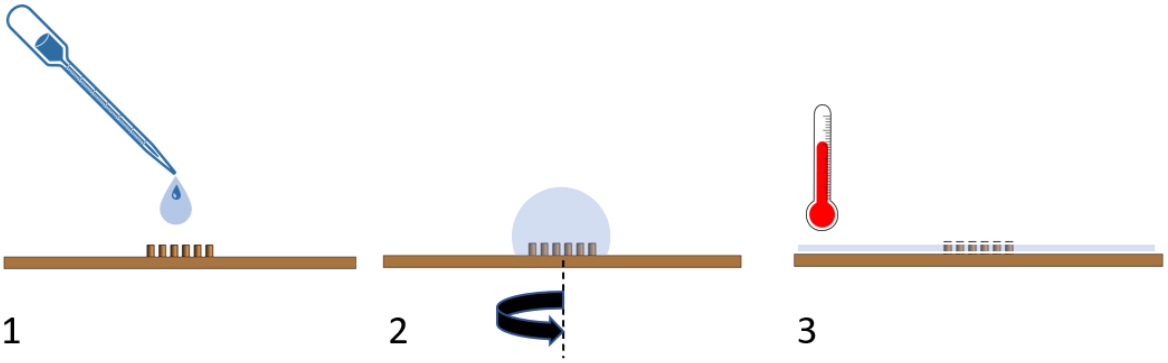

(1) PDMS prepolymer with base to resin ration 10:1 was pipetted in the center of a substrate with 3D printed pillars to which surface treatment has been done to make it easy to remove PDMS after curing.
(2) The substrate was spun in a spin coater at 2500 rpm for 5 minutes to form a 10 μm layer of the prepolymer.
(3) The substrate with the spin coated prepolymer was put on a hot plate at 150 °C for 5 minutes to cure the PDMS.

Figure 4.14: Manufacturing procedure for the porous membrane

To assemble the actuator, an actuator half layer was placed on a thin layer of uncured PDMS prepolymer and then placed onto the porous membrane. The thin prepolymer layer was then cured and the porous membrane peeled off the substrate with the help of the half actuator layer. Membrane areas covering the vacuum channels are cut out manually and removed with tweezers. Another half actuator layer was bonded this, using the same method as above, to complete the actuator. Holes were punched in the assembled actuator layers for access to the basal chamber. See Figure 4.15 for the step wise assembly procedure for the actuator.

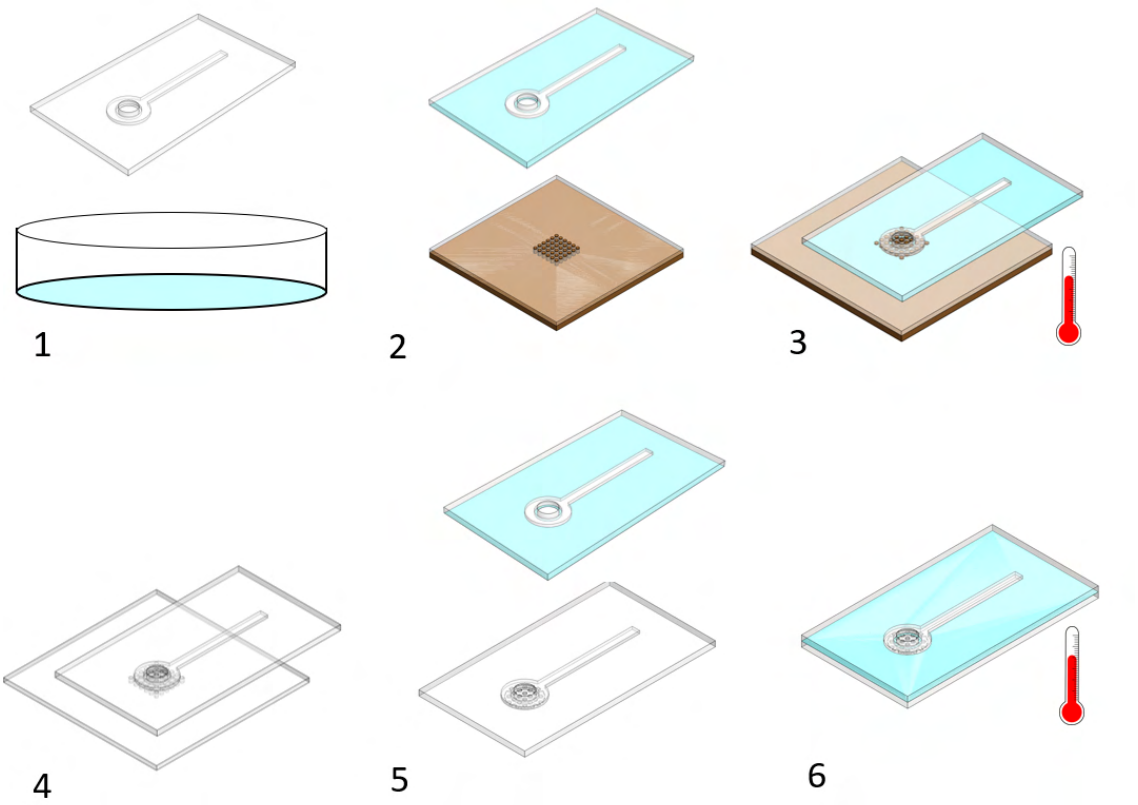

(1) An actuator half layer was placed on a 25 μm spin coated layer of PDMS prepolymer to coat its lower surface evenly with the uncured PDMS.
(2) The actuator half layer, coated with uncured PDMS, was placed on the porous membrane, still on the substrate.
(3) The thin layer of PDMS was cured at 50°C for 1 hour to bond the actuator half layer to the porous membrane.
(4) The porous membrane was peeled off from the substrate with the help of the actuator half layer bonded to it.
(5) Parts of the membrane covering the vacuum channels were removed manually and an access hole for the vacuum channel was punched out in the actuator half layer. Another actuator half layer coated with uncured PDMS was placed on top of it.
(6) To bond the actuator half layer to the other actuator half layer bonded to the porous membrane, the thin layer of prepolymer was cured at 50°C for 1 hour.

Figure 4.15: Procedure for actuator assembly

The channel layers were made out of a 200 μm PDMS layer, with a recess in the shape of the channel, sandwiched between two 1.5 H glass coverslips. Holes for making connections for vacuum, gas flow and culture media flow, as well as, the central membrane access hole, were laser cut in the coverslips. The PDMS layer was spin coated on a polystyrene petri dish and cured at room temperature. Scotch tape was used to aid the cutting of a channel in the PDMS layer and for transferring the cut PDMS channel layer to the coverslip. With the help of an alignment stage, another coverslip was placed on top of the PDMS channel layer, ensuring that the connection holes and the central membrane access hole for both the coverslips were aligned, to form the channel. The step wise manufacturing procedure for the channels is shown in Figure 4.16.

The gas channel was plasma bonded on the top surface of the actuator and the culture media channel was plasma bonded on the lower surface. To make the resealable coverslips for sealing the channels, 9 mm × 9 mm squares were laser cut from a 1.5 H coverslip and bonded to a 40 μm layer of PDMS. A step, made by punching out a cylinder from a PDMS slab of desired thickness and slicing off the sides, was also bonded to the lower coverslip. For making connections, 90° bent needle tips were attached to the device.

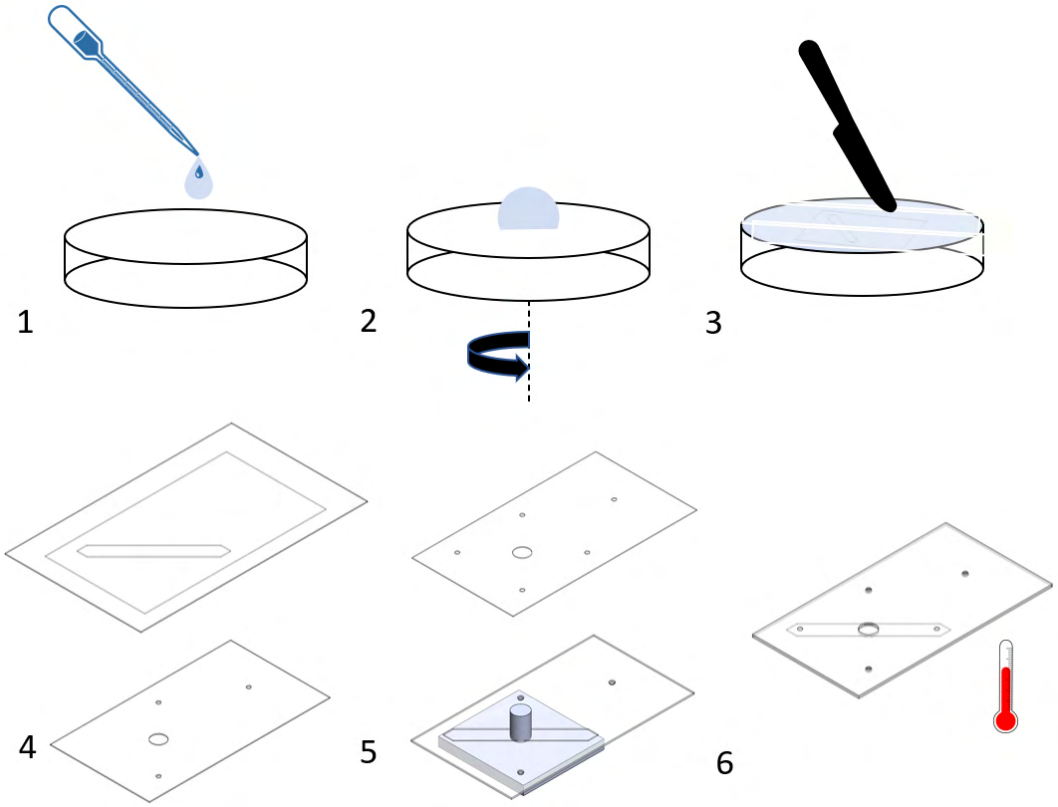

(1) PDMS prepolymer with base to resin ration 10:1 was pipetted onto a PS petri dish.
(2) The substrate was spun in a spin coater at 400 rpm for 1 minute to form a 200 μm layer of the prepolymer.
(3) The prepolymer was left at room temperature for 48 hours to cure. The cured PDMS was covered with scotch tape and then cut in the shape of channel layers.
(4) The cut channel layer was transferred to a glass layer using another layer of scotch tape. The tape was removed after the placement.
(5) Another glass layer was placed on the channel layer to form the complete channel. An alignment stage was used to ensure that the glass layers were aligned.
(6) The assembled channel was placed on the hot plate at 80°C for 2 hours to heat bond the glass layers to the PDMS channel layer.

Figure 4.16: Manufacturing procedure for channels

5

Device Testing

The device was tested in order to verify whether it worked as per the set requirements (1.1) or not. This included testing the pneumatic actuator and quantifying the linear strain that it can subject the porous membrane to. The channels were tested for flow and the effect of the liquid flow on the membrane was also looked into. The suitability of the porous membrane for long term cell culture and of the device for cell imaging was verified.

5.1. Pneumatic Actuator

The manufactured PDMS pneumatic actuator was tested by applying cyclic negative pressure. Initial tests were aimed at establishing a proof of concept and later extensive testing was done to study the effect of the manufacturing process on the maximum linear strain that the actuator could apply on the membrane. These tests formed the basis for making a choice between different manufacturing methods for the actuator.

Test Setup:
For controlling the pressure applied to the actuator OB1 MK3+ microfluidic flow controller from Elveflow was used. The device can be used to apply negative pressure upto -900 mbar. The device was connected to the pressure controller using polytetrafluoroethylene (PTFE) tubing with standard luer lock connectors and a syringe filter.

Proof of Concept:
The actuator samples, made from two actuator half layers and a non-porous membrane, were subjected to cyclic negative pressure. Negative pressure was applied at 0.2 Hz in the form of a triangular wave with the pressure varying between 0 mbar and -900 mbar. The actuator was tested for being seal tight by putting a drop of tinted water in the chambers on either side of the membrane while the negative pressure was applied. This test was used to select the method for bonding actuator half layers to the membrane. The results showed that **bonding using uncured PDMS** was more reliable than plasma bonding. The file `Actuator proof of concept.mp4` in the supplementary files shows a video of the working actuator. It can be seen in the video that there is also noticeable deflection in parts other than the actuator wall as well, which is not desired. This is due to the absence of glass layer 2 and 3 in the sample and highlights the **importance of the stiff glass layers** for ensuring that the actuator deforms as intended.

Actuator Deflection:
The deflection of the actuator wall was measured as negative pressure was gradually applied to the actuator wall. A microscope with an attached digital camera was used to record videos of the actuator wall and later ImageJ software was used to measure the wall deflection. Figure 5.1 shows the actuator wall before and after applying -900 mbar pressure.

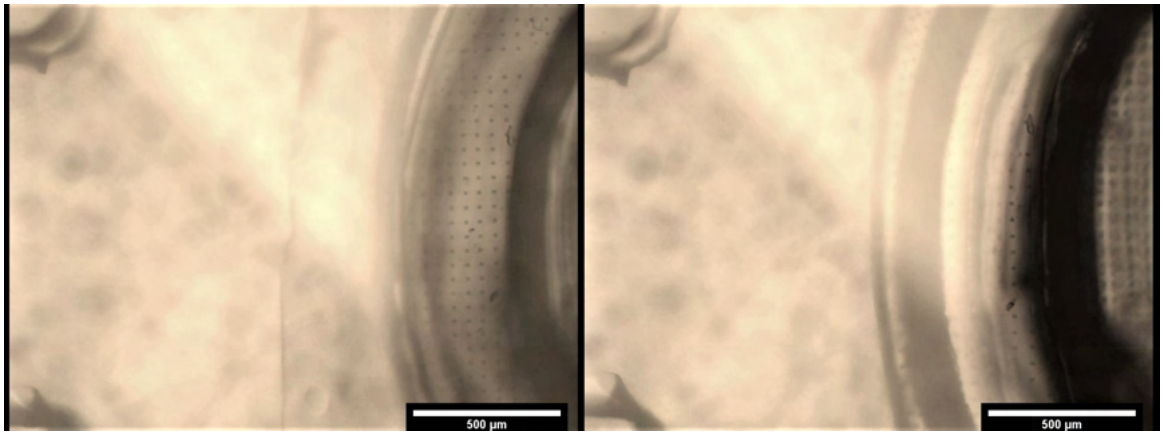

Figure 5.1: Actuator wall before (left) and after (right) applying -900 mbar pressure.

Based on the measurements obtained from these tests the curing temperature for the PDMS was decided. The graph in Figure 5.2 shows the effect of the curing temperature on the wall deflection with respect to the pressure applied for an actuator with a wall height of 1 mm and a wall thickness of 0.4 mm. Higher curing temperature resulted in a stiffer actuator wall, resulting in a lower deflection of the actuator wall. Thus, it was decided to cure the PDMS at **room temperature for 48 hours** with the **base polymer to resin ratio as 10:1**.

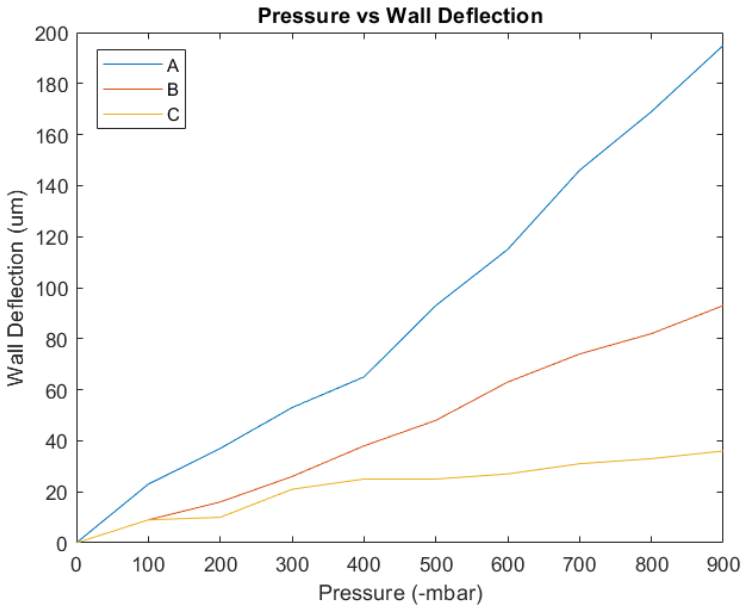

Curing time and temperature for 10:1 PDMS- A: 48 hours at room temperature, B: 3 hours at 60°C, C: 2 hours at 75°C .

Figure 5.2: Effect of curing temperature of PDMS on the in plane deflection of the actuator wall with respect to the negative pressure applied.

The maximum wall deflection at -900 mbar and the wall deflection at -700 mbar, the limit for most commercially available vacuum pumps for OOC application, was measured. For a room temperature cured PDMS actuator, with a wall height of 1 mm and a wall thickness of 0.4 mm, the maximum in plane deflection for -900 mbar of the wall was found to be 195 μm which corresponds to a 13% liner strain for the membrane. For -700 mbar this was found to be 146 μm and corresponds to 9.73% linear strain for the membrane. As this value of liner strain was lower than the desired 20% linear strain, it was decided to **increase the height of the actuator wall to 1.4 mm** , keeping other dimensions same as before. With these dimensions **the wall deflection at - 900 mbar was 370 μm , which corresponds to 24% liner strain** for the membrane. For -700 mbar this was found to be 302 μm , which corresponds to 20% linear strain for the membrane.

Heating of the PDMS actuator at high temperatures post curing was also found to reduce the wall deflection. For the same dimensions, an actuator made of actuator layers cured at room temperature and bonded to the glass layers of channels by heating under pressure for 2 hours was found to have a maximum deflection of 118 μm compared to a deflection of 195 μm for a device made using plasma bonding of the actuator to the glass layers. Thus, **plasma bonding** was selected as the method for bonding glass layers with the actuator. A reduction in the maximum wall deflection is also expected over the time the device is in use at 37°C for more than four weeks in the incubator.

Membrane Strain:
To measure the strain on the membrane, videos of the porous membrane were taken while being actuated using cyclic negative pressure. The videos were processed using ImageJ to measure the linear strain. At first, the pores were identified and then the path of the center of each pore was mapped for the cyclically stretching membrane using TrackMate [112]. The distance between the centers of two selected pores was compared in the stretched and unstretched state and the linear strain was calculated. The Figure 5.3 shows the processed images of the porous membrane showing the path of each pore center. The maximum linear strain measured under -900 mbar pressure for a device with actuator wall height 1 mm was found to be 14%, which is comparable to the value calculated using actuator wall deflection. For devices with 1.4 mm wall height, the linear strain was found to be to be 25% and 20% for -900 mbar and -700 mbar pressure respectively.

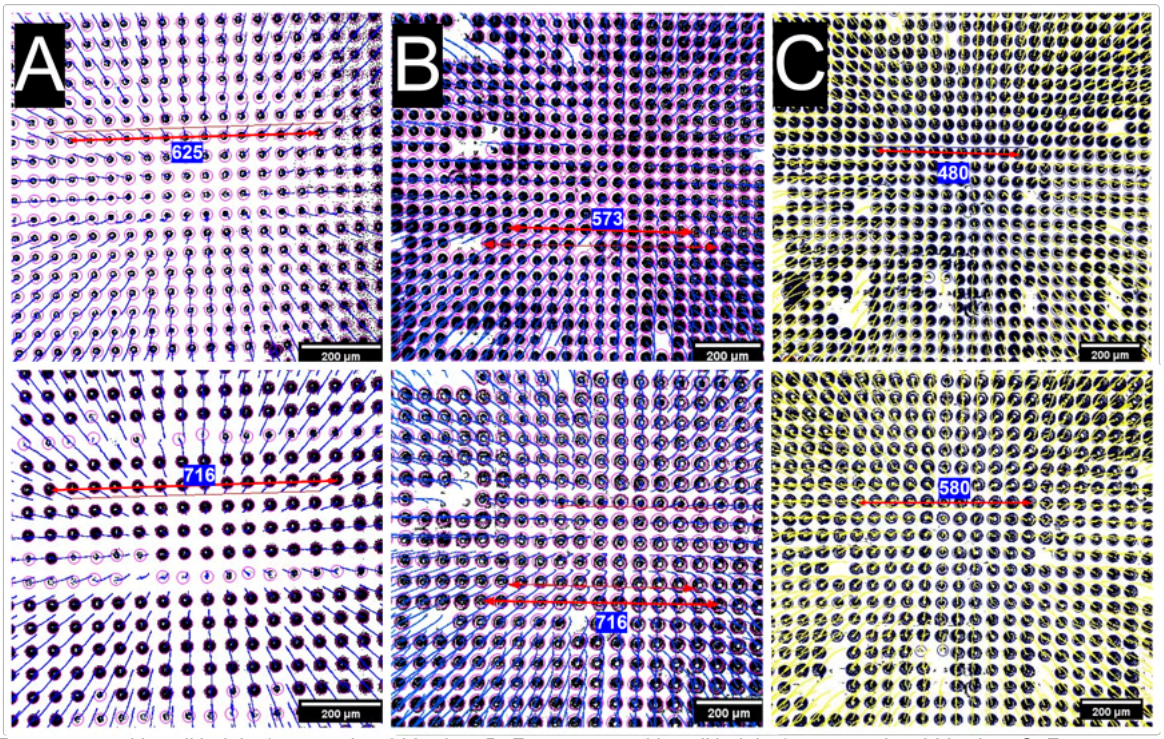

A- For actuator with wall height 1 mm under -900 mbar, B- For actuator with wall height 1.4 mm under -900 mbar, C- For actuator with wall height 1.4 mm under -700 mbar

Figure 5.3: Membrane pore distance before and after applying negative pressure

Some out of plane deflection was also observed, as can be seen in the pore paths, however, it was not considered important to measure this out of plane deflection of the membrane as when the device is in use the out of plane deflection of the membrane will depend on the pressure difference between the apical chamber and basal chamber. The pressure in the basal chamber depends in turn on the inlet pressure and outlet pressure of the culture media flow channel. For the above membranes, there was no flow present. The final deflection of the membrane will be a sum of the in plane stretching by the pneumatic actuator and the out of plane stretching due to the culture media flow. The section 5.3 describes the test to measure out of plane deflection of the membrane.

Videos of the membrane under cyclic stretch at 0.2 Hz (triangular wave) for -700 mbar and -900 mbar maximum negative pressure, along with the processed videos for strain measurement, can be seen in the supplementary files

5.2. Flow in the Channel

The LOC has gas flow in the apical chamber and culture media flow in the basal chamber. The gas channel provides low resistance to gas flow, and thus, little difference is required between the inlet and outlet pressure. For the flow of culture media, according to calculated estimates, the resistance provided by the channel requires a pressure difference between the inlet and the outlet to be in the range 0.7-2 mbar, exact value depends up on the shear stress that is to be applied to the endothelial cells.

Flow Generation Methods:
The desired method for flow generation is by using a **pressure driven flow controller**, as for this method the **out of plane deflection of the membrane can be mitigated** by adjusting the pressure to be equal in the apical and basal chamber. To recirculate the culture media, commercially available recirculation packs can be used [8, 12]. These packs allow for control of the inlet and the outlet pressure of a channel. This method also results in least deviation from the set flow rate [30]. A pressure controller can also be used to set just the inlet or outlet pressure, this will lead to some out of plane deflection of the membrane.

Syringe pumps and peristaltic pumps are other popular methods for flow generation. If the user decides to use them, there will be some out of plane deflection of the membrane. If a **syringe pump** is used there will be upward or downward deflection of the membrane based on weather the pump is used in injection or withdrawal mode. A major disadvantage of the syringe pump is that it does not support recirculation of culture media which is required for the device (see 3.3.1). **Peristaltic pumps** provide an option for recirculating the culture media for long term cell culture experiments. The disadvantage is that the flow is pulsed and due to that there will be undesired fluctuation in the shear stress that the endothelial cells are subjected to. This also results in fluctuation in the out of plane deflection of the membrane.

It is possible to use **hydrostatic pressure** to flow liquid in the channel by placing a reservoir connected to the chip at a height with respect to the chip. The flow rate can be controlled by the height difference. To incorporate recirculatuion in this setup the liquid needs to be collected from the chip outlet and pumped back into the reservoir.

To compare the flow generated by controlling the pressure at the channel inlet and channel outlet to the flow generated by infusion, COMSOL models for both the scenarios were compared. In case of flow due to infusion, the model estimated a maximum out of plane deflection of 300 μm and for pressure controlled flow the model estimated a maximum out of plane deflection of 54 μm. The shear stress on the membrane due to flow was also found to be more uniform in the latter case. This comparison also suggests that pressure driven flow is the suitable method for flow generation for this device. The file `Membrane Shear Stress.gif` shows the shear stress on the membrane in case of flow due to infusion and the file `Membrane Shear Stress (pressure controlled flow).gif` shows shear stress on the membrane in case of the flow due to pressure control at the channel inlet and outlet.

Flow Tests:
The flow in the channel was tested with a **syringe pump in suction mode**. Cyclic negative pressure was applied to the actuator to stretch the membrane and a resealable coverslip was used to seal the channel. For suction mode, the coverslip remained securely attached while the actuator was moving. When the liquid was flown in infusion mode, the coverslip detached, partially or completely, after some time leading to a leak. For using the syringe pump in infusion mode, a holder needs to be made to hold the coverslip tight against the glass surface or the coverslip needs to be glued to the device after the cells have been seeded.

A **peristaltic pump** was used to circulate tinted liquid in the culture media chamber. The placement of the channel in the recirculation loop, Figure 5.4 B, ensured that the media is pulled out of it by the pump. This allowed the coverslip to stay in contact while the liquid was flown in the channel. Some out of plane deflection of the membrane was observed due to the fluctuations in the flow provided by the pump, as can be seen in the file `Flow Fluctuation with Peristaltic Pump.mp4`. The setup was left running for 5 days and it was observed that air bubbles leaked into the channel due to some leak at the connections. This highlights the importance of sealing the connection points well for avoiding air bubbles in all modes of flow where the fluid is being sucked out of the channel.

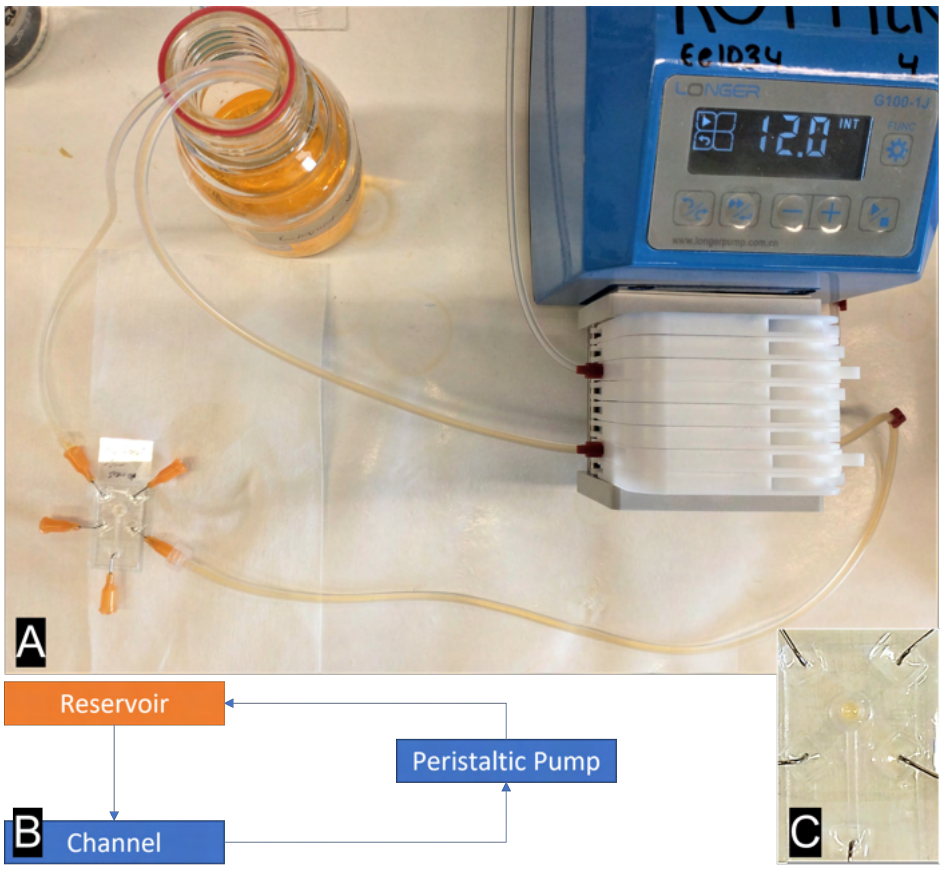

A- The test setup for recirculation of liquid using a peristaltic pump, B- The block diagram of the recirculation loop. The arrows show flow direction, C- Zoomed in view of the chip with tinted liquid flowing through it.

Figure 5.4: Recirculation of tinted liquid using a peristaltic pump

5.3. Membrane Deflection Due to Flow

The out of plane deflection of the membrane depends on the pressure difference between the apical chamber and the basal chamber. If the inlet and outlet pressures for the culture media channel are selected to ensure that pressure on both sides of the porous membrane is the same, then there will be **no out of plane deflection of the membrane**. This is the ideal condition and will ensure little variation in shear stress for all the endothelial cells on the membrane. However, for such a condition a pressure controller with positive and negative outlets will be needed to control the pressure at both the inlet and the outlet of the channel. Another usage scenario could be in which the user only wants to use negative (or positive) pressure at the outlet (or inlet). In this case, there will be an out of plane deflection of the membrane.

To estimate the out of plane deflection of the membrane, a syringe pump was used to flow water in the culture media channel. No connections were made to the upper channel, making the pressure in the apical chamber equal to the atmospheric pressure. Without any step on the coverslip, the height of the basal chamber is 1.6 mm, see 3.4.2. A step of a minimum height 0.4 mm ensures that most of the culture media does not flow straight across the channel and is deflected into the basal chamber.

Thus, the chamber height has to be 1.2 mm or lower. Figure 5.5 gives the flow rates corresponding to different chamber heights for 0.55 Pa shear stress on the membrane.

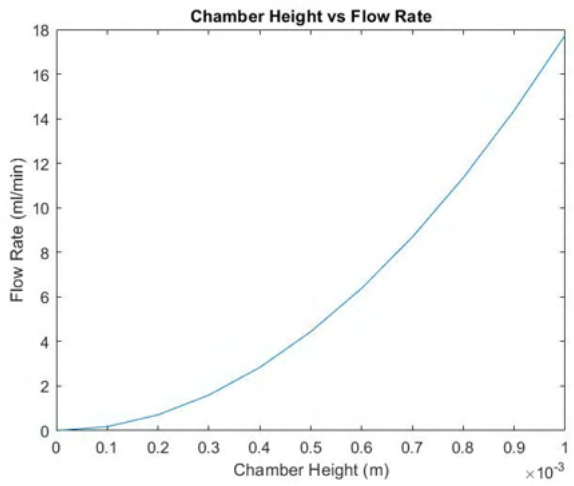

Figure 5.5: Flow rates corresponding to chamber height for 0.55 Pa shear stress.

Test Setup:
Bruker **white light interferometer** was used for measuring the out of plane deflection of the membrane. An LOC device without the top air channel was made to make it possible to focus on the membrane using the interferometer objective. The device was sputtered with a thin layer of gold so that the white light interferometer can detect the membrane, as can be seen in Figure 5.6. The inlet of the channel was connected to a reservoir filled with water at atmospheric pressure and the outlet was connected to a **syringe pump**. The pump was run in withdrawal mode and infusion mode at varying flow rates. The 0.25x zoom objective was used to get a scan of the membrane in deflected and undeflected states.

The measurement showed the central part of the deflected membrane and the top flat surface of the actuator half layer, as can be seen in Figure 5.7. The deflection was calculated by subtracting the distance between the membrane and the top surface at no flow from the corresponding distance at different rates of liquid flow. For withdrawal mode of the syringe pump, the membrane deflected into the chamber and came in to **contact with the step** for flow rates corresponding to a shear stress of 0.55 Pa. This is not desirable and will cause damage to the cell layer. Thus, for suction mode, deflection for different flow rates was measured with a step of 0.8 mm. For infusion mode, chamber heights of 0.4 mm and 0.6 mm were chosen for flow rates 3 ml/min and 7ml/min respectively. The results can be seen in Table 5.1. Here the negative sign represents flow in withdrawal mode and deflection into the basal chamber. The measurement data can be seen in appendix I.1.

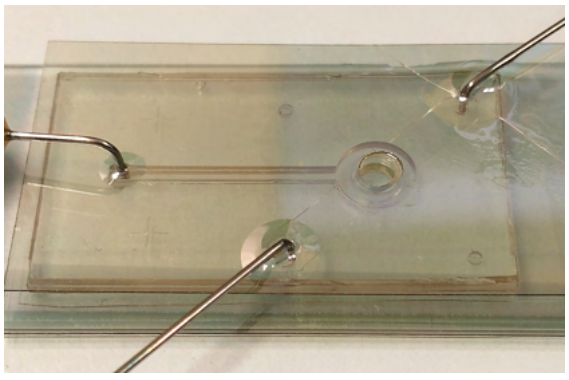

Figure 5.6: Gold Sputtered sample for white light interferometry

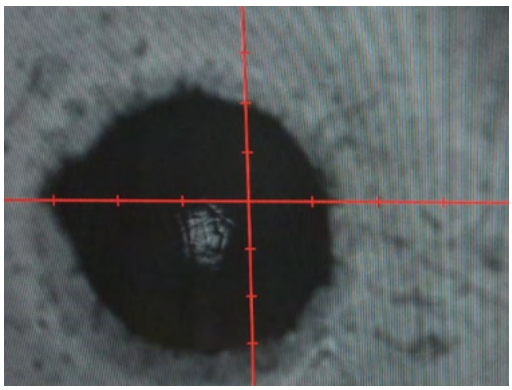

Figure 5.7: Deflected membrane as seen using the white light interferometer software

Table 5.1: Out of plane deflection of 10 μm PDMS membrane due to liquid flow in culture media chamber

Flow Rate (ml/min)	Chamber Height (μm)	Deflection (μm)
7	600	567
-7	800	-628
3	400	321
-3	800	-453
-6	800	-620
-2.6	800	-443

5.4. Cell Culture

To set up the LOC, cells need to be cultured on the porous PDMS membrane. Cells prefer to attach to hydrophilic surfaces and as PDMS is **hydrophobic** by nature it requires surface treatment to make it suitable for long term cell culture. The method used for surface treatment depends up on the type of cells to be cultured, the duration for which the cells are to be cultured and the mechanical forces (shear stress or cyclic stretching) the cells are going to be subjected to [7, 28, 126]. Long term media flow and cyclic stretching increase the rate of cell detachment and cell death. As the LOC device requires the cells to endure stretching and culture media flow, surface treatment of the PDMS membrane is essential.

Treating the PDMS surface with plasma makes the surface hydrophilic. Extracellular matrix (ECM) proteins can then be adsorbed by the surface, making it suitable for cell culture [126]. This effect is temporary and the surface regains its hydrophobic nature. This leads to the cells cultured on it to detach over time and, thus, this method is only suited for short term cell culture applications. For long term cell culture applications, such as in case of this device (greater than 4 weeks), methods to **covalently bond ECM proteins like collagen** and fibronectin to the PDMS surface have been proposed [7, 77, 92]. These methods make the surface suited for long term culture and show reduction in the rates of cell death under culture media flow and cyclic stretching [7, 28]. Figure 5.8 shows the method used by Leivo et al. to covalently bond collagen to PDMS. Leivo's method AA1, which used ascorbic acid in PBS, was considered to be suitable for the designed device and was tested for the porous PDMS membrane samples [7].

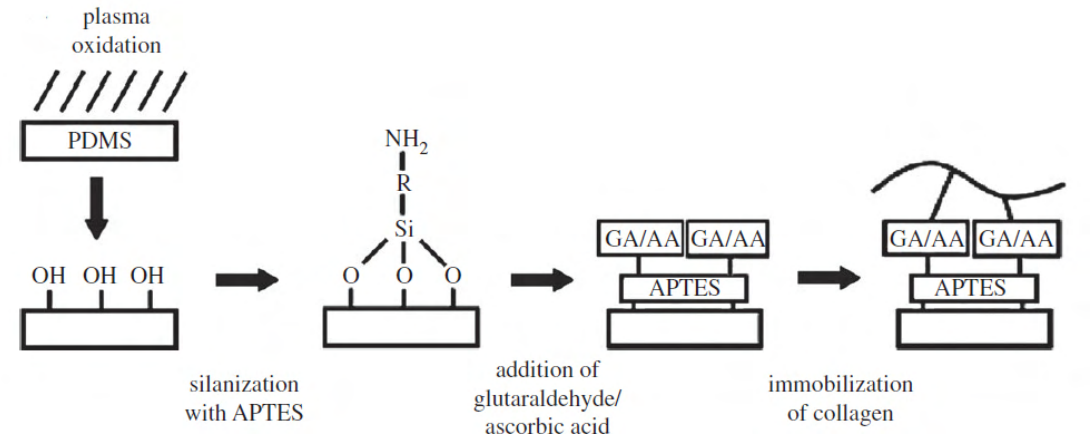

Figure 5.8: Step-by-step process for covalently bonding collagen to PDMS [7]

To make the samples for cell culture tests the porous PDMS membrane was attached to a holder made out of a rectangular PDMS slab with a 3.5 mm hole punched out in the middle. After surface treatment, cells were cultured on these samples and how well they attached to the membrane and grew on it was observed over two weeks. Around 1.33×10^4 cells were seeded per sample resulting in **1.38 ×10^3 cells/mm^2 on a membrane with 4.34 ×10^2 pores/mm^2** . The surface treatment and cell culture procedure along with the results observed for different samples is as follows:

1. **Sample 1**
   Surface Treatment: The sample was treated with air plasma for 15 seconds using ETP BD-20 laboratory corona treater. After this it was dipped in 10 mg/ml fibronectin, 30 $\mu g/ml$ PureCol and 10 $\mu g/ml$ bovine serum albumin (BSA) in PBS.
   Cell Culture: Human PBECs were seeded on the membrane and cultured in KSFM (Thermofisher 17005-034) + P/S (Penicillin/Streptomycin) + epidermal growth factor (EGF) (Thermofisher 17005-075) + BPE (Thermofisher 17005-075) for 13 days.
   Results: After 13 days of culture the cells were **alive but a confluent cell layer was not present**. A reduction in the number of alive cells was observed over time and the number of cells present after 13 days were less than that present after 7 days. This can be attributed to the regain of hydrophobicity of the PDMS surface. After 13 days the cells were fixed, permeabilized and stained using 4′,6-diamidino-2-phenylindole (DAPI) and Phalloidin[3]. DAPI binds to the DNA in the nucleus of the cell and phalliodin binds to the actin filaments, both can be imaged using a confocal microscope to visualize the cells. The membrane was mounted on a glass slide and a cover slip was placed on top. It was then observed under a confocal microscope and the results can be seen in Figure 5.9.

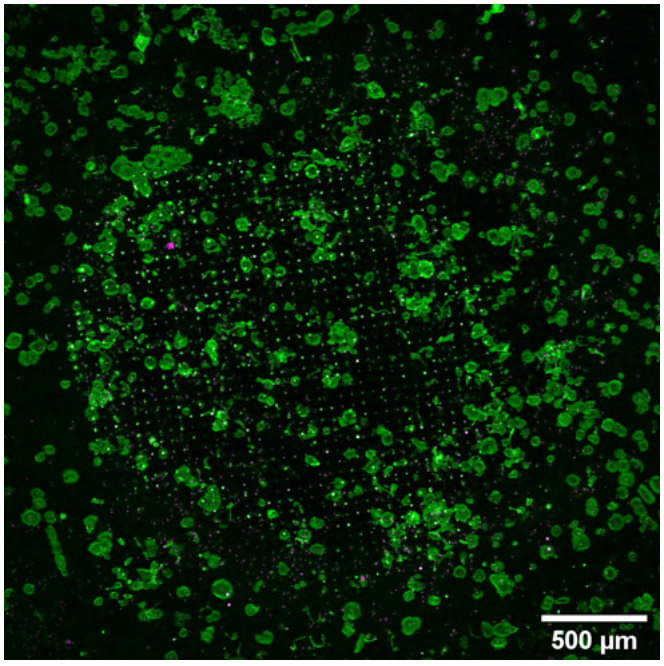

Figure 5.9: Human PBECs on porous PDMS membrane after 13 days of cell culture. DAPI staining can be seen in magenta and phalloidin staining can be seen in green.

2. **Sample 2**
   Surface Treatment: The sample was treated with air plasma for 3 minutes using Diener Femto Plasma System. After this, it was put in 10% APTES solution in ethanol for 1.5 hours. The sample was then washed twice with DI water and then put in ascorbic acid in PBS (200 mg/ml) for 1 hour. After this, it was incubated in 50 $\mu g/ml$ type 1 collagen diluted in 0.01 M acetic acid for 1 hour.
   Cell Culture: Before cell seeding, the sample was stored at 4°C in the collagen for 4 days. Human PBECs were seeded on the membrane and cultured in KSFM (Thermofisher 17005-034) + P/S (Penicillin/Streptomycin) + EGF (Thermofisher 17005-075) + BPE (Thermofisher 17005-075). The cells were exposed to air after 5 days of culture and the culture medium was changed to BEGM .
   Results: After 5 days the cells were found to evenly cover the membrane and a confluent layer of cells was observed after 16 days in culture.

3. **Sample 3**
   Surface Treatment: The sample was treated with air plasma for 15 seconds using ETP BD-20, a hand held laboratory corona treater. After this, it was put in 10% APTES in ethanol solution for 2 minutes. The sample was then washed twice with DI water and then put in ascorbic acid in PBS (200 mg/ml) for 1 hour. After this, it was incubated in 50 $\mu g/ml$ type 1 collagen diluted in 0.01 M acetic acid for 1 hour.
   Cell Culture: Before cell seeding, the sample was stored at 4°C in the collagen for 4 days. Human PBECs were seeded on the membrane and cultured in KSFM (Thermofisher 17005-034) + P/S (Penicillin/Streptomycin) + EGF (Thermofisher 17005-075) + BPE (Thermofisher 17005-075) for 5 days after which the media was replaced by BEGM.
   Results: The cells were found to be alive after 16 days and a confluent cell layer was also observed.

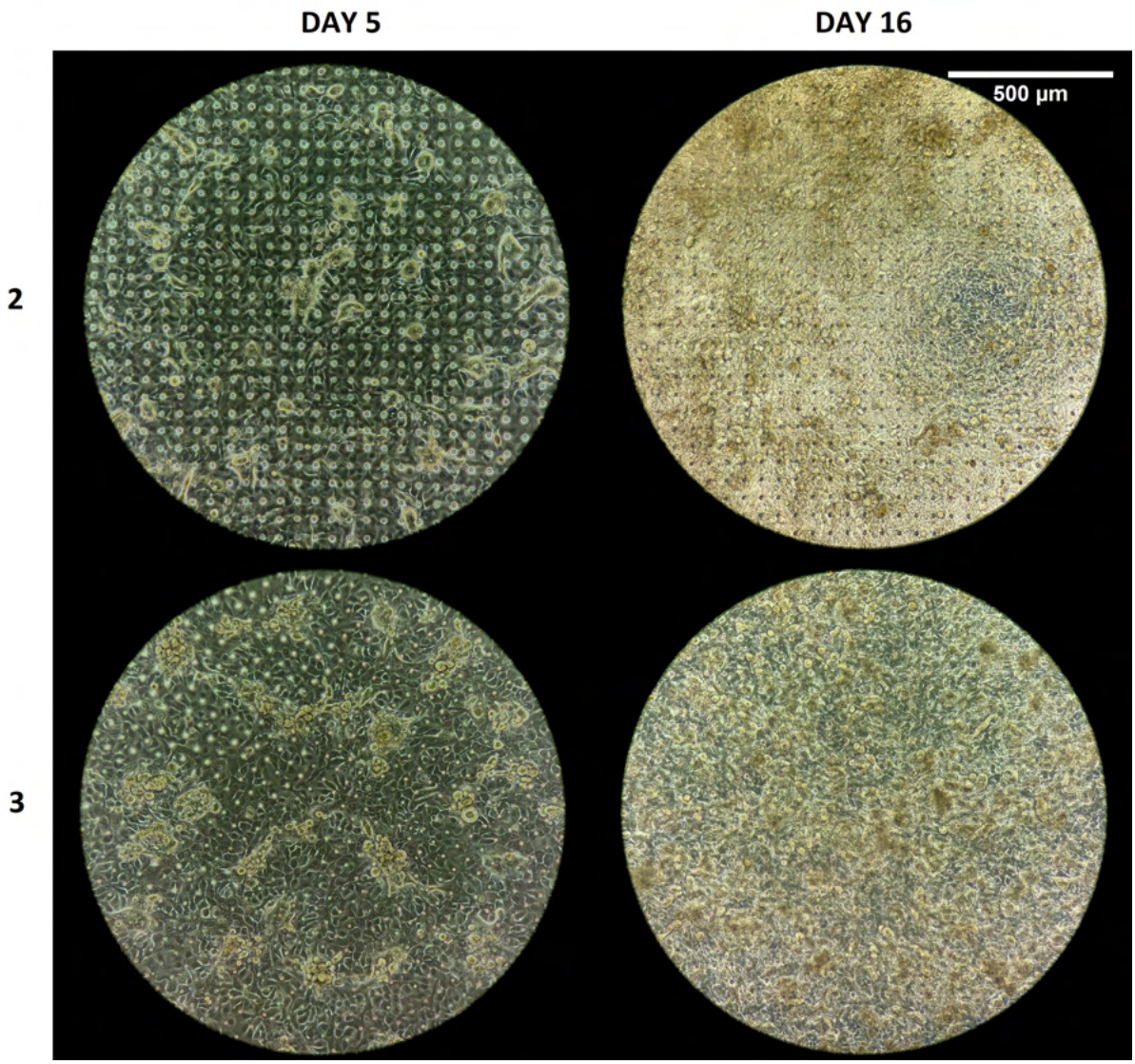

Figure 5.10: Human PBECs cultured on the porous PDMS membrane. Results for sample 2 and 3.

4. **Sample 4**
   Surface Treatment: Same as sample 2.
   Cell Culture: Calu-3 cells were seeded on the membrane and cultured in Dulbecco's Modified Eagle Medium (DMEM) + 10% fetal bovine serum (FBS) + P/S. The cells were exposed to air after 5 days of culture and the culture medium was changed to BEGM.

Results: The cells were found to be alive after 16 days, however, a confluent cell layer was not present. The area covered by cells was less than sample 5, where the cells were kept submerged in media for the whole duration.

5. **Sample 5**
   Surface Treatment: Same as sample 3.
   Cell Culture: Calu-3 cells were seeded on the membrane and cultured in DMEM + 10% FBS + P/S, the medium was changed to BEGM after 5 days.
   Results: The cells were found to be alive after 16 days, however, a confluent cell layer was not present.

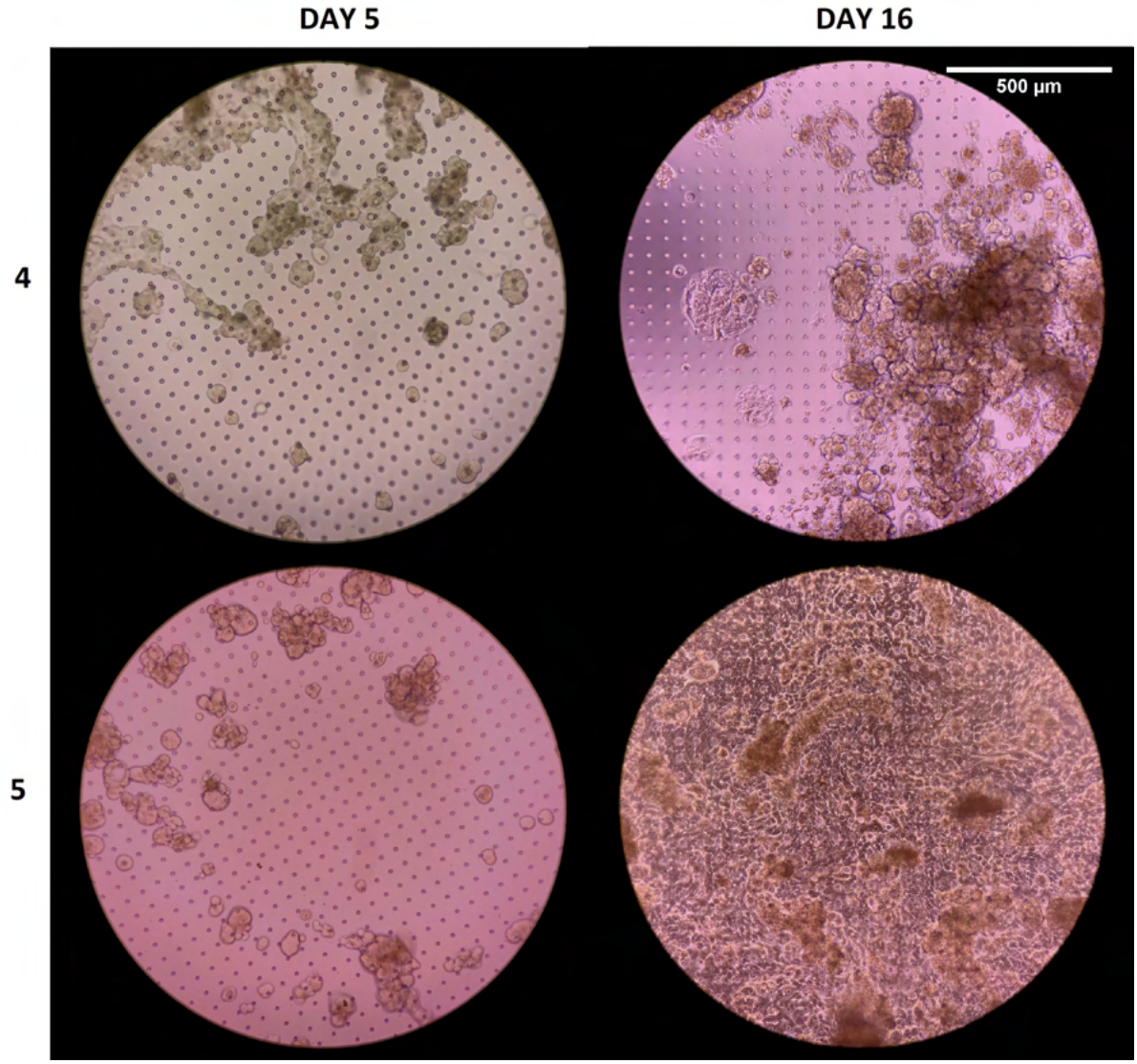

Figure 5.11: Calu-3 cell line cultured on the porous PDMS membrane. Results for sample 4 and 5.

The results for the culture of PBECs are shown in Figure 5.10. The pictures were taken using the 10× plan fluorite phase objective of revolve microscope. Comparing the results for sample 1 with those of sample 2 and 3, where collagen was covalently bonded to the membrane, a confluent cell layer was found in the later samples after two week of culture. For sample 2 and 3 the type of culture media was also changed to differentiation media, BEGM, after 5 days, when the cells were found to fully cover the membrane. The combination of surface treatment and culture media change for the latter samples was found to be **suitable for long term culture of PBECs on the manufactured porous PDMS membrane.**

Figure 5.12: The LOC device placed in the sample holder of the Leica SP5 confocal microscope

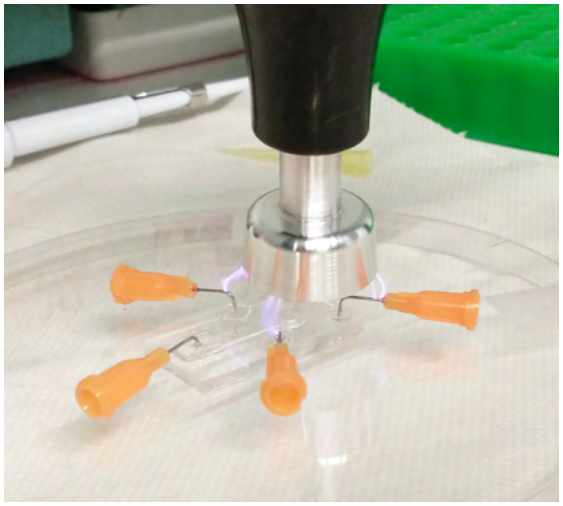

Figure 5.13: Syringe tips interfering with the working of the hand held plasma generator.

The results for the culture of Calu-3 are shown in Figure 5.11 . It should be noted that the images only show a part of the 3.5 mm diameter membrane, the image of sample 5 after 16 days might give the impression that a confluent layer of Calu-3 cells was covering the membrane while in fact there were patches where cells were not present. The reason for absence of a confluent cell layer for Calu-3 cells was discerned to be the low number of cells seeded initially on the membrane. As these cells behave in a different manner than the primary cells more of them should have been seeded on the membrane.

The cells were also left in culture for another week more and then fixed. The cells on the samples 2 and 4 were exposed to air to allow them to differentiate. However, staining did not show any differentiation even though the cells were exposed to air for more than 2 weeks. As there was only one sample with PBECs which was placed at ALI no conclusion can be drawn from it. Images of the full membranes after three weeks in culture for the samples can be seen in the supplementary files, there was some damage to the sample 2 while attaching it to the coverslip.

The cell culture was done at **Erasmus MC** by **K.F. Skarp** and **M.C. Iriondo Martinez**. The procedure for cell culture for the above samples was also provided by them.

5.5. Compatibility with Microscopy

The device needs to be compatible with the confocal microscope to allow for live cell imaging. The device was designed to be compatible with the **HCX PL Fluotar L 40x objective**, with a working distance of 1.9-3.3 mm, connected to the **Leica SP5**. To test the compatibility, the porous membrane in the LOC device was observed using the confocal microscope and a bright-field image was taken by a phone camera through the eyepiece. Two different coverslips, one with no step and other with 1.2 mm step were used to seal the channel while taking the images. The device was found to be compatible with the confocal microscope, as it was possible to focus on the membrane with both the coverslips. The device also fit the sample holder of the confocal microscope and was easy to place in the space for the samples, as seen in Figure 5.12. In Figure 5.9 it can also be seen that apart from some retention of the cell staining dyes in the pores, the membrane itself has **low autofluorescence** and it is possible to image the stained cells.

5.6. Device Usage

In this section some suggestions about how to use the LOC device are included. Learnings from trials to set up the chip have also been included.

Sterilization
It is essential to sterilize the device before use. The recommended method is to use **70% ethanol**, as it does not change the mechanical properties of the PDMS. Methods which involve heating up the device, like boiling and autoclaving, lead to stiffening of the PDMS [40, 84]. Autoclaving could be used, however, it will reduce the maximum strain that the actuator can subject the membrane to. Using UV or gamma radiation to sterilize the device is another option that does not change the mechanical properties of the PDMS. UV light can also been used to sterilize PDMS with collagen covalently bonded to it [77].

Cell Culture
The volume of the apical and basal chamber is **8.5** μl. It is necessary to ensure that the volume of the chemicals for pre-treatment pipetted on the membrane does not exceed this volume. If the liquid volume is more than that, then it is observed to flow into the channel due to capillary action. Similarly, the volume of the culture media with cells also needs to be equal or less than the chamber volume. Only after the cells have attached to the membrane, should the whole channel be filled with culture media and only after a confluent layer of cells has been achieved the culture media should be flown in the channel. The endothelial cells are to be seeded first and after they have attached to the membrane the device can be flipped to seed the epithelial cells.

During trials it was observed that the hand held plasma generator did not work well with the assembled device as the syringe tips interfered with the generation of plasma, as can be seen in Figure 5.13. No such effect was seen in the Diener Femto Plasma System and such a system would be suitable for plasma activation of the membrane.

Culture Media Flow
After the cells have attached to the membrane, the cover slip with the step should be used to seal the channel. For initial filling up of the channel, culture media should be slowly, at a flow rate 0.1 ml/min or lower, flown into the channel. This is important for allowing all the air to be pushed out and for no bubbles to be trapped in the basal chamber.

In trials it was found that it was very difficult to clean the glass surface of the device enough, with the cell layer present on the membrane, to fully bond the coverslips on to it. This resulted in the culture media leaking out of the basal chamber and points out the need for an external holder or gluing the coverslips on to the glass layers once the cells have been seeded.

A list of anticipated failure modes of the device, based on the various trials that were carried out, was made. See Appendix J for the list of failure modes and steps to prevent them.

5.7. Chapter Summary

The device was tested to check how well it satisfied the set requirements, and, if needed, the manufacturing process was modified to make the device satisfy the requirements. The pneumatic actuator was tested by applying cyclic negative pressure and the linear strain that it imparted to the membrane was measured. Based on the test results, it was decided that for making the actuator half layers the PDMS prepolymer, with **base polymer to resin ratio 10:1**, would be cured at **room temperature for 48 hours**. The tests showed that bonding using uncured PDMS was more suited than plasma bonding for assembling the actuator. Based on the test results that revealed that for a 1 mm height the linear strain on the membrane for -700 mbar was 10% and this increased to the desired value of **20% by increasing the actuator wall height to 1.4 mm**. Thus the actuator wall height was set to 1.4 mm. Stiffening of the actuator post curing, due to being subjected to high temperatures, was noted. Based on that it was decided to plasma bond the channels above and below the actuator instead bonding them by heating under pressure.

The culture media can be flown in the basal chamber using equipment like pressure driven flow controllers, syringe pumps, peristaltic pumps or even by placing a reservoir connected to the channel at a height. The device was tested by **flowing tinted water** through the lower channel using a syringe pump. A peristaltic pump was used to recirculate tinted water through the channel. These tests pointed out that the removable coverslip was successful in sealing the channel when the liquid was withdrawn from the channel and detached when liquid was injected into the channel.

Pressure driven flow, where the pressure at the inlet and outlet of the channel is set to make the pressure in the basal chamber equal to the pressure in the apical chamber, ensures that there is **no out of plane deflection of the cell culture membrane**. For any other method of generating flow in the channel, there will be some out of plane deflection of the membrane. This deflection was measured using white light interferometry. For a basal chamber height of 0.8 mm, the deflection of the membrane was found to be **0.443 mm** into the channel for water being flown at a rate of **2.6 ml/min** by a syringe pump in withdrawal mode.

Human PBECs were cultured on the porous PDMS membrane to determine the suitability of the manufactured membrane for **long term cell culture**. Surface treatment is required to make the PDMS surface hydrophilic so that the cells attach to it. Surface treatment methods such as plasma treating the PDMS surface, that make it hydrophilic temporarily, were found to be unsuitable for long term culture. **Covalently bonding collagen to the PDMS surface** is the recommended surface treatment method, as this resulted in a confluent cell layer after 16 days in culture.

For sterilizing the chip, using 70% ethanol or UV light is recommended over methods such as boiling and autoclaving, which involve heating the device to a high temperature. To set up the chip it is recommended that, after surface treatment of the membrane, the endothelial cells should be seeded first and once they have attached the chip can be flipped to seed the epithelial cells. The resealable coverslips, by themselves, were found to be an inadequate solution for sealing the channels of a chip. This is because the bond between glass and PDMS is sensitive to any impurity present on the surface and it is difficult to ensure impurity free surfaces while the device is in use. Therefore, **holding the coverslip in place with the help of a cell culture compatible glue or an external holder is required**.

6

Conclusion and Future Scope

In this work a LOC device was designed, manufactured and tested. The LOC device provides an environment, which mimics the in vivo environment, in which cells can be cultured to recreate the alveolar-capillary barrier in vitro. This includes cyclic stretching of the porous membrane, on which the cells are cultured, to replicate breathing strains and culture media flow, which provides the required shear stress to the endothelial cells, to replicate blood flow in the capillaries. In comparison to the state-of-the-art LOC devices, which compromise one of these two aspects to fulfill the other, the device strikes a **balance between recreating breathing strains and recreating shear stress due to blood flow**. It stretches the cultured membrane bi-axially, resulting in linear strain and surface area strain values equal to the observed in vivo values. And at the same time it provides the required shear stress to the endothelial cells without any significant variation in the shear stress value, from the desired value, for all the cells.

The porous membrane for ALI cell culture is 10 μm thin, a value comparable to the membrane thickness of commercially available LOC devices [34, 47]. The device includes a pneumatic actuator that cyclically stretches the cells at 0.2 Hz to provide a maximum liner strain of 20% for -700 mbar pressure. A shear stress of 0.55 Pa on the lower surface of the membrane, where the endothelial cells are to be cultured, is provided by culture media flowing at 2.6 ml/min in the basal chamber with height 400 μm.

Culture media could be flown in the basal chamber using pressure driven flow controllers to mitigate out of plane deflection of the membrane. Devices such as peristaltic pumps, which can be used to set up a loop for recirculating the culture media through the basal chamber, can also be used at the cost of loss of uniformity of shear stress on the endothelial cells. These also result in some out of plane deflection of the membrane that provides an undesirable permanent strain, on top of the cyclic breathing strain, on the membrane .

The device allows the user to access the cell culture membrane directly, which makes it possible to seed the cells onto the membrane by directly pipetting them and to retrieve the cells after an experiment. Unlike the OOC devices which require using tubes to seed the cells in the chip, resulting in loss of cells that are left in the tubing, there is no loss of cells. Live imaging of the cells cultured in this device is possible, as it is compatible with confocal microscopy. This makes the device user friendly and well suited for cell culture experiments .

Future Scope:
A **holder** that keeps the coverslip in place to ensure that the channels are sealed, with no leaks present, needs to be designed. The holder should also include connectors eliminating the need for attaching syringe tips to each chip. Designing a holder also provides the opportunity to combine the channels and coverslips. For this, the glass layers on either side of the actuator need to be bonded to it. The PDMS layers, with the recess for the channel, bonded to the top and bottom glass layers without central access hole, would be aligned and held tight against the other glass layers with the help of the holder. This would also allow making the top and bottom glass layers out of thicker glass coverslips, $\sim$ 400

μm, which are less prone to breakage in comparison to the 1.5 H coverslips.

A device with the LOC device as a unit that is repeated in an array, on the lines of a culture well plate, would be suited for most biological experiments which require setting up multiple ALI models simultaneously. Appropriate layout needs to be designed for the connections for vacuum and media flow to ensure that all the units of the the array are functional as stand alone LOCs, and no unit should have undesired influence on the results of the neighbouring units.

The device could be manufactured using materials that are more suited for cell culture applications than PDMS. The pneumatic actuator could be made out of SEBS by **hot embossing or injection moulding**. The channels could be made out of medical grade elastomers [71] or hot embossed into COC or PC. This shift from PDMS to polymers such as SEBS and COC will also help in making the device suitable for large scale production as injection moulding and hot embossing these polymers is possible.

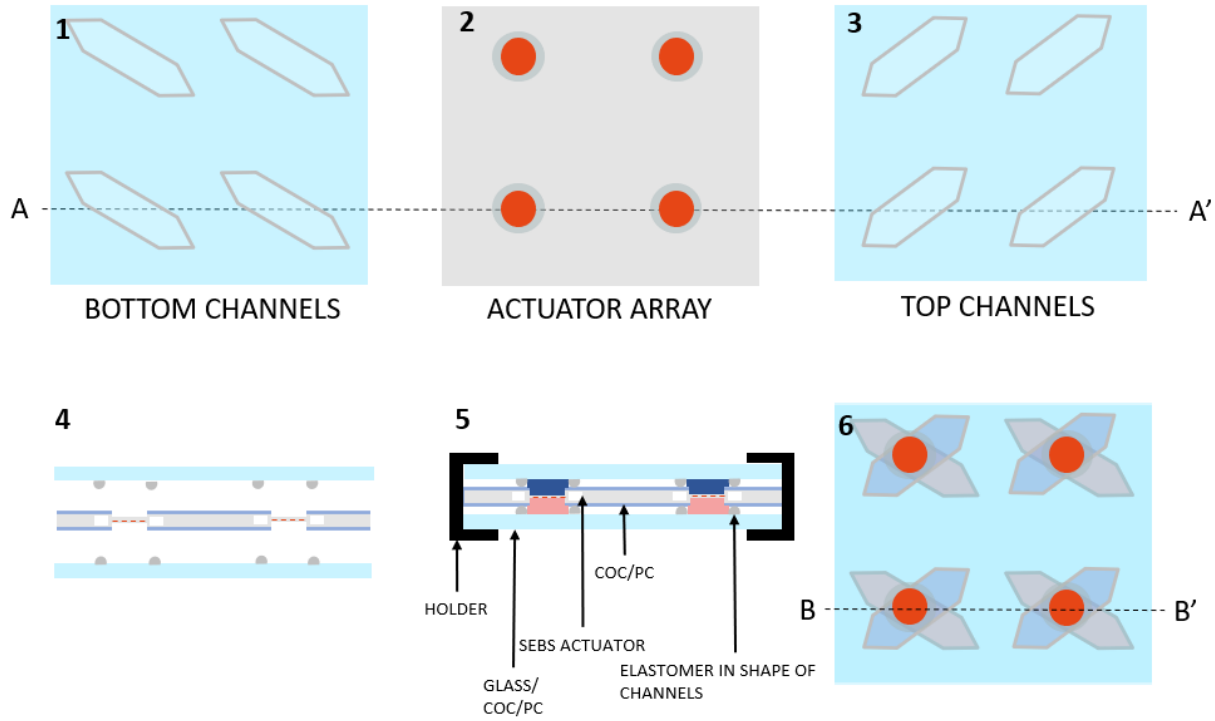

(1) Array of bottom channels (2) Array of actuators with membranes (3) Array of top channels (4) AA' section view of the three layers stacked on top of each other. (5) BB' section view of the assembled array plate 6.The top and bottom channels are drawn using an elastomer [71] on a glass/COC/PC layer. The actuator is made of SEBS and permanently bonded to a layer of COC/PC. A holder holds the three layers together. (6) The assembled array, the elastomer channels are held against the COC/PC layer of the actuator by the holder. This seals the channels.

Note: The connections to the flow channels and the vacuum channels are not depicted in the image. The image is not to scale.

Figure 6.1: Concept of culture plate with 2 × 2 array of the LOC device

Sensors for measuring the TEER, pH, O_2 concentration, CO_2 concentration and temperature would increase the information that can be obtained from cell culture experiments. The device has been designed keeping in mind the integration of such sensors into the device in future A.4. Optical sensing is suggested for measuring the pH, O_2 concentration and CO_2 concentration and no change in the device manufacturing process needs to be made for this. On the other hand, for TEER measurement metal electrodes need to be included in the device while it is being manufactured and similarly for temperature measurement there is a need to include the sensors in the manufacturing stage.

All these improvements can be combined to make an array plate, like the one shown in Figure 6.1, out of materials such as SEBS and COC, with integrated sensors and a holder which aids in making connections to the plate.

Appendices

A

Literature Review

A.1. Lungs

The lung is the organ responsible for gas exchange. Gas exchange takes place in the alveoli. The alveolar region comprises of over 90% of lung volume [74]. The rest is made up of the conducting airways which branch over several generations. The **tracheobronchial tree**, as shown in the Figure A.1, begins with the trachea, named generation 0, divides into two bronchi, one for each lung, which further divide into progressively smaller bronchioles till they end in the alveoli at the generations 10 through 23 [42]. The first 15 generations provide the conducting airways, the bronchi and the bronchioles, while the last 8 generations contain the gas exchanging units, the acini [118]. The respiratory zone makes up most of the lung surface area.

	Generation		Diameter, cm	Length, cm	Number	Total cross sectional area, cm^2
Conducting zone	Trachea	0	1.80	12.0	1	2.54
	Bronchi	1	1.22	4.8	2	2.33
		2	0.83	1.9	4	2.13
		3	0.56	0.8	8	2.00
	Bronchioles	4	0.45	1.3	16	2.48
		5 ↓	0.35 ↓	1.07 ↓	32 ↓	3.11 ↓
	Terminal bronchioles	16	0.06	0.17	6×10^4	180.0
Transitional and respiratory zones	Respiratory bronchioles	17	↓	↓	↓	↓
		18				
		19	0.05	0.10	5×10^5	10^3
	Alveolar ducts	T_3 20	↓	↓	↓	↓
		T_2 21				
		T_1 22				
	Alveolar sacs	T 23	0.04	0.05	8×10^6	10^4

Figure A.1: Tracheobronchial Tree [56]

Blind ended functional units containing clusters of alveoli are called acini and there are 30,000 acini [119] in the lung containing a total of 480 million alveoli [117] in a human lung [74]. The alveolar surfaces have a network of capillaries running around them. Blood flows through these capillaries and the O_2 and CO_2 exchange happens here as shown in Figure A.2.

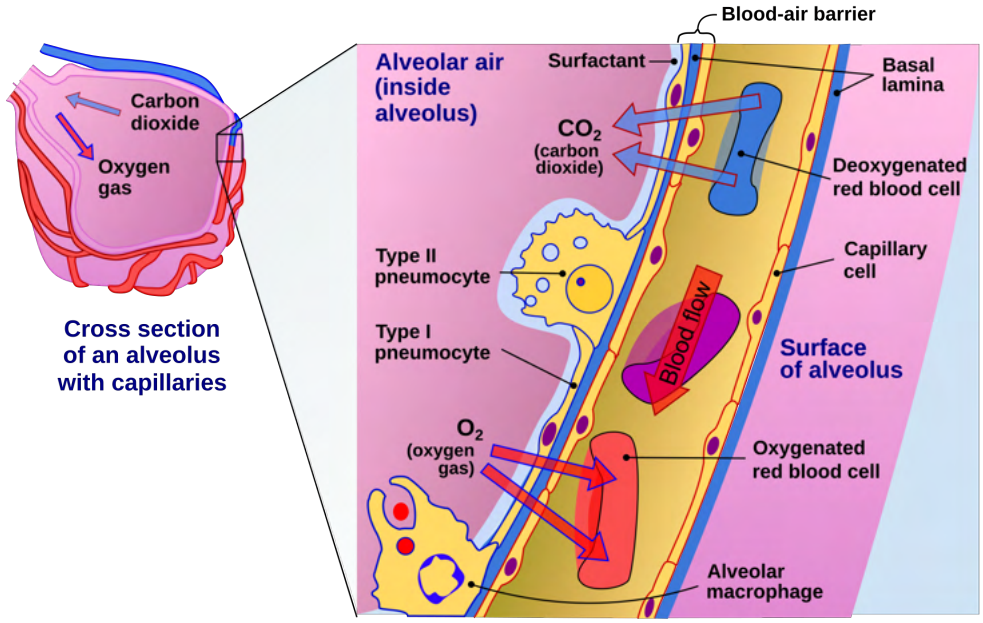

Figure A.2: Gas exchange [5]

The inter-alveolar septum, as shown in Figure A.3, allows contact between the alveolar airspace and the capillary lumen and provides the surface for gas exchange. It is designed to provide a **large surface area (140 m^2)** and **thin diffusion barrier (2 μm)** for efficient gas exchange [74]. The **blood-gas barrier** is comprised of three layers- the alveolar epithelial layer, the interstitial layer and the endothelial layer of the capillaries. The **alveolar epithelium** is made up of type I alveolar epithelial cells, which cover 95% of the alveolar area, and the type II alveolar epithelial cells. The type II cells are responsible for surfactant secretion and repair and renewal of the epithelial layer. The mechanical stretch of type II epithelial cells stimulates changes in surfactant secretion, cell injury or death, permeability and cell migration [94]. A single alveolus has about 47 type I cells and 97 type II cells and an average surface area of 220,000 μm^2, each type I cells covers approximately 5098 μm^2 and each type II cell covers 100 μm^2. Alveolar macrophages, 57 per alveolus, may be attached to the epithelial surface and capture foreign material present on the alveolar surface to maintain sterility [118]. The diameter of an alveolus varies from 100μm to 300 μm and accordingly the number of cells are proportional to the diameter [98].

The interstitial space consists of **ECM**, which provides structural support to the cells. The embedded fibroblasts are the most abundant cells present, 210 per alveolus, and they produce and maintain the ECM. The extracellular network of fibers, making up the basement membrane, consist of elastin fibers and collagen fibers. These fibers transmit the distending forces, generated by the pressure difference between the acinar airspace and pleural cavity, to the interior of the lung. Elastin fibers have a linear stress-stain relationship till over 200% strain and thus provide elastic recoil to allow the alveolus to return to its original shape. Collagen fibers form meandering structures at low volume and become straight at higher volumes, after which they follow a highly non-linear stress-strain relationship on further increasing the strain. The blood-gas barrier has thick sections, where the cell nuclei and the fiber network for structural support are, and thin sections, **less than 1 μm in thickness** and covering half of the blood-gas barrier surface. The thin sections have a common basal lamina separating the epithelial and endothelial layers. Each alveolus has about 170 **endothelial cells** with each cell covering 1350 μm^2. Capillary tubes are within 6 μm in diameter and 8 μm long and generally two endothelial cells line it. In an adult lung a single capillary layer is spread over the alveolar surfaces on the two sides of the alveolar-septa [74, 118]. The endothelial cells are subjected to shear stress due to blood flow,

which is $9.55 N/m^2$ for the thinnest capillaries [75].

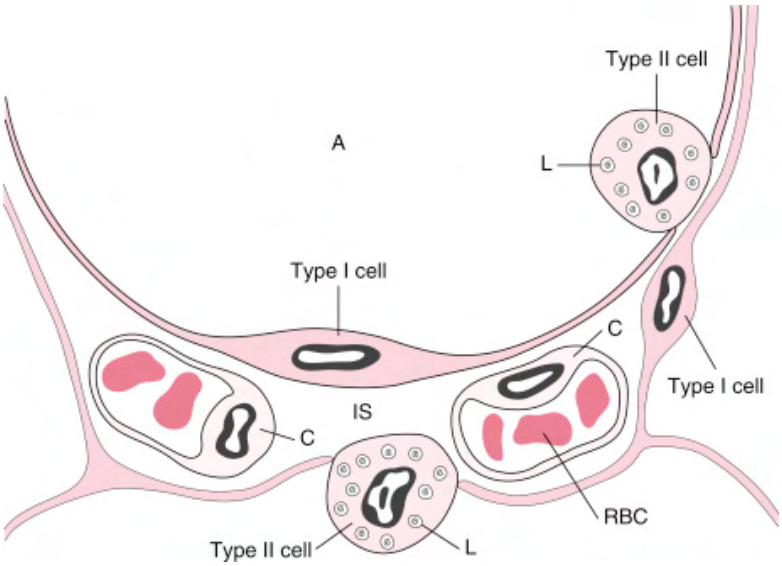

Figure A.3: Inter-alveolar septa with the type I and type II epithelial cells. Capillaries (C) with red blood cells (RBC) are also shown. A, alveolar surface; IS, interstitial space; L, lamellar body, source of surfactant.[120]

Breathing mechanisms

The distal airspaces are subjected to volume changes during a breathing cycle. The deformation is described in terms of strain, size of a structure after deformation in relation to the baseline size. The functional residual volume is taken to be the baseline volume for the lungs. This volume consists of stale air, which mixes with fresh air inhaled in each breathing cycle. The strain in alveoli is usually stated for the length, instead of area and volume. In general the strain fields in tissues are considered to be nonuniform. During tidal breathing, between 40% and 80% of the total lung capacity (TLC), the one dimensional strain is 4% to 10% and can also increase to 20% for deep sighs or exercise [74]. The TLC is defined as the volume at maximal inspiratory effort [94]. The breathing frequency is 0.2 Hz at rest, which corresponds to 12 breaths per minute [62].

The difference between the pressure levels in the alveolus and in the pleural space is known as the transpulmonary pressure ($P_T = P_{ALV} - P_{PL}$). This determines the lung volume, as the pressure in the pleural cavity falls due to the contraction of the diaphragm this causes an increase in P_T and causes the lungs to expand. For a healthy lung P_{ALV} is the same for all the alveoli and the only pressure difference occurs at the pleural surface. Thus the distension forces due to P_T are transmitted throughout the lungs by tissue attachments and not due to pressure difference between the alveoli [94]. The lungs contract due to natural elastic recoil of the lung and the chest wall for normal breathing and the contraction can be accelerated by contraction of abdominal muscles for heavier breathing [64]. The surfactant causes a reduction in surface tension with air expiration to impart stability to the alveolus [74]. The presence of hysteresis in the pressure-volume relation of the alveoli is also due to the surfactant [94]. Gil et al.[59] proposed **four mechanisms** for the lung volume change due to alveoli:

1. Recruitment and derecruitment of alveoli
2. Balloon-like isotropic stretching and destretching
3. Alveolar shape change along with volume change
4. Folding and unfolding of alveolar walls like an accordion

Recruitment of alveoli occurs when collapsed or fluid filled alveoli are filled with air, this results in significant volume increase. Derecruitment is the opposite and refers to the collapse of the alveolus. During normal breathing the lung volume does not fall below the functional residual volume and thus the derecruitment/recruitment of alveoli has not been observed in vivo in healthy lungs. Till the volume filled by gas is 80% of the TLC the alveolar volume increases by folding/unfloding of septal walls, and

then by alveolar shape change. At higher lung volumes up to 100% TLC is the stretching of the basal layer of the inter-alveolar septa encountered was dominant [74]. During normal breathing the lung volume is not low enough for folding and unfolding of septal walls and thus in vivo volume change of the alveoli can be considered as a combination of stretching and destretching and shape change [94]. These mechanisms for deflation are shown against the pressure-volume curve shown in Figure A.4.

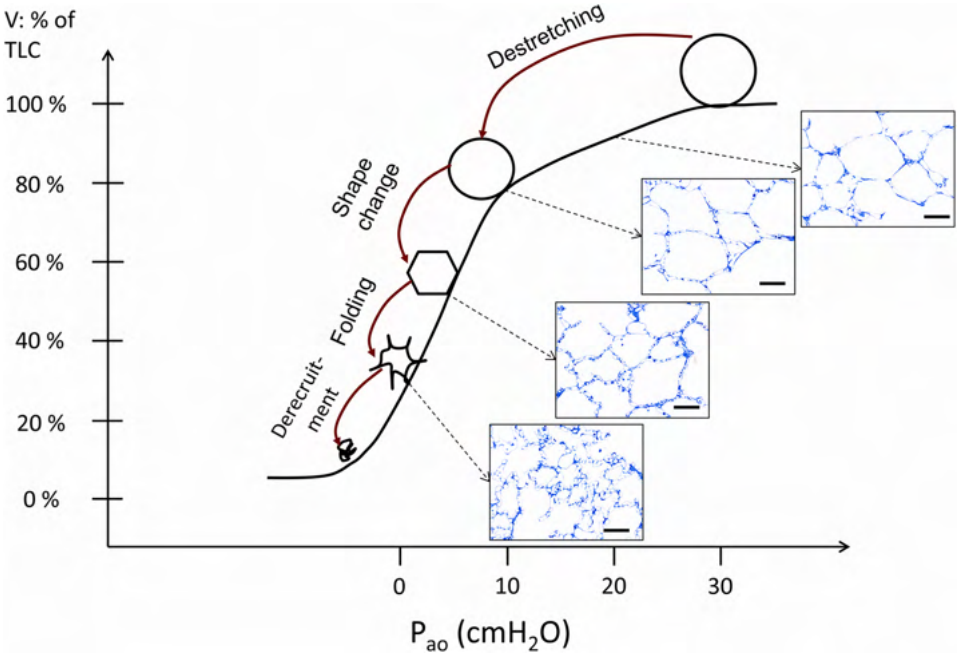

Figure A.4: Micromechanisms for alveolar volume change during deflation shown against the pressure-volume curve of the alveolus. Scale bar $50\mu m$[74]

A.2. In vitro models of the lung

In vitro models of the lung find applications in **physiological studies, disease modelling and toxicology studies**. They also play a critical part in **drug development** and are used to test drug efficacy and drug toxicity. Such models can be designed to recreate the complexity of human physiology and have some advantages over the animal models used for drug testing, which show interspecies variations and are associated with ethical issues. These models can help to detect drug toxicity or insufficient efficacy at an earlier stage, than the high-cost large-scale animal and human testing, and this provides a major economic drive for improving in vitro lung models so that they closely mimic the in vivo environment. These models are also used to study lung injury and repair mechanisms along with the reaction of lungs to toxins and allergens [98, 103].

Planar static culture systems are the most common models and include cell monolayers in **culture dishes, flasks and wells**, as shown in Figure A.5. The main difference between them is limited to shape and the culture surface is similar. The surfaces are specially treated to control cell adhesion and may be coated to simulate the ECM. Culture dishes and flasks are usually made of **borosilicate glass or clear plastics like PS or PC** which allow the cells to be observed under a microscope [1]. Culture wells are structured in an array on to culture plates with one plate containing 4-1536 wells on a plate. These plates are made of PS which can be clear to aid microscopic observation, white to aid luminescent assays or black to aid fluorescent assays [1, 14, 97]. These models lack the 3D micro-architecture of the ECM, the mechanical strain the cells are subjected to and the interaction of different cell types as in the body. The culture media is also stagnant and fails to replicate the continuous blood flow [103]. Culture plates are the most popular type of in vitro modelling devices as they provide an option for low cost, highly automated, high throughput testing. The other models still lack those aspects, making them the suitable option for fast large scale screening of therapeutics.

(a) Culture Dish (b) Culture Flask (c) Culture Well Plate

Figure A.5: 2D static cell culture platforms

Cell culture **inserts** have porous membranes and can be hanged in culture wells to allow for cell culture on both the sides of the membrane and to have different media on either side. The porous membrane is usually made of PC, polyethylene terephthalate (PET), PTFE or polyester [1][14]. The pore density and pore size is selected according to the application. To model an **alveolar-capillary barrier**, human lung epithelial cell lines are seeded on top of a PC membrane insert, and primary human pulmonary microvascular endothelial cells are seeded on the bottom, the membrane can be coated to mimic the ECM. This coating, however, lacks the dynamics and physiology of connective tissue. Afterwards the culture media is removed from the top side of the membrane to establish the air-liquid barrier [65]. A diagram of the co-culture can be seen in Figure A.6. The epithelial airway was modeled by co-culturing epithelial cells along with macrophages on one side and dendritic cells on the other side of the insert [95]. Similarly the complexity can be increased by including more cells to mimic the in vivo environment, however, there is still absence of perfusion/flow of media, 3D ECM and mechanical cues.

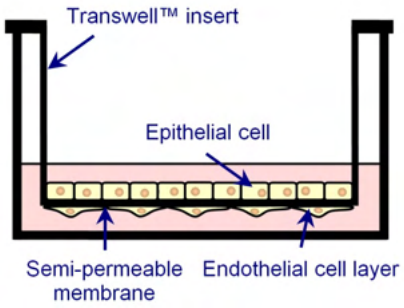

Figure A.6: Alveolar-Capillary barrier modeled on an insert [27]

Incorporating dynamic flow of gas and media to the culture insert systems will allow for closer mimicking of in vivo environment. This has been realized, for instance, by including fluidics by React4life in their MIVO® systems, as shown in Figure A.7. The double flow system allows subjecting the pulmonary air-liquid interface to dynamic flow of aerosols and gases. Noncommercial models with fluidics have also been demonstrated in an attempt to replicate the in vivo behaviour more accurately [37].

Organoids are in vitro models which aim to recreate the 3D structure in which the cells can be co-cultured. They usually lack the media circulation, air-liquid interface, and mechanical cues [103]. **3D scaffolds** for cell culture can be made artificially or by decellularizing tissue. Providing dynamic flow to such systems has also been attempted for repopulation of the ECM by human induced pluripotent stem cells (iPS)–derived alveolar epithelium [58]. Although lung organoids are an expanding field of research, they will not be discussed in detail here as they are not the focus of the review.

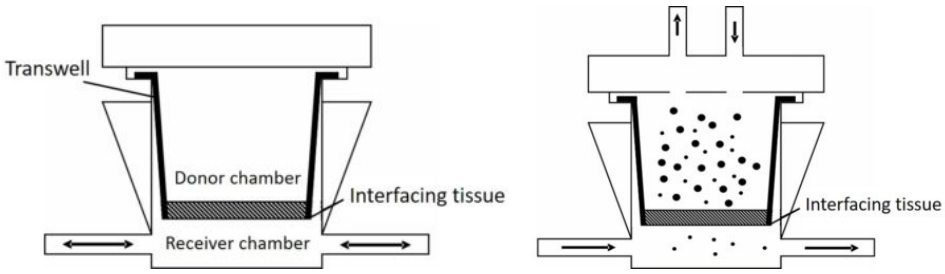

(a) Mivo® Single Flow (b) Mivo® Double Flow

Figure A.7: MIVO® in vitro fluidic multi-chamber

Lung-on-a-chip devices provide an environment which replicates the in vivo dimensions and structure for the 3D cell culture, incorporates the mechanical cues and the continuously flowing media in place of blood flow. LOC models aim to overcome many of the shortcomings of the in vitro models described in the preceding section. The LOC models have several advantages over the other in vitro models and the animal testing models. They provide an environment that replicates the in vivo cellular environment closely and thus the cell behavior is similar to that it would have been in the body. Co-culture of different types of cells is possible. The models use human cells and thus the results obtained through them could be closer to reality than animal models. The animal models recreate the total body physiology, a feature that the OOC models still lack. The amount of cells required and the media consumed is less in comparison to other in vitro devices due to the micro scale of the cell culture area. The equipment and skills required to operate OOC devices are still not available in many labs and LOC devices are still not produced at a large scale. This has limited their large scale use for in vitro modelling. A comparison of in vitro lung models is presented in Table A.1.

Table A.1: Comparison of in vitro models of the lung

	Air-Liquid Interface	**Mimicking ECM**	**Media Flow**	**Breathing Strain**
Culture Dishes, Flasks and Wells	-	(+)	-	-
Culture Inserts	++	+	(+)	-
Organoids	-	++	(+)	-
Lung-on-a-chip	++	+	++	++

Key: - : Not present, +: Present but in a limited fashion, ++: Well Present, (+): Possible in a limited way

A.3. State-of-the-art

For this review all the LOC devices in literature were studied. The layout and mechanism of these devices was focused up on. The materials used in the devices, along with the manufacturing techniques, were also studied. The devices that were chosen for the study either fulfilled all or most of the specifications of LOC devices. Similar aspects of commercial LOC devices were studied. The aim was to get a complete understanding of the different approaches for designing LOC devices.

A.3.1. Lung-on-a-Chip devices in literature

Lung-on-a-chip (LOC) models incorporate microfluidics for continuous perfusion to mimic **blood flow** [36, 47, 66, 91, 99, 102, 124], cyclic mechanical strain to mimic **breathing motion** [47, 50, 54, 66, 107, 108, 123], a porous membrane to mimic the basal lamina for cell culture and allow for the co-culture of various cells present in the lung. This makes LOC the in vitro model that most closely replicates the breathing human lung. While porous polymer membranes made of PDMS [47, 66, 107], PET [36, 87, 99, 111], PTFE [99] and PC [101] have been commonly used for cell culture in LOC models, more sophisticated membranes and surfaces that **replicate the ECM** better have also been demonstrated. A PGLA nanofiber membrane [122] replicated the thin blood-gas barrier dimensions. Biological surfaces for cell culture include membranes and barriers made with a

gel of different combinations of collagen, elastin and Matrigel. This biological ECM replicating surface can be made by injecting the gel in passages [69, 87, 124], pipetting the gel onto a gold mesh with holes with alveolus comparable dimensions [123] or by making a lumen using a temporary mould around which the gel is set [33]. Incorporation of fibroblasts for the purpose of recreating the functional aspects on top of the structural aspects of the ECM has also been demonstrated [33, 87, 91, 99, 122]. Thus, LOC models can be seen to replicate the in vivo structural dimensions and ECM properties in a better way than other in vitro models.

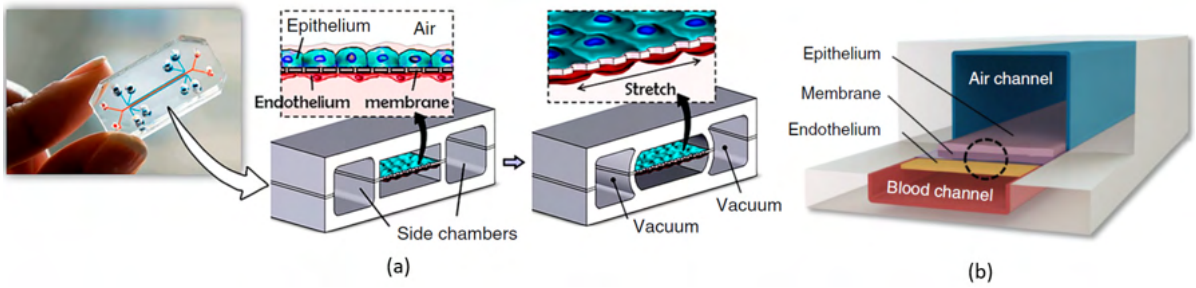

Figure A.8: (a) A LOC device with vacuum channels to create cyclic strain. [67] (b) A LOC device with the blood-gas barrier. [35]

LOC devices are being steadily adopted for a number of applications like physiological studies, toxicological studies, disease modelling and drug testing. By incorporating cyclic strain the LOC models were shown to replicate the metabolic activity and cytokine secreation [47, 66, 107] as present in vivo. This was used to demonstrate the inflammatory response to nanoparticles [47]. Hou et al.[66] studied the effect of cigarette smoke extract on the epithelial cells and their malignant transformation in a self made chip using an alveolus-on-a-chip with breathing strain. The effect of breathing strain on epithelial wound healing has also been studied [52].

Benam et al. demonstrated an airway-on-a-chip that was used to model lung inflammation, due to COPD, and to study drug responses [36]. The same device was also used to model normal and COPD airways and then study the effect of exposing them to cigarette smoke [34]. Shreshta et al.[101] demonstrated airway-on-a-chip device and used it to study the effects of cigarette smoke extract CSE on the airway. Xu et al.[121] studied the effect of PM 2.5 on the lungs by using a LOC with matrigel filled passage as the barrier between epithelial cell and endothelial cell layers and found increased permeability of the blood-gas-barrier and inflammation.

Lung diseases and infections are modeled using LOC and drug efficacy can be tested using them. Bacterial infection caused by E. Coli [47] was modeled and the phagocytic effect of neutrophils, recruited from the media flowing on the other side of the barrier, was demonstrated. Deinhardt-Emmer et al.[45] used a commercial multi-organ tissue flow chips to infect the lung cells with a bacterial infection, a viral infection, as well as, a co-infection and studied the effect of the infections on the air-liquid barrier in the presence of macrophages. The barrier integrity was found to be most impaired in case of a co-infection also resulting in the highest immune response. Lung-tumour-on-a-chip was used to evaluate an tumour drug Gefitinib [122].

Co-culture of different types of cells is essential in replicating the lung response accurately. Mejias et al.[87] demonstrated an airway-on-a-chip device with a vasculature layer with endothelial cells and fibroblasts cultured on it, which allowed the study of fibroblast-epithelial interaction. It was used for pathophysiological studies like to model cancer and cystic fibrosis and neutrophil recruitment. Sellgren et al.[99] demonstrated an airway-on-a-chip with triple co-culture of airway epithelial cells, fibroblasts and endothelial cells. Punde et al.[91] demonstrated an airway chip with a co-culture of epithelial cells, fibroblasts and endothelial cells and used it to study protein induced lung inflammation. Humayun et al.[69] made a chip with a hydrogel layer supporting epithelial cells on the top side and smooth muscle cells on the bottom side. This chip was used to study the interaction of the two types of cells as this determines the behaviour of large and medium airways.

Monoculture chips, even though lacking the blood-gas barrier, can be used for a number of studies

like injury inflicted to the epithelial cell layer due to air plug propagation and rupture [68], epithelial cell damage due to fluid and solid mechanical stresses during mechanical ventilation [50] and studying cytotoxicity of cancer drugs [71]. The presence of mechanical cues due to strain and fluid flow make them superior to the 2D static monoculture culture models. Microfluidic chips with anatomically inspired geometry and scale, recreating the anicus in vitro, have been used to culture epithelial cells for studying pulmonary alveolar physiology and anicar flows, including aerosol particle dynamics and deposition, during fetal lung development, as well as, in adults [54, 55, 110, 111]. A summary of the state-of-the-art LOC models, along with the images, is presented in Appendix B.

A.3.2. Cell types used for culture

The cells cultured in vitro can be classified into three types:

1. **Human Primary Cells:** These types of cells are derived directly from parent tissue. Individual cells are extracted from the tissue, using certain enzymes, and then divided to get the desired number of cells. These include cells like primary human pulmonary alveolar epithelial cells (pH-PAEC) [47, 107, 123], primary human bronchial epithelial cells (pHBEC) [33], primary human tracheo-bronchial epithelial cells (AE) [99], primary human airway epithelial cells (hAECs) [36], primary human umbilical vein endothelial cells (HUVECs) [107], primary human lung fibroblasts [99], primary human lung microvascular endothelial cells (MvE) [36, 99] and human bronchial smooth muscle cells (hBSMCs) [70]. These cells retain more of the in vivo cell characteristics in comparison to immortalized cell lines, but have a limited lifespan.
2. **Immortalized Cell Lines:** These types of cells are derived from primary cells and have a longer lifespan. These include cells like human alveolar basal epithelial cells A549 [50, 86], human airway epithelial cell line Calu-3 [70, 102], human bronchial epithelium cells BEAS-2B [66, 91] and lung cancer cells NCI-H1437 [71]. During their development from primary cells they undergo various changes. As they do not have all the characteristics of the in vivo cells their behavior can be different.
3. **iPS:** These cells can be derived from any donor and then differentiated into the desired cell type. To derive them adult cells from donors are reprogrammed into stem cells. The use of induced pluripotent stem cells would allow avoiding the invasive procedures required to extract primary cells. They can prove to be cost-effective. However, protocols for generation of lung cells from iPS cells need to be further developed before they can be used in LOC [103]. Laniece attempted to obtain alveolar epithelial cells and microvasculature endothelial cells from iPS cells using a self made LOC device. The results lacked full differentiation and thus suggestions for future protocol optimization were also mentioned [78]. Use of iPS cells to derive alveolar epithelium has been successfully demonstrated in organoids [58].

A.3.3. Layout of LOC devices

To recreate the blood-gas barrier it is necessary to provide a surface to culture the epithelial cells on one side and endothelial cells on the other side. This surface provides the function of the ECM. The current models that achieve that can be divided into three categories based on their layout:

1. Vertically stacked channels
2. Channels in the same horizontal plane
3. Culture well over a channel

In the **first type** of layout, which is also the most popular one, a membrane separates the two chambers, it provides the surface for cell culture while the channels are used for initially seeding the cells and then for providing media flow. The epithelial cells are seeded on the top surface and the endothelial cells are seeded on the bottom surface of the membrane. The membrane is often made of polymers and is coated with ECM material to make it compatible with the cells.[91] [36][66][47] Sellgren et al. [99] created an airway model with three vertically stacked channels separated by two separate membranes, making the central thin channel available for the ECM cells. Humayun et al.[69] have a similar three layered chip with a channel in the thinner middle layer for placing hydrogel which acts as a membrane.

The gas in the alveoli has a higher percentage of water vapour than the air and thus has a reduced partial pressure of O_2. Therefore, an option of providing a gas that has the composition of alveolar gas is possible if a channel is present over the blood-gas barrier. Laniece made an alveoli-on-a-chip device with this layout. The chip was made reversible, allowing retrieving the membrane whenever required, and a holder with magnets was used to seal the layers [78].

The **second type** layout was demonstrated by Zhang et al. [124], it had three channels in the same plane. The central channel was filled with Matrigel which served as a membrane for seeding endothelial cells on one side and epithelial cells on the other. Mejias et al.[87] made a chip with the layout a hybrid of the first and the second types, it had three vertically stacked layers with the middle one being the membrane layer. The top layer consisted of the air chamber above the membrane. The bottom layer had five channels partitioned by microposts, the central channel below the membrane was seeded with endothelial cells along with idiopathic pulmonary fibrosis human lung fibroblasts, the two channels flanking the central channel contained the culture media and the outer two channels contained normal human lung fibroblasts.

In the **third type** of layout the top channel is replaced by a well that provides direct access to the top surface of the membrane. Shrestha et al.[101] chose this configuration over the closed channel, which allows for uniform flow, as the open well provides easy access to the membrane for ECM coating, cell seeding, sample collection and fluid manipulation for functional tests. Stucki et al. [107] provided a third layer below with pneumatic controls for the valves and breathing motion. This layout is suited for studies using aerosol drugs as they allow for recreation of particle dynamics as present in vivo [48]. This layout also helps to avoid inhomogeneous cell distribution and loss of cells in the fluidic network [107].

The different layout categories are shown in Figure A.9. Several chips were also fabricated in an array which allows for carrying out multiple and parallel experiments by just manufacturing the device once [69, 87, 107, 108].

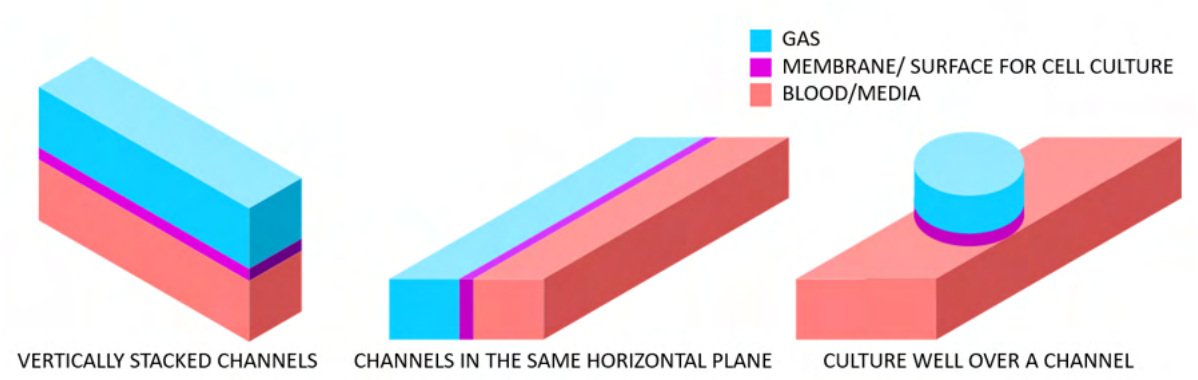

Figure A.9: Layout Categories for LOC

A.3.4. Commercially available LOC devices

A number of microfluidic devices for LOC application are commercially available in the market. These devices are either designed specifically for the lung or have a flexible design that allows to use them for different tissues. These chips are available along with compatible flow control systems, tubing and other accessories required to run the set up.

Devices demonstrated by Huh et al. [47], for an alveolus, and Benam et al. [36], for an airway, have been developed by the Wyss Institute for Biologically Inspired Engineering at Harvard University and are made commercially available by **Emulate**, Inc [19]. **AlveoliX** has made the chip, for the alveolus, demonstrated by Stucki et al. [108] commercially available as the AX12, which is based on the 96 well format and has 12 independent culture wells [16], as shown in Figure A.10. Other commercially available devices also allow for the culture of cells to form the blood-gas barrier. Membrane chips manufactured by Microfluidic ChipShop GmbH [17] were used to set up an alveolus-on-a-chip [45].

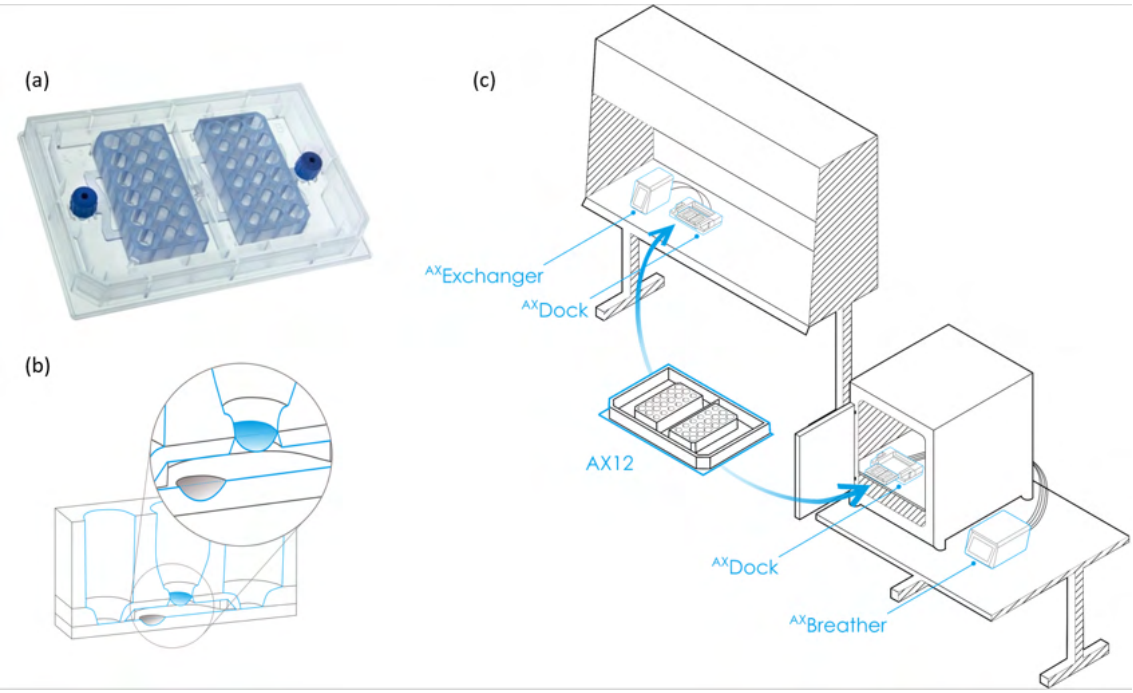

Figure A.10: (a) AX12, 12 alveolus-on-a-chip chambers (b) Design of the alveolus-on-a-chip with breathing mechanism (c) Set up for the device to exchange media and create breathing strain

Micronit manufactures resealable OOC devices. These devices provide the option of seeding the cells on the membrane outside the microfluidic device and to easily retrieve the membrane after completing the experiment. The chips have integrated optical oxygen sensors provided by PreSens and are compatible with Fluigent pressure based flow control platform. The chips come along with a holder, which can accommodate one chip or an array of four chips, that ensures that the device layers are pressed tight to avoid without any leaks [21].

Mimetas manufactures OrganoPlate® 3-lane has chips with three lanes present in the same horizontal plane. One each for the epithelial tubule and the endothelial tubule, separated by an ECM tubule. The central channel is defined by phase guides that ensure that the gel stays in the channel. The chip occupies a 9x9 grid on the 384-well-plate, allowing for 40 chips on the plate. OrganoFlow® can be used to maintain perfusion, by rocking the plate in a see-saw manner, in the apical and basal channels [22]. This method is thus gravity driven and does not require pumps [22].

Other commercially available chips that can be used for LOC application are HUMIMIC Chip by TissUse GmbH [24], µ-Slide Membrane ibiPore Flow by ibidi [20], two chamber culture device by Aline [18] and SynALI chips -IMN2 linear by Synvivo [23]. The HUMIMIC Chips by TissUse GmbH can be used to set up multi-organ chips for up to 4 different organs on one chip and are aimed to create a human-on-a-chip. As OOC is currently an expanding field of research, new devices are being developed and made commercially available by a number of manufacturers. The list of commercial devices mentioned here is not complete, but does aim to include the major manufacturers. The challenge for manufacturers lies in proving to the end user that the technology is useful and to make it user friendly, affordable and reliable so that it can be easily adopted.

The **layout categories** for commercial devices are the same as the devices found in literature, described in subsection A.3.3. Vertially stacked channels is the most popular layout and can be found in the chips manufactured by Emulate, Micronit, ibidi, Aline and Microfluidic ChipShop. Channels in the same horizontal plane can be found in chips manufactured by Mimetas and Synvivo. AlveoliX chip has a culture well over channel layout. A summary of the commercially available devices, along with the materials used, is presented in Appendix C.

A.3.5. Materials and manufacturing

PDMS is the most popular material used to manufacture lung-on-a-chip devices and microfluidic devices in general. Soft lithography is commonly used to fabricate the PDMS layers with microchannels and fluid compartments. The moulds are made using photolithography, stereolithography (SLA), digital Light Synthesis (DLS), and conventional micromachining processes. The prepolymer is poured into the moulds and cured to make the structures cast in PDMS hold shape.

Huh et al.[47] used a silicon wafer, with positive relief of the microchannels made of photoresist by photolithograhy techniques, to cast PDMS prepolymer. Similarly, silicon moulds prepared by photolithography were used by other authors as well ([54, 66, 86, 87, 91, 99, 111, 122, 124]).The silicon moulds were coated by vapour deposition with fluorosilane for anti-adhesion [99].The photolithography based approach for making moulds requires clean room facilities and trained workers. 3D printing of the moulds is in comparison low cost, faster and allows for complex geometric shapes. SLA [63] and DLS [101] have been used to make moulds for PDMS casting. The moulds were treated with oxygen plasma to ensure easy detachment of the cured PDMS. Each device layer is separately cast and then bonded to form the lung-on-a-chip device. Stucki et al.[107] used hard plastic moulds which were in turn made using structured aluminium moulds.

Thin PDMS layers were fabricated by spinning prepolymer, on a PE sheet attached to a silicon wafer, at 1700 rpm for 60 seconds [107], by lamination on a Kapton film carrier [99] or by spinning on a silanized glass slide at 300 rpm for 90 seconds [50]. Holes are punched [86, 87, 99, 101] or drilled [91] in the cured PDMS layer for inlet and outlet ports. Another method used for manufacturing using PDMS is etching. Dry and wet etching has been demonstrated for PDMS, with dry etching being more precise than wet etching but also more time consuming. Dry etching has a high degree of anisotropy which ensures higher precision than wet etching which is highly isotropic [31, 57]. Isotropic etching was done without any masks using tetrabutylammonium fluoride (TBAF) mixed with N-methylpyrrolidinone(NMP). Etchant was flown at 200 $\mu l/min$ for the required duration, it was flown in the microchannels using hydrostatic pressure or vacuum suction at outlet ports, to get the desired dimensions of the vacuum microchannels and completely dissolve the PDMS membrane present in it [47]. To make the surface of PDMS hydrophilic it was treated with oxygen plasma [50]. In devices that were made of glass PDMS gaskets were used for better sealing [71].

Though the optical transparency, elasticity, biocompatibility and ease of fabrication make PDMS a suitable material for organ-on-a-chip applications it also has some drawbacks like high absorption and adsorption of small molecules [115].

Poly(methyl methacrylate) (PMMA) layers were used by Humayun et al.[69] to make the chip by micromilling the features into them. PMMA is bioinert, optically transparent, low cost and compatible with mass production processes and all these qualities make it suitable for biological applications. Like PDMS, it has the drawback of adsorbing small molecules and leaching bioactive contaminants, however, unlike PDMS it doesn't absorb small molecules.

Khalid et al.[71] used soda lime **glass** layers with elastomer (Nusil medical grade silicone-MED-6033) channels, printed onto them using an ink-jet printing system for their device. In comparison to PDMS and PMMA, glass has an advantage of being non-permeable to chemical molecules and outer environment gas. This can be useful while carrying out drug related studies for molecules that are absorbed by PDMS and PMMA. The flow passages have the **critical dimension** $\sim 100\mu m$ or more for the PDMS devices, $\sim 500\mu m$ or more for the the glass-elastomer device and $\sim 700\mu m$ or more for the PMMA device.

Topas, a COC, is used for commercial scale production of OOC chips by Microfluidic Chipshop [17]. Cyclo-olefin polymer (COP) devices are suitable for OOC applications due to chemical inertness and optical transparency of the material. For low-cost production injection moulding, hot embossing and nanoimprint lithography are replication methods can be used. It is also possible to use such materials for rapid prototyping by using laser ablation and micromilling [25].

The table A.2 gives a list of materials used for LOC devices along with their pros and cons.

Table A.2: Materials used for LOC devices

Material	Pros	Cons
PDMS	Biocompatible Elastic Optically transparent Microfabrication compatible Low autofluorescence	Small molecule absorption Small molecule adsorption High gas permeability* Leaches contaminants
Acrylic - PMMA	Biocompatible Optically transparent Microfabrication compatible Low autofluorescence	Small molecule adsorption Not autoclavable Gas permeability* Brittle, not elastic* Leaches contaminants
Glass	Biocompatible Low adsorption Optically transparent Not permeable to gas Microfabrication compatible Very low autofluorescence Sterilized with ethanol, autovclave	Not elastic* High manufacturing costs Elastomer required for sealing Low Design Freedom
Topas, COC	Biocompatible Low leachables and extractables Optically transparent Microfabrication compatible Low autofluorescence Autoclavable	Brittle, not elastic*
PS	Biocompatible Optically transparent Microfabrication compatible Low autofluorescence	Not elastic Gas permeability* Not autoclavable

*Could be either a pro or a con depending upon application. So categorized according to LOC application.

Membranes
Huh et al.[47] made a 10 μm porous **PDMS membrane** by spin coating PDMS prepolymer at 2500 rpm for 10 minutes on a silanized wafer, with an array of 50μm tall and 10 μm wide pentagonal posts made by photolithography, followed by curing overnight at $65°C$. Stucki et al.[107] used PDMS to make the membrane as well by sandwiching PDMS prepolymer between a silicon wafer, patterned with micropillars with heights 3.5μm-10μm and diameters 3μm or 8μm, and a polyethylene sheet and clamping them together for curing. The height of the micropillars determined the membrane thickness. Punde et al[91] manufactured a porous membrane out of a **silicon chip** by using photolithography.

Yang et al.[122] fabricated a 3 μm **poly(lactic-co-glycolic acid) (PGLA) nanofiber** membrane by electrospinning 10% (w/v) PLGA dissolved in 2,2,2-trifluoroethanol, as shown in Figure A.11 a. A similar membrane was made by Laniece for her device by electrospinning a solution of gelatin over a gold coated poly(ethylene glycol) diacrylate (PEGDA) honeycomb mesh with holes of diameter 400 μm. The thickness of the membrane was of less than 1 μm, the thinnest in literature and closest to the in vivo dimension [78].

Commercial polymer membranes made of hydrophilized PTFE, polyester (PET) [34, 86, 87, 111], and PC [101] membranes were used in several devices [99]. When tested for lung-on-a-chip application epithelial cells preferred PTFE membranes while endothelial cells preferred PET membranes [99].

Polymer membranes need treatment and ECM coatings to make them hydrophilic, biocompatible and suitable for cell seeding. An alternative is to use **biological membranes** which are inherently compatible with the cells. Zamprogno et al.[123] made a membrane out of collagen and elastin. Collagen-elastin solution was pipetted onto a 15 μm thin gold mesh with a pore size of 260 μm, comparable to the size of an alveolus. The solution is held in shape by surface tension forces till it dried to form a suspended membrane. Membrane thickness was proportional to the volume of solution pipetted on to the

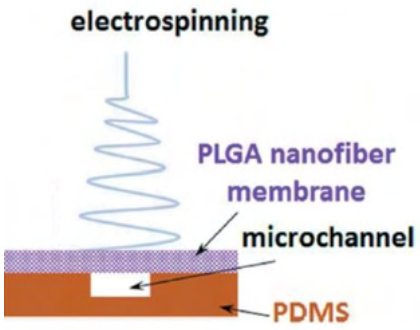

(a) Electrospinning PGLA to form membrane. [122]

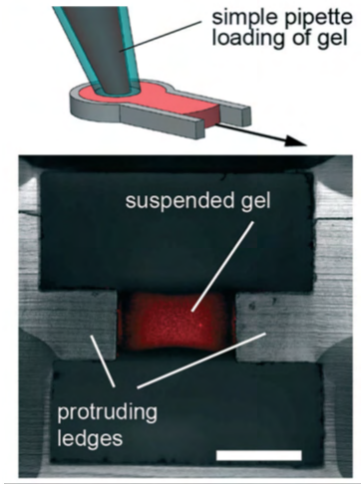

(b) Suspended hydrogel formed by pipetting. [69]

Figure A.11: Manufacturing of membranes

mesh, the thinnest membrane that was achieved was $\sim 4.5\mu m$. The ratio of elastin to collagen in the solution also determined the membrane thickness that could be achieved, with thickness decreasing with decreasing elastin that also resulted in deteriorating viscoelastic properties.

Zhang et al.[124] used a microchannel filled with **Matrigel** to act as the surface for cell culture, with epithelial cells on one side and endothelial cells on the other. Mejias et al.[87] made vitrified **collagen** membrane by pipetting collagen solution onto a channel punched out in a PDMS layer, the hydrophobicity of PDMS kept the solution out of the channels and ensured that the solution dried to form a thin layer covering the channel. This was done by incubating at 37°C for about an hour and then drying at room temperature. Alternatively, the solution can also be dried on a separate PDMS slab and then transferred over the microchannel after it has dried to form a thin film [85]. Humayun et al.[69] pipetted pre-polymerised hydrogel, made out of collagen-I and Matrigel, between two protruding PMMA ledges which it flowed along by assisted capillary action to form a thin film of the hydrogel which dried to form a membrane, as shown in Figure A.11 b. Barkal et al.[33] used temporary PDMS rods to make lumens for cell culture in a 3D matrix of collagen and pulmonary fibroblasts. In this way surfaces for cell culture were made which were not on a membrane but still allowed for interaction between different types of cells.

Bonding:
The PDMS surface was treated with corona plasma [47] or O_2 plasma [107] followed by bringing in contact the two PDMS surfaces, or a PDMS and a glass surface [54, 124], that are to be bonded. For bonding PC and PET membranes to PDMS, the membranes were aminofunctionalized and then contact bonded with plasma treated PDMS surface. The layers were then thermocompressed under a compressing force. PTFE membranes were bonded by sandwiching them between silanized PDMS layers and then thermocompressing under a weight overnight followed by high temperature treatment in an autoclave [99]. Another method to bond PET membranes involved plasma treating the membrane and then dipping it in APTES, after which it was taken out and dried. This was then sandwiched between two oxygen plasma activated PDMS layers.

Reversible bonding between PDMS layers was achieved by bringing the surfaces into contact and pressing manually, PC was coated with a layer of PDMS to make it suitable for irreversible bonding with PDMS layers [107]. However, this type of bonding was found to be insufficient by Laniece if pressure variations had to be used for stretching the membrane. So to still maintain a reversible bond, a chip holder with magnets embedded in PDMS was used [78].

Solvent assisted thermal bonding was used for PMMA layers. 99% ethanol was pipetted onto the surfaces and then the layers were aligned and pressed under a weight at 70°C for 1 minute.Bonding

of multiple layers was done in succession [69].

Sterilization:
The devices were sterilized by techniques using UV light [101, 124], ozone gas [107] or autoclave [123]. The media chambers and channels were flushed with 70% ethanol in some cases [69].

A.3.6. Incorporation of mechanical strain to mimic breathing

The mechanical strain is between 5-12% linear elongation for normal breathing and can go up to 45.4% for mechanically ventilated lungs [50, 116]. While the exact mechanism for the volume change due to breathing can be complex, as described in the breathing mechanisms section, the result is volume expansion during inhaling air which can be measured as a positive line, area or volume strain.

Huh et al.[47] demonstrated the first breathing chip which used two hollow channels flanking to the membrane, by applying cyclic negative pressure change in these channels the membrane stretched to mimic breathing motion, as shown in Figure A.8 (a). The membrane was subjected to 10% linear strain at 0.2 Hz. Hou et al.[66] used a similar approach and mimiced physiological breathing motion by periodic suction of air, at 0.25 Hz, from a pneumatic chamber below the membrane. In both these approaches the flexibility of PDMS assures that the stretch is transferred to the membrane.

Stucki et al.[107] created a chip with a thin layer of PDMS that acted as the diaphragm and transferred 3D cyclic stretch to the membrane unlike the 2D stretch provided in the earlier models. Cyclic negative pressure was applied in the small chamber below the diaphragm and the volume of this chamber determined the maximum stretch of the diaphragm. The maximum stretch corresponded to 10% linear strain. The stretch was transferred to the membrane by the incompressible liquid media, present in the chamber between the two layers, according to Pascal's law. Using this principle for stretching the membrane has a drawback that it doesn't allow for flow of media during breathing motion. The mechanism is shown in Figure A.12. The pressure wave was modelled as a sinusoidal wave [107] or a triangular wave [108] with a frequency of 0.2 Hz.

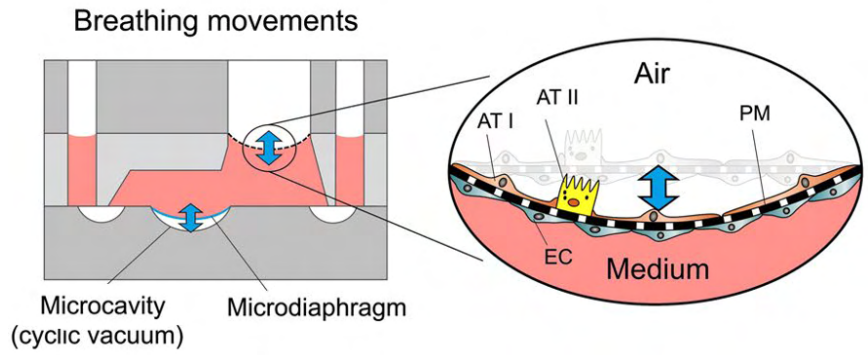

Figure A.12: Use of a diaphragm to transfer stretch to the membrane through an incompressible liquid. [108]

Fishler et al.[54] incorporated breathing motion onto their chip by deforming thin PDMS side walls by changing water pressure, using a syringe pump, in water filled chambers surrounding the wall. The top surface of the chip was also deformed periodically through the water filled compartment made out of a syringe embedded into the PDMS top layer over it.

A biological membrane was stretched by applying negative pressure to the chamber beneath it [123] and another similar membrane was stretched by applying positive pressure above it [78]. A pore less PDMS membrane was stretched by changing the fluid volume in the chamber beneath it using a programmable syringe pump [50].

A.3.7. Drawbacks in the current models

Several drawbacks of the current available LOC models have been identified till now. The lack of **biological complexity** means that the cells do not behave as they would in vivo. Thus including

human primary cells, structural cells and immune cells can improve the models. The ECM recreated in the LOC models also usually lacks the 3D spatial arrangement and is limited to 2D surfaces.

The LOC devices still lack the recreation of the cell culture **substrate structure** according to the in vivo stiffness and dimensions. The blood-gas barrier reaches values below $1\mu m$ [103] for half of the alveolar area, however the LOC models, with membranes at least three times thicker than that, have not been able to recreate that. The present LOC models also have a low ratio of alveolar to ductal volume [111]. The much higher liquid to cell ratio than in vivo results in the dilution of cell secretions and metabolites which can affect cell behaviour. The extensive use of PDMS, which absorbs hydrophobic drugs, is another issue to be tackled [103]. This can result in wrong results while testing drugs. There is a need for identifying materials that are more suited for OOCs and simplifying the fabrication procedure.

A number of additional characteristics will be useful in improving LOC models. The automation of microfluidic cell culture along with efficient **sensing and monitoring** of biological responses will make OOC suitable for large scale applications. High throughput would be an advantage for speedy testing. Long-term culture is required for a number of studies.

A.4. Integration of sensors

The functionality of a lung-on-a-chip microfluidic device increases with the integration sensors for the measurement of TEER, pH, O_2, CO_2 and temperature. Such sensors have been integrated before in organ-on-a-chip devices and microfluidic devices. Optical sensors have the advantage of not making the chip bulky with extra parts and does not interfere with the experiment being carried on, thus maintaining the sterility and fluidic integrity of the chip. They are commonly used to measure pH, O_2, CO_2. Thin film electrodes made of metals also have the advantage of not taking up excess space on the chip and are used for sensing the temperature and TEER. These can also be designed to sense pH, O_2 and CO_2. Incorporating readout on the chip is also a needed development. Compatibility of the device with imaging systems would allow for the use of various fluorescent intracellular probes.

TEER sensor
Khalid et al.[71] created a 500 nm thin TEER sensor by using indium tin oxide (ITO) electrodes patterned, using photolithography, on the inner sides of the top and bottom glass surfaces of the chip. ITO electrodes being semitransparent allow for the optical monitoring of the cells, they were however seen to deteriorate the image quality obtained from the digital microscope camera. Gold and titanium thin film electrodes were also demonstrated for the same use. As the barrier needs to be in contact with the sensor electrodes through a liquid, which will act as a conductor and complete the circuit, DMEM was introduced in the apical compartment [6].

Apart from permanent integration of the TEER sensors other methods have also been used to measure the resistance. Wire electrodes (silver/silver chloride) were inserted in the inlet of the alveolar compartment and the outlet of the vascular compartment, respectively. The resistance value of the chip without the cells was subtracted to get the trans-bi-layer resistance measurements [47]. Wire electrodes can also be permanently incorporated on the chip [49]. These are inserted in the microgrooves made in the chip and have an advantage over the film based sensors, as they don't delaminate from the substrate when the substrate has stretching present due to incorporation of mechanical strain on the OOC.

Temperature sensor
Platinum resistance temperature sensors (Pt - RTD) are the most popular temperatures sensors due to their reliability. The change in resistance due to temperature change is almost linear over a large range of temperature. It is also possible to deposit the sensors as a thin film using standard lithography processes [106] or to use a probe with resistance wires.

O_2 sensor
Optical O_2 sensors include a patch of phosphorescent material on the inner surface of the channel, containing dissolved O_2 or gaseous O_2. The patch is excited using an optical fiber which also collects the phosphorescent signal for further quantification [15]. This means that the access window to the

sensor must be made of transparent glass or polymer. Commercial sensors with different coatings for varying concentration ranges can be bought along with a read out oxygen meter that measures the value of the signal obtained by the optical fiber [60]. A method for fabrication of the sensor spots using a specially prepared platinum (II) meso-tetra (4- fluorophenyl) tetrabenzoporphyrin (PtTPTBPF) solution requires pipetting the solution spot onto the substrate and then drying it [125].

Another optical method involves a film of immobilized O_2 sensitive dye on a surface separated by the flow channel by a layer of PDMS that only allows 0_2 to pass through. This is illuminated by a high-power blue LED and the change in luminescent intensity was measured using two Si photodiodes [100]. One of the photodiode detects the light passing through just the filters and the other detects light passing through the dye along with the filters. This sensor works for both gaseous and dissolved O_2.

CO_2 sensor
Commercially available sensor spots along with compatible optical fiber read out meters are the most convenient solution to measure partial pressure of dissolved CO_2. Flow cells with the sensor spots attached inside are available for quick integration into the LOC setup [60].

pH sensor
Commercial optical self-adhesive sensor spots along with compatible optical fiber pH meters are available in the market and can be easily integrated with a LOC device with transparent windows [60]. An optical pH sensor was made using a white LED, an optical filter, a photodiode [71]. The color of the fluid changed upon acidification due to the presence of phenol red. The sensor works by detecting the change in the intensity of the light passing through the fluid passing in a highly transparent microfluidic tube. The light is emitted by the LED and sensed by the photodiode.

Apart from the above mentioned sensors there is also a possibility of using microsensors that work on other principles. However, if they are not available already in the market that would also mean self fabricating the sensor, developing a readout system for the sensors and testing the efficiency of the sensor. In comparison of-the-shelf sensors are easy to implement and provide a readout that can also be stored in the computer. A number of sensors that have been described in the literature have a well developed manufacturing and testing procedure by now. The readout methods have also been already devised and thus using such sensors can be the easiest solution next to the commercial sensors. The optical sensing can be performed in a flow cell present outside the OOC to allow for ease of use and better accessibility. This also removes the chance of contaminating the cultured cells with leached out materials from the sensors, if any. Sampling or monitoring of the media coming out of the chip, to test for specific molecules, would also increase the device functionality.

B

LOC Devices in Literature

Table starts on the following page.

Lung-on-a-chip devices in literature

	Author and Focus	Image	Material	Features
1	Huh et al. [47] Alveolus	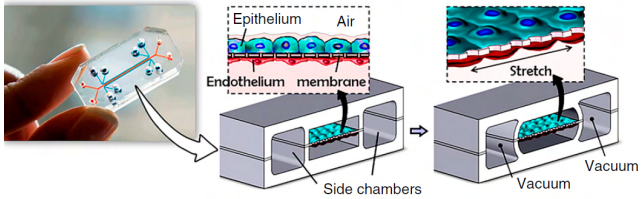	Device: PDMS Membrane: PDMS	Co-culture- Epithelial cells and Endothelial cells Media Flow: Yes Breathing motion: Yes Layout: Vertically stacked channels
2	Stucki et al. [107, 108] Alveolus	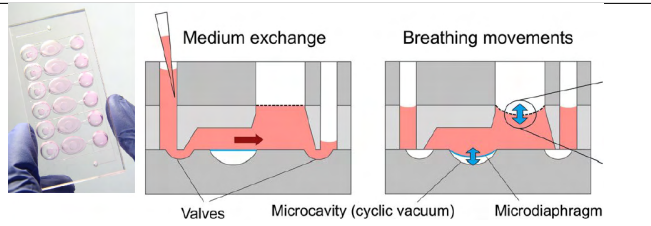	Device: PDMS Membrane: PDMS	Co-culture- Epithelial cells and Endothelial cells Media Flow: Not continuous Breathing motion: Yes Layout: Culture well over a channel Array
3	Zamprogmo et al. [123] Alveoli	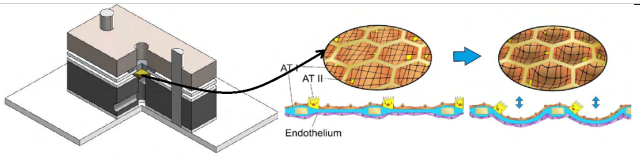	Device: PDMS Membrane: Collagen-elastin on gold mesh	Co-culture- Epithelial cells and Endothelial cells Media Flow: No Breathing motion: Yes Layout:Reservoirs
4	Hou et al. [66] Alveolus	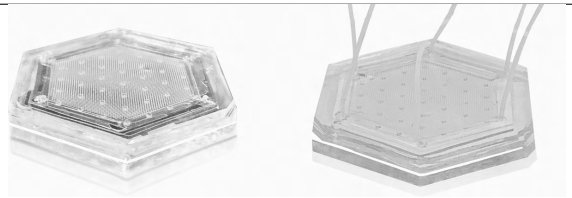	Device: PDMS Membrane: PDMS	Co-culture- Epithelial cells and Endothelial cells Media Flow: Yes Breathing motion: Yes Layout: Vertically stacked channels
5	Xu et al. [121] Alveolus	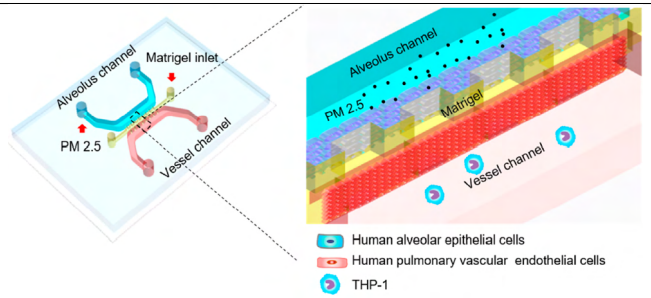	Device: PDMS Cell culture surface: Matrigel	Co-culture- Epithelial cells and Endothelial cells Media Flow: Yes Breathing motion: No Layout: Channels in the same horizontal plane

Lung-on-a-chip devices in literature

	Author and Focus	Image	Material	Features
6	Laniece [78] Alveoli	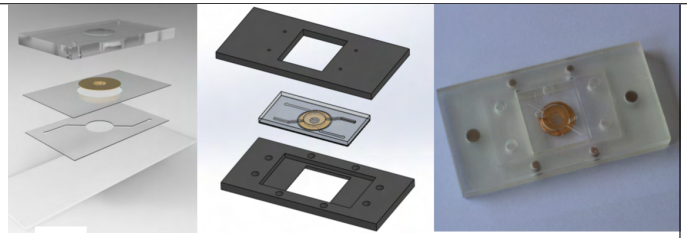	Device: PDMS Membrane: Gelatin on PEGDA mesh	Co-culture- Epithelial cells, Endothelial cells Media Flow: Yes Breathing motion: Yes Layout: Vertically stacked channels Resealable
7	Mejias et al. [87] Airway	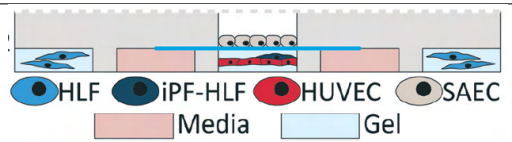	Device: PDMS Membrane: PET or Collagen	Co-culture- Epithelial cells, Endothelial cells and Fibroblasts Media Flow: No Breathing motion: No Layout: Reservoir, 96 well format
8	Sellgren et al. [99] Airway	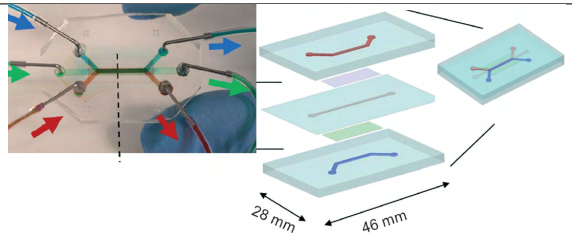	Device: PDMS Membrane: PTFE, PET	Co-culture- Epithelial cells, Endothelial cells and Fibroblasts Media Flow: Yes Breathing motion: No Layout: Vertically stacked channels
9	Barkal et al. [32] Airway	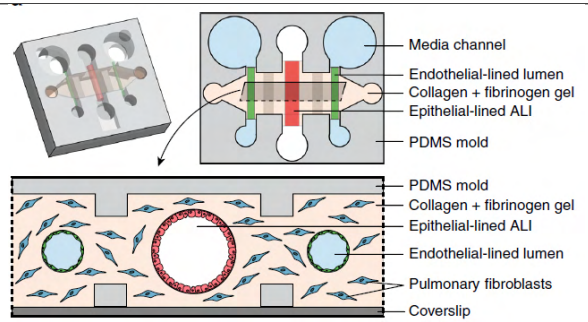	Device: PDMS Cell culture lumens: Collagen + Fibrinogen	Co-culture- Epithelial cells, Endothelial cells and Fibroblasts Media Flow: No Breathing motion: No Layout: Reservoir

	Author and Focus	Image	Material	Features
10	Punde et al. [91] Airway	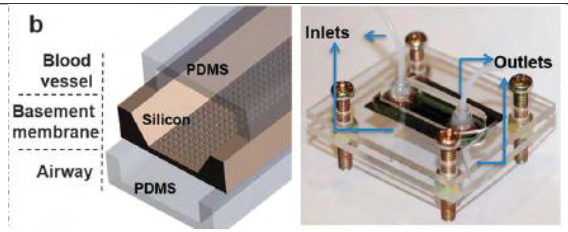	Device: PDMS Membrane: Silicon	Co-culture- Epithelial cells, and Fibroblasts Media Flow: Yes Breathing motion: No Layout: Vertically stacked channels
11	Humayun et al. [69] Airway	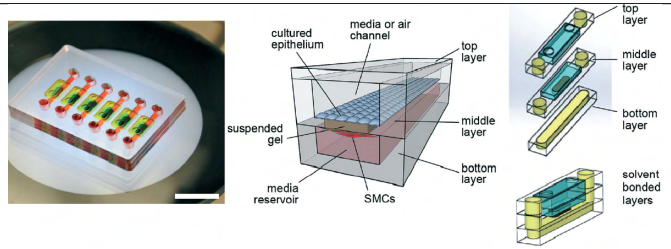	Device: PMMA Cell Culture surface: Hydrogel	Co-culture- Epithelial cells, Smooth muscle cells Media Flow: No Breathing motion: No Layout: Vertically stacked channels Array
12	Shrestha et al. [102] Airway	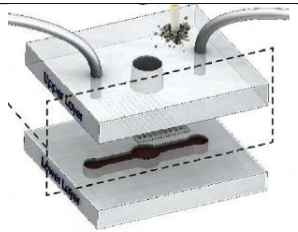	Device: PDMS Membrane: PC	Monoculture- Epithelial cells Media Flow: Yes Breathing motion: No Layout: Culture well over a channel
13	Benam et al. [35] Airway	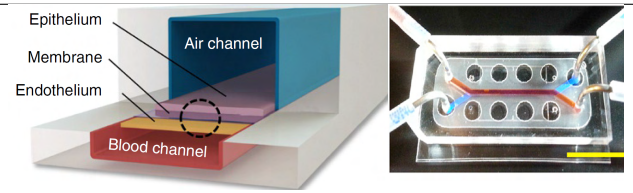	Device: PDMS Membrane: PET	Co-culture- Epithelial cells and Endothelial cells Media Flow: Yes Breathing motion: No Layout: Vertically stacked channels

	Author and Focus	Image	Material	Features
14	Yang et al. [122] Tumour	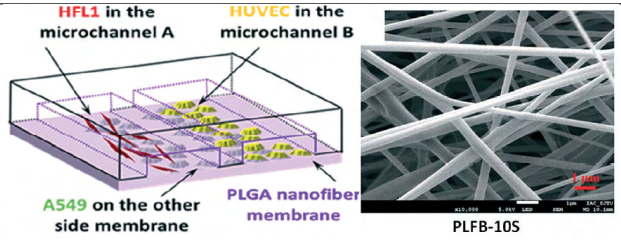	Device: PDMS Membrane: PLGA nanofiber	Co-culture- Epithelial cells, Endothelial cells and Fibroblasts Media Flow: No Breathing motion: No Layout: Vertically stacked channels
15	Tenenbaum-Katan et al. [110, 111] Fishler et al. [54, 55] Acinus	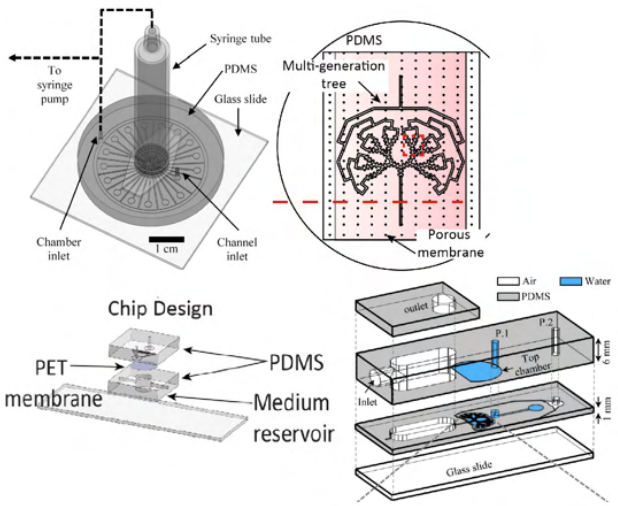	Device: PDMS Membrane: PET	Monoculture- Epithelial cells Media Flow: Yes(in some) Breathing motion: Yes (in some) Layout: Vertically stacked over reservoir
16	Nalayanda et al. [86] Alveolus	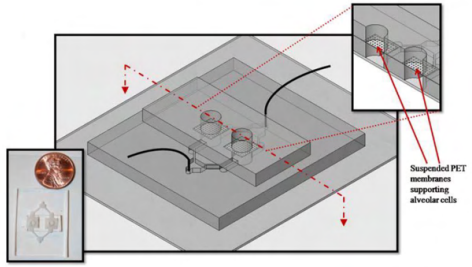	Device: PDMS Membrane: PET	Monoculture- Epithelial cells Media Flow: Yes Breathing motion: No Layout: Culture well over a channel Array

Lung-on-a-chip devices in literature

	Author and Focus	Image	Material	Features
17	Huh et al. [68] Airway, Bronchioles	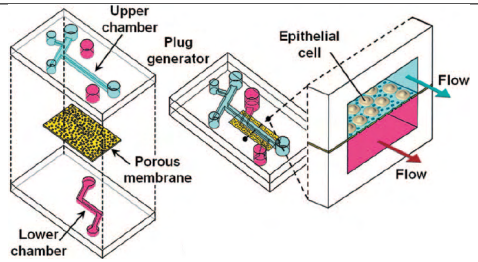	Device: PDMS Membrane: Polyester	Monoculture- Epithelial cells Media Flow: Yes Breathing motion: No Layout: Vertically stacked channels Plug generator
18	Douville et al. [50] Alveolus	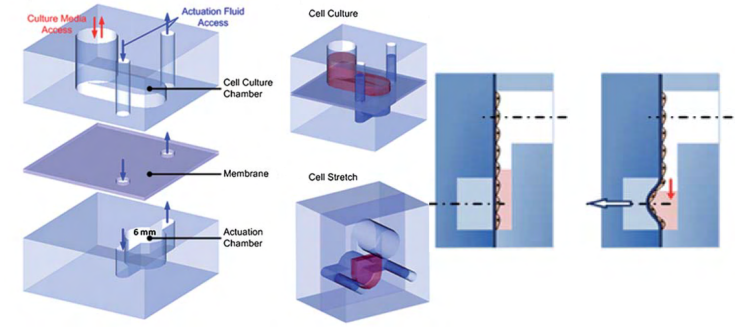	Device: PDMS Membrane: PDMS	Monoculture- Epithelial cells Media Flow: No Breathing motion: Yes Layout: Vertically stacked over reservoir
19	Khalid et al. [71] Lung Cancer	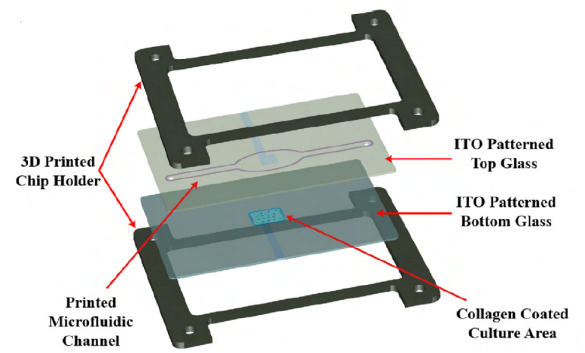	Device: Soda lime glass Nusil silicone elastomer	Monoculture- Lung Cancer cells Media Flow: Yes Breathing motion: No Layout: Single channel

C

Commercially Available Devices

Table starts on the following page.

Commercially available devices

	Commercial Device	Image	Material	Features
1	Chip-S1 Organ-Chip by Emulate [19]	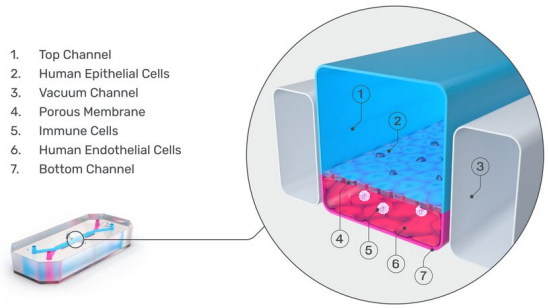	Device: PDMS Membrane: PDMS	Media Flow: Yes Breathing motion: Yes Layout: Vertically stacked channels
2	AX12 by AlveoliX [16]		Device: PDMS Membrane: PDMS	Media Flow: Not Continuous Breathing motion: Yes Layout: Culture well over a channel Array of 12
3	Membrane chips by Microfluidic ChipShop [17]	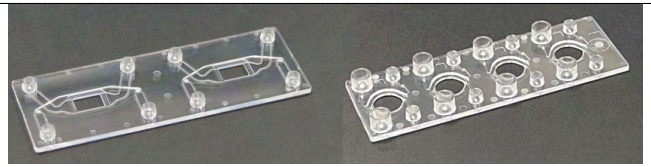	Device: Topas Membrane: PS or PET	Media Flow: Yes Breathing motion: No Layout: Vertically stacked channels
4	Organ-on-a-Chip by Micronit [21]	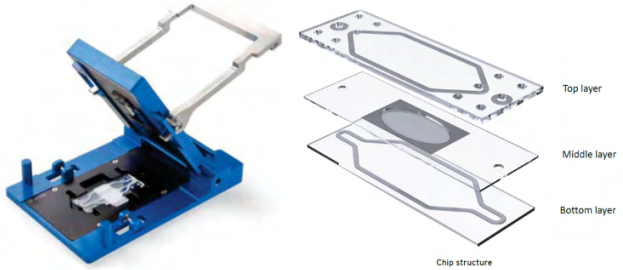	Device: Borosilicate Glass Elastomer gasket Membrane: PET, PS or PC	Media Flow: Yes Breathing motion: No Layout: Vertically stacked channels Resealable Array of 4 chips possible

Commercially available devices

	Commercial Device	Image	Material	Features
5	OrganoPlate® 3-lane by Mimetas [22]	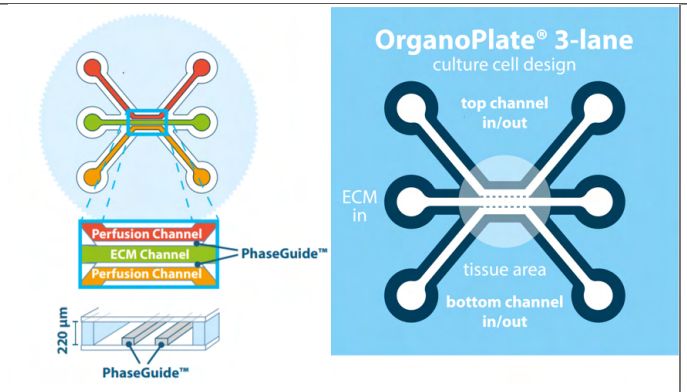	Top plate: Virgin polystyrene. Plate bottom: optical quality 150 µm glass Microfluidics: glass, proprietary polymers, biocompatible and low compound-absorbing Cell culture surface: ECM Gel in the middle tube	Media Flow: Yes, Perfusion by rocking Breathing motion: No Layout: Channels in the same horizontal plane Array of 40 chips
6	µ-Slide Membrane ibiPore Flow by ibidi [20]	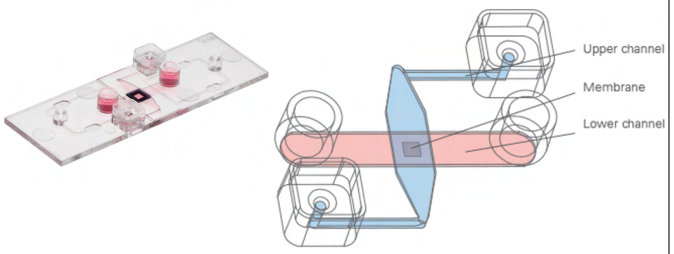	Top: Glass coverslip Bottom: ibidi Polymer Coverslip Membrane: Porous Glass	Media Flow: Yes Breathing motion: No Layout: Vertically stacked channels
7	Organ-on-a-Chip by Aline [18]	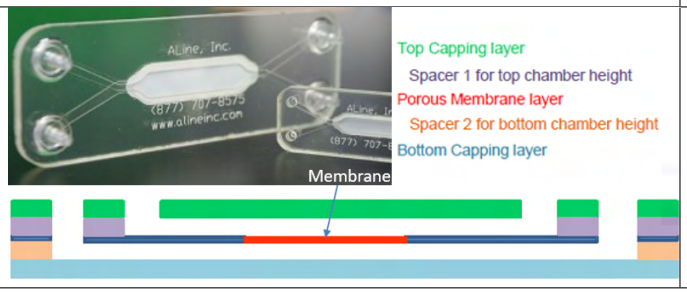	Top Capping layer: Acrylic, COC or COP Spacers: Silicone adhesive/PET Bottom Capping layer: Glass slide, Acrylic or Polystyrene (breathable) Membrane: PET, PC or PS	Media Flow: Yes Breathing motion: No Layout: Vertically stacked channels

Commercially available devices

	Commercial Device	Image	Material	Features
8	IMN2 Linear by Synvivo [23] [109]	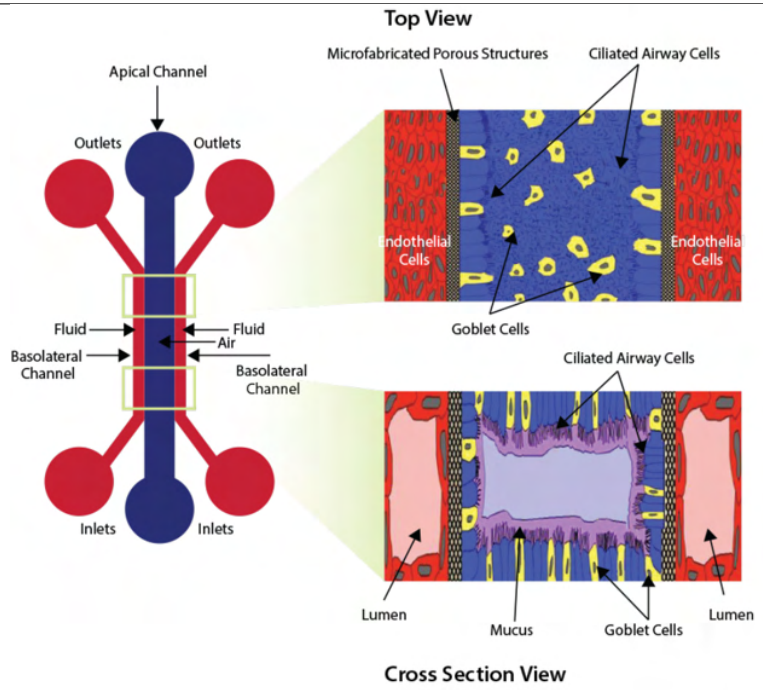	Device: PDMS on glass slide Membrane: PDMS [83]	Media Flow: Yes Breathing motion: No Layout: Channels in the same horizontal plane

D

Matlab Codes

D.1. Channel Design

The matlab file `Flow_in_the_channel.m` can be found in supplementary documents. It gives the required flow rate for getting the desired shear stress on the top wall of a rectangular channel for given channel dimensions and culture media properties. The distribution of the shear stress on the wall is plotted.

```
% For flow measurements in channels
clc
clear

% Fluid Parameters

eta = 0.6913e-3  ; % viscosity in kg/ms % water 20 deg = 0.001, 37 deg = 0.6913e-
3 ,blood = 0.004 % XG in DMEM 6e-3 % dextran 20% w/w =20e-3
rho = 993.18 ; % density in kg/m^3 % water 1000, blood 1060 % DMEM 1.00 + 0.1 XG
% dextran 20% w/w =1060

% Channel geometry Parameters

h =  0.0003 ;% height for rectangular channel in m
w =  0.0032 ;% width for rectangular channel in m
L =  0.02; % length for rectangular channel in m

% Hele-Shaw shear for h<<w

%tau = 6*eta*Q/(w*(h^2))% shear in Pa
tau = 0.55 % Pa

Q_l_hr = (tau*w*(h.^2)./(6*eta)).*3.6e6 % l/hr
Q = (tau*w*(h.^2)./(6*eta)) %m3/sec
Q_d = Q*6e10 %ul/min

% Flow rate according to Poiseuille flow

% here p = pressure N/m^2 ,
%R_hyd = hydraulic resistance kg/m^4s 0r Pa s/m^3, Q = Flow rate m^3/s
```

```
R_hyd = (12*eta*L)/((1-0.63*(h/w))*(h^3)*w)
R_hyd_acc    =    (12*eta*L)/((h^3)*w)*(1/(1-(0.630    -    (192/pi^5)*(1-
tanh((pi/2)*(w/h))))*(h/w)))

% Reynolds number
A = w*h;
P = 2*(w + h);
D_h = 4*A/P;

v = Q/A % velocity m/s

Re = rho*D_h*v/eta

Re_eff = Re*(h/L)    % Effective Reynolds number


% velocity field for poiseuille flow in rectangular channel
y = 0;
z = h/2;
syms k x xg

x = vpa(symsum((1/((2*k+1)^3))*(1-(cosh((2*k+1)*pi*y/h)/cosh((2*k+1)
     *pi*w/(2*h))))*(sin((2*k+1)*pi*z/h)), k , 0, Inf));
v_max = (4*(h^2)*R_hyd*Q/((pi^3)*eta*L))*x % max velocity at center

no =  6;% data points
yg = linspace(-w/2,w/2,no);
zg = linspace(0,h,no);
[Y,Z] = meshgrid(yg,zg);

xg = vpa(symsum((1/((2*k+1)^3)).*(1-(cosh((2*k+1)*pi.*Y./h)./
cosh((2*k+1)*pi*w/(2*h)))).*(sin((2*k+1)*pi.*Z./h)), k , 0, 1000));

% velocity profile in rectangular channel
vx_yz = (4*(h^2)*R_hyd*Q/((pi^3)*eta*L))*xg;
V = vx_yz/v_max; % normalized

M = zeros(no);
M ;
for i=1:no j=1:no;
    M(i,j)=V(i,j);
end

surfc(Y,Z,M) % cross-section vs normalized velocity
daspect([1 1 1000])

% Shear rate and shear force

gamma_d = 2*v_max/h % average shear rate
tau_b = eta*gamma_d % shear according to average shear rate

syms ys zs xs

xs = symsum((1/((2*k+1)^3)).*(1-(cosh((2*k+1)*pi.*ys./h)./cosh((2*k+1)
*pi*w/(2*h)))).*(sin((2*k+1)*pi.*zs./h)), k , 0, 1000);
```

```
%velocity profile in a rectangular channel
v_sym = (4*(h^2)*R_hyd*Q/((pi^3)*eta*L))*xs;

A = diff(v_sym,ys); % delv/dely
B = diff(v_sym,zs); % delv/delz


ys = linspace(-w/2,w/2,no);
zs = linspace(0,h,no);
[Y1,Z1] = meshgrid(ys,zs);

%delv/dely
A1 = vpa(-(1125899906842624*Q*R_hyd*h*pi.*symsum((sinh((Y1.*pi*(2*k + 1))./h).
*sin((Z1.*pi*(2*k + 1))./h))./(cosh((w*pi*(2*k + 1))/(2*h))*
(2*k + 1)^2), k, 0, 1000))./(8727491006471547*L*eta),10);

%delv/delz
B1 = vpa(-(1125899906842624*Q*R_hyd*h*pi*symsum((cos((Z1.*pi*(2*k + 1))./h).
*(cosh((Y1.*pi*(2*k + 1))./h)./
cosh((w*pi*(2*k + 1))/(2*h)) - 1))
./(2*k + 1)^2, k, 0, 1000))./(8727491006471547*L*eta),10);

gamma_d_local = sqrt(A1.^2 + B1.^2); % local shear strain depends on y and z
Gamma = gamma_d_local./gamma_d;

G = zeros(no);

for i=1:no j=1:no;
    G(i,j) = Gamma(i,j);
end

surfc(Y1,Z1,G) % cross-section vs normalized shear
daspect([1 1 1000])
```

The normalized velocity profile (`contourf(Y,Z,M)`) obtained for a channel height of 300μm is as follows:

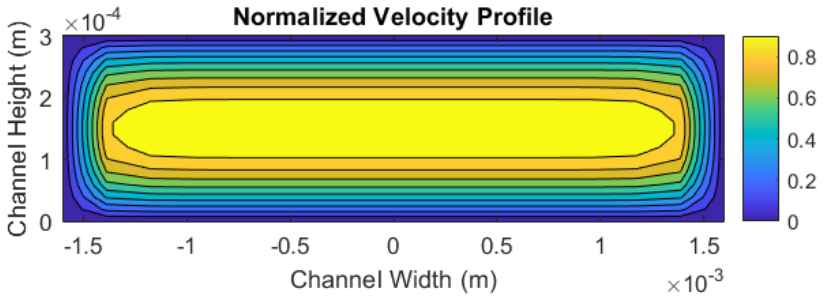

Figure D.1: Normalized Velocity Profile

The normalized shear rate (`contourf(Y1,Z1,G)`) obtained for a channel height of 300μm is as follows:

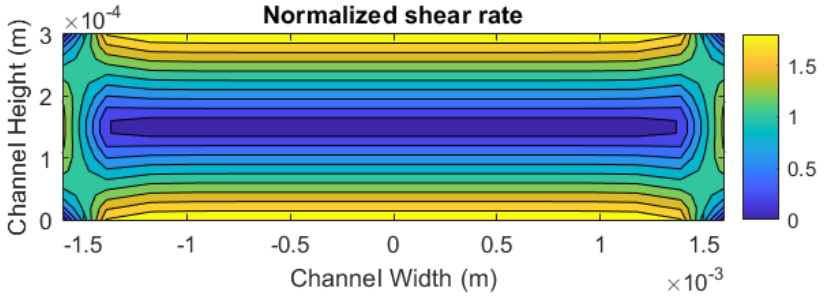

Figure D.2: Normalized Shear Rate

E

Detailed Drawings

E.1. Actuator Mould

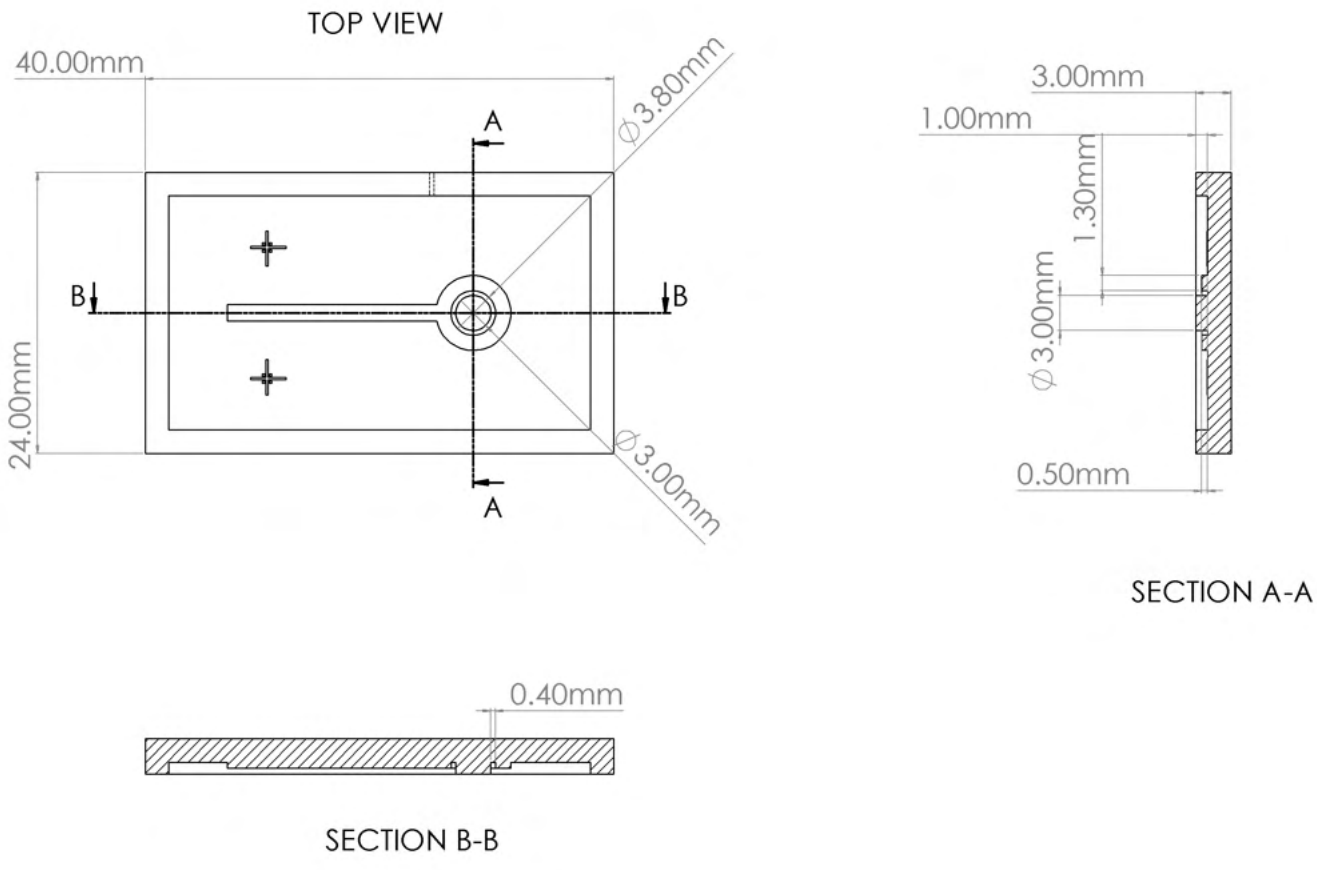

Figure E.1: Actuator Mould Drawing

E.2. Glass Layers

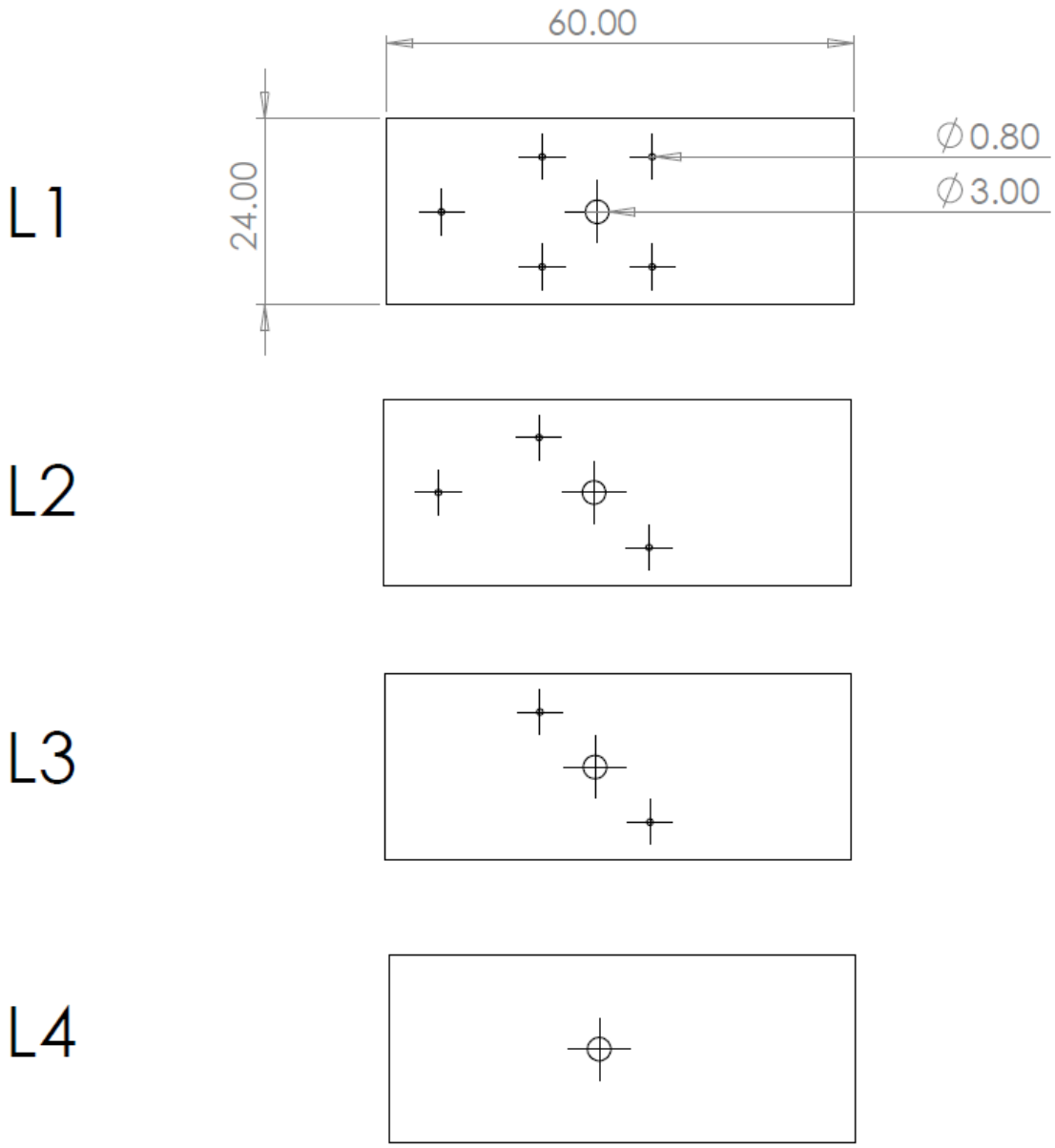

Figure E.2: Glass Layers Version 1 Drawing

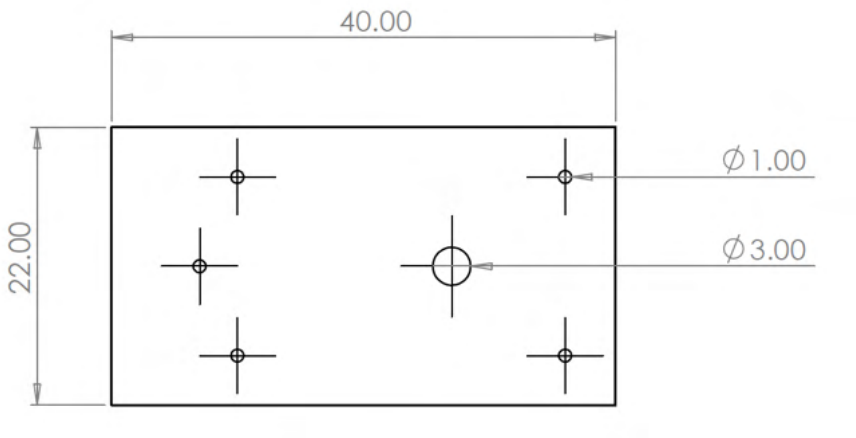

Figure E.3: Glass Layer 1 of Version 2 Drawing

F

Plasma Bonding Procedure

PDMS can be bonded to glass and PDMS by first activating the surface using plasma and then bringing the activated surfaces into contact. Diener Femto Plasma System was used to activate the surfaces. The recipe for bonding was perfected by trying out different combinations of the process parameters. Recipes used by previous users to obtain PDMS-PDMS and PDMS-Glass bonds proved to be very helpful in determining the recipe.

Before bonding it should be ensured that the PDMS and glass surfaces must be clean and free from dirt and dust. If the PDMS surface is unclean clean it using the following methods:

1. For almost clean surface with some dust particles- Use an air gun to remove the dust particles.
2. For moderately clean surface with some dust and debris- Wipe clean using IPA and clean room wipes. Then use an air gun to remove and residual particles.
3. For dirty surface- Put the PDMS part in a beaker containing ethanol. Put the beaker in the ultrasonic cleaner for 5 minutes. Use an air gun to remove and residual particles.

To clean the glass surface wipe it with IPA using a clean room wipe and then use the air gun to remove any particles on the surface.

F.1. PDMS-PDMS bonding

Table F.1: Plasma Bonding PDMS to PDMS

Gas	Power	Time	Pressure	Bond Quality
Oxygen	80 W	0.5 min	0.12 mbar	–
Oxygen	80 W	0.7 min	0.12 mbar	–
Oxygen	80 W	1 min	0.12 mbar	–
Oxygen	60 W	2 min	3.5 mbar	–
Air	60 W	2 min	0.2 mbar	–
Air	60 W	2 min	3.5 mbar	+
Air	40 W	3 min	3.5 mbar	++

Key: – : No bonding, +: Bonded, ++: Strong Bond

Previous user, M. Looman bonded PDMS surfaces by activating them using air plasma for 3 minutes with a power of 60 Watt at 4 mbar [81].The author pointed out that the process parameters differ for PDMS cured at different temperatures. The author's recipe is for PDMS cured at 70°C for 3 hours. The recipes in the table were tried for PDMS cured at 75°C for 2 hours. From the above results the following protocol was made to bond PDMS to PDMS.

Procedure for bonding PDMS surfaces:

1. Ensure all the PDMS surfaces are clean and dry.
2. Put the parts, with the surface to be bonded facing upwards, in the plasma cleaner.
3. **Expose the surfaces to air plasma for 3 mins with a power of 40 W at 3.5 mbar.**
4. Bring the PDMS surfaces into contact ensuring the no air is trapped in between the surfaces.
5. Apply pressure manually on the two layers for 30s after contact to ensure that the layers do not debond due to surface undulations or and debris on the surface.
6. Wait for 10 mins before further working with the bonded layers.
7. Do not apply any force to pull the surfaces apart for the next 24 hours.

F.2. PDMS-Glass bonding

Table F.2: Plasma Bonding PDMS to Glass

Gas	Power	Time	Pressure	Bond Quality
Oxygen	80 W	0.5 min	0.12 mbar	–
Oxygen	80 W	0.7 min	0.12 mbar	–
Oxygen	80 W	1 min	0.12 mbar	–
Oxygen	40 W	1 min	3.5 mbar	–
Air	40 W	1 min	0.2 mbar	–
Air	40 W	1 min	3.5 mbar	++

Key: – : No bonding, +: Bonded, ++: Strong Bond

Previous user, S. Soons bonded PDMS to glass by activating the surface using air plasma for 1 minute with a power of 40 Watt at 3 mbar [105]. The protocol for PDMS-glass bonding using air plasma by the author describes the step by step procedure for using the Diener Femto Plasma System to achieve the results and was followed with the parameters mentioned below. From the above results the following protocol was made to bond PDMS to glass.

Procedure for bonding PDMS to glass:

1. Ensure all the surfaces are clean and dry.
2. Put the parts, with the surface to be bonded facing upwards, in the plasma cleaner.
3. **Expose the surfaces to air plasma for 1 minute with a power of 40 W at 3.5 mbar.**
4. Bring the glass surface into contact with the PDMS surface ensuring that no air is trapped in between.
5. Apply pressure manually on the PDMS layer for 30s after contact to ensure that the layers do not debond due to surface undulations or and debris on the surface. Ensure that the glass layer is on a flat surface so that it does not break.
6. Wait for 10 minutes before further working with the bonded layers.
7. Do not apply any force to pull the surfaces apart for the next 24 hours.

G

Alternative Methods and Materials

G.1. Actuator Materials and Methods

G.1.1. Actuator Material

Commercially available **SEBS sheets, Flexdym** [11] were tried out for making the actuator half layers. Flexdym pieces, 20 mm x 36 mm, cut out from a 150 mm x 150 mm sheet of thickness 1.2 mm, were hot embossed using the 3D printed mould using the hot embossing press made by Sarah Aalbers [26]. The sample and the mould were preheated to 100°C and then the hot embossing was carried out by raising the temperature to 130°C and applying pressure equal to 0.3 MPa for 3 minutes. After the features were hot embossed into the sheet, the pressure was removed and the Flexdym sheet was peeled off from the mould while still hot. The results obtained can be seen in Figure G.1.

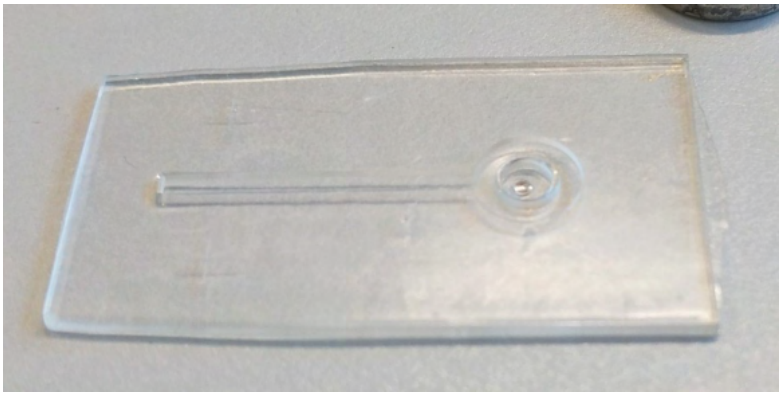

Figure G.1: Hot embossed Flexdym sheet for actuator half layer

Some of the features were obtained with **rounded edges**. Increasing embossing temperature to 150°C and time to 5 minutes did not solve this issue completely. To bond two actuator half layers, they were aligned together and placed between two glass slides held under pressure with the help of clips. This arrangement was placed in the oven at 80°C for 1 hour. The bond obtained was not strong enough to ensure an air tight seal at the actuator wall. The reason for this could be that the surfaces of the Flexdym actuator half layers had some undulations which do not allow for proper contact. Lack of a set-up which could apply distributed pressure for bonding could also be another reason.

Flexdym does not bond well to PDMS and a method to make porous Flexdym membranes would have to be developed. Due to these reasons **hot embossing of Flexdym was not chosen as the method to manufacture actuator half layers**. According to the manufacturers porous Flexdym membranes

should be commercially available by the end of 2021. That, along with the optimization of the bonding process, could make the use of this material suitable for the designed LOC device.

The Flexdym sample sheets were provided by Eden Tech representative Marjan Abdorahim (marjan.abdorahim@eden-microfluidics.com) on request.

G.1.2. Actuator Assembly Method

An alternative method for actuator assembly. This method is only suited for membranes up to 25 μm in thickness as at higher thickness the bonding between the two may not be proper due to the step created by the membrane. To accommodate thicker membranes the actuator wall height needs to be reduced.

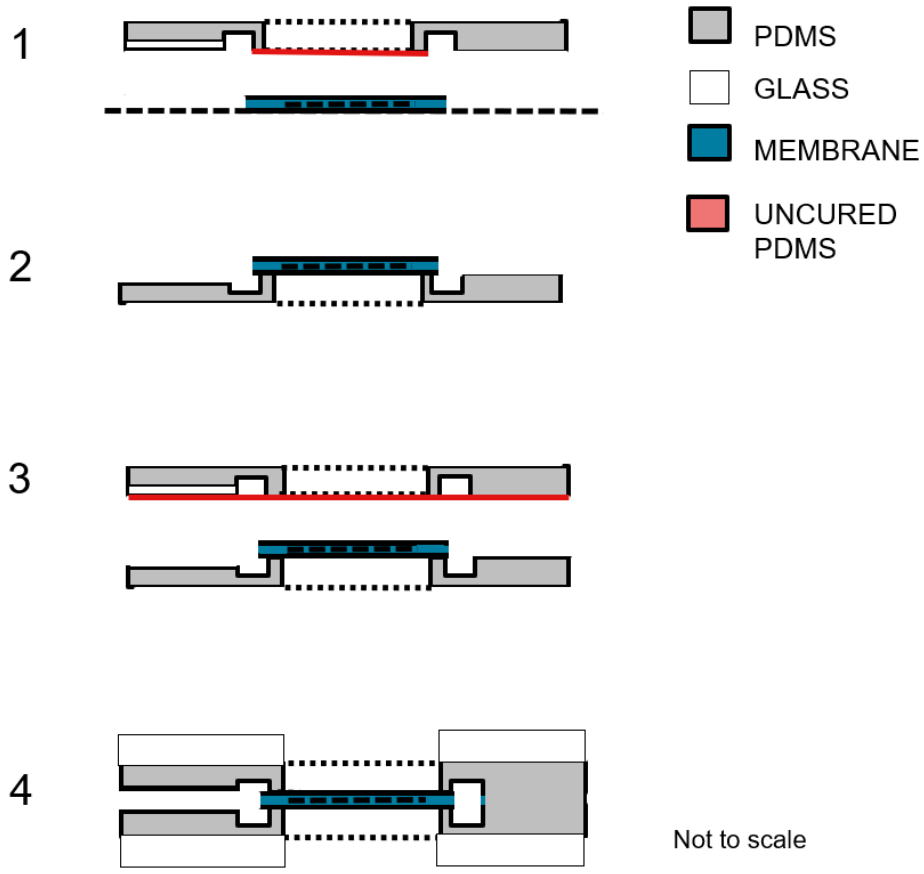

Figure G.2: Sequence for assembling the actuator. (1) Bond the half PDMS actuator layer to the PDMS membrane. (2) Peel the membrane from the substrate. (3) Bond the other half actuator PDMS layer on top. (4) Sandwich the actuator layer between glass layers to provide support to the actuator walls.

G.2. Porous PDMS Membrane

A **laser cutter** was used to make pores in a cured PDMS membrane. A 25 μm layer of PDMS prepolymer was spin coated onto a glass slide coated with Pluronic® F-127. It was cured at the desired temperature and then the pores were laser cut using OPTEC laser cutter. The laser has a resolution of 20 μm so pores smaller than that are not possible to achieve. Thus a pore array with pitch 150 μm was cut out, the pores were drawn as points in the input drawing for the laser. The results obtained can be seen in Figure G.3. The pore diameter was found to be $40 \pm 5 \mu m$ which was too large for the required application. There was also significant damage to the PDMS membrane on the edges of the

cut pores. In cell culture experiments the cells passed through the pores while being seeded on to the membrane and none of the cells survived after 7 days of seeding onto this porous membrane. Damage to the PDMS in the zone around the pores can be responsible for this.

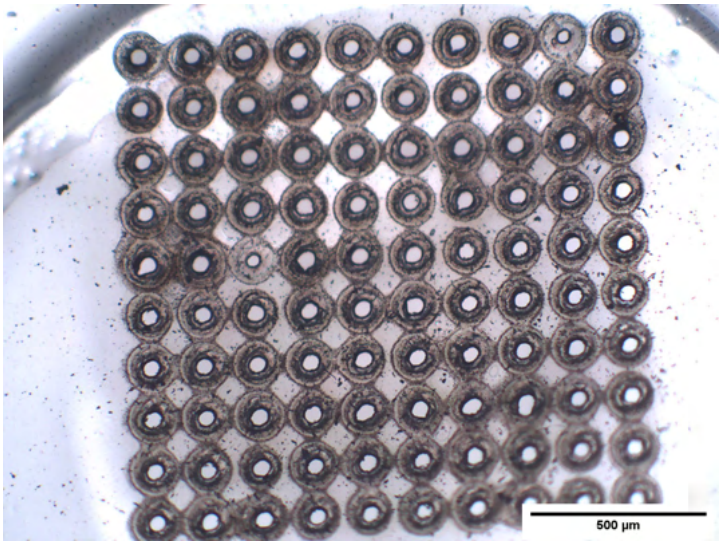

Figure G.3: Laser cut pores in 10μm thick PDMS membrane. The pores have a diameter of $40 \pm 5\mu m$ and a pitch of 150μm

G.3. Channels

G.3.1. Channel Material

The channels can also be made by hot embossing COC or PC. The same was tried using Sarah's press. A 1 mm thick TOPAS sheet was embossed as per the method devised by Sarah [26]. For the 0.25 mm thick PC sheet the hot embossing was done at 153°C under 0.3 MPa pressure. The PC sheet being thinner had a lot of undesired deformation as well. The results can be seen in Figure G.4. It was noticed that COC and PC sheets thinner than 0.5 mm were flexible and could be easily bent. Bonding the embossed channel sheet to another sheet to close the channels and then bonding the channels to the actuator was more complex than just using plasma to activate the surface as in case of PDMS and glass. For these reasons, these materials were not considered further. However, methods to bond PDMS to COC, PDMS to PC and SEBS to COC have been demonstrated and can be considered if the channels are to be made out of these materials [11, 43].

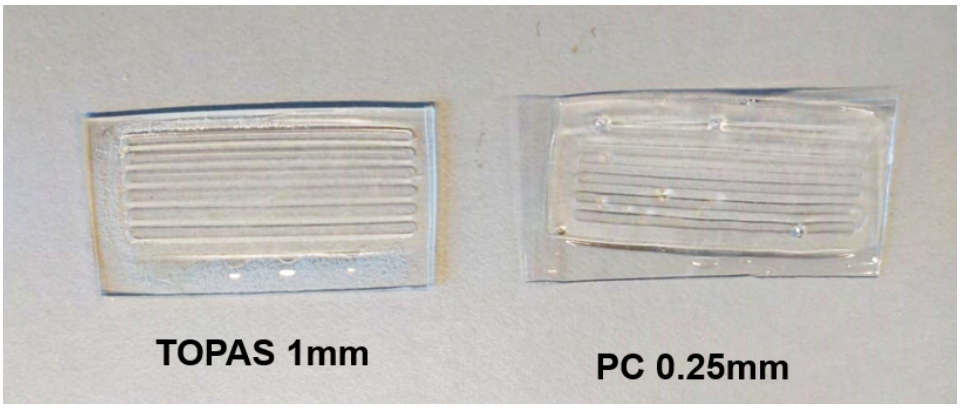

Figure G.4: Channels hot embossed into TOPAS and PC

G.3.2. Channel Layout

A different layout of the channels was also tried out, as shown in Figure G.5. This layout does not require the cover slip to be laser cut and a standard 18 mm x 18 mm cover slip can be used. But the dead volume is greater than the selected channel layout. This layout was not selected as during testing it turned out that a larger area of the cover slip made removing the cover slip with the thin PDMS layer from the substrate tougher and the surface of the thin PDMS layer is not completely flat and has undulations which cause low quality bonding. Such undulations increase with increasing the surface area. The cut out channels can be seen in Figure G.6.

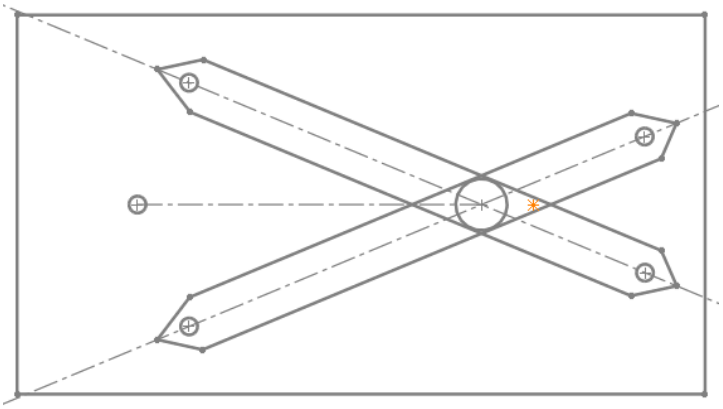

Figure G.5: Drawing for tracing out channels Version 2.

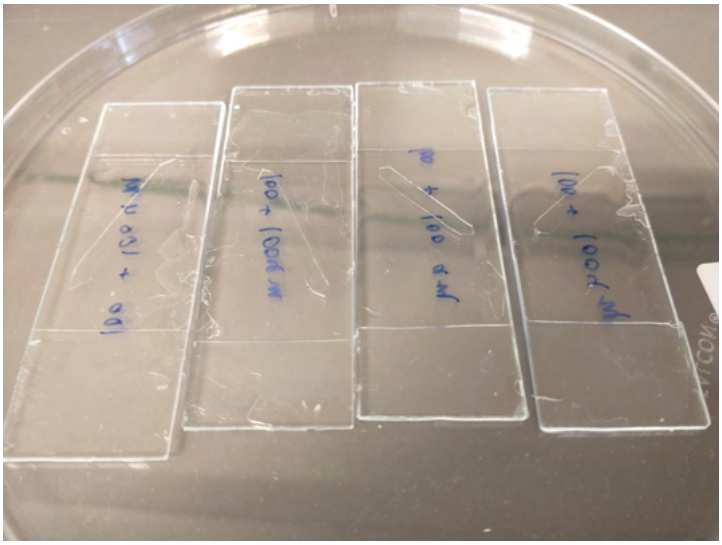

Figure G.6: Channels cut out in 200 μm thick PDMS layer on a glass slides.

H

Manufacturing

H.1. PDMS Spin Coating

The thickness of a spin coated layer of PDMS depends on the spinning speed, spinning time, PDMS base polymer to resin ratio, temperature, placement and volume of PDMS prepolymer on the substrate [76]. For the purpose of this project the spinning time and duration were controlled, the results with this were found to be more than satisfactory for the current application. For thinner PDMS membranes other parameters may also need to be controlled. The spinning speed and duration used for this project are given in Table H.1[41].

Table H.1: Spin coating of PDMS layers

Thickness	Spinning Speed (rpm)	Spinning Duration
10 μm	2500	5 min
25 μm	1000	5 min
40 μm	1000	2.5 min
100 μm	750	1 min
200 μm	400	1 min

H.2. Pillar Mould

The procedure for making the pillars for making the porous membrane as provided by Ahmed Sharaf:

"Pillars of 8 μm made of IP-S material were printed on Silicon substrates via two-photon polymerization using the Nanoscribe PPGT+ 3D printer (Nanoscribe GmbH Co. KG.) in dip-in laser lithography (DiLL) configuration. The wavelength of the femtosecond laser used for printing was 780 nm. The pillars were designed in SOLIDWORKS and then exported as (stl) files before they were sliced into vertical layers and hatched into horizontal lines in Describe program which is the proprietary program of Nanoscribe GmbH Co. KG. Printing took place in Galvo mode in which the structure was printed line by line (horizontally) and layer by layer (vertically).

Prior to printing, the Silicon substrates were treated with oxygen plasma at 0.2 mbar and 80 W for 10 minutes and then coated with 3-(Trimethoxysilyl)propyl methacrylate (MAPTMS) (2% v/v in ethanol) to improve the adhesion of structures to the substrate. The objective used for printing was a 25x Zeiss objective (0.8 numerical aperture). The laser power used was 50 mW and the scanning speed was 100,000 micrometer/s.

After printing, the samples were developed in propylene glycol monomethyl ether acetate (PGMEA) for 25 minutes to dissolve the unpolymerized resin and then directly moved to iso-propyl alcohol for 5 minutes to wash off the residues of the PGMEA/resin solution. Afterwards, they were dipped for 30 seconds in methoxyperfluorobutane before they were dried by a gentle stream of air using an air gun. Methoxyperfluorobutane was used as a last step owing to its very low surface tension which guaranteed applying as little stress on the structures as possible to prevent their collapse."

Testing Data

I.1. White Light Interferometry Data

The different measurements for the 10 μm PDMS membrane corresponding to different flow rates are given in Figure I.2. The Figure I.1 summarizes the measurement data and gives the calculated deflection.

	Distance from top surface	Deflection
Zero flow	1080 um	0
7 ml/min	513 um	567 um
- 7 ml/min	1708 um	-628 um
3 ml/min	759 um	321 um
- 3 ml/min	1533 um	-453 um
-6 ml/min	1700 um	-620 um
-2.6 ml/min	1523 um	-443 um

Figure I.1: Membrane out of plane deflection

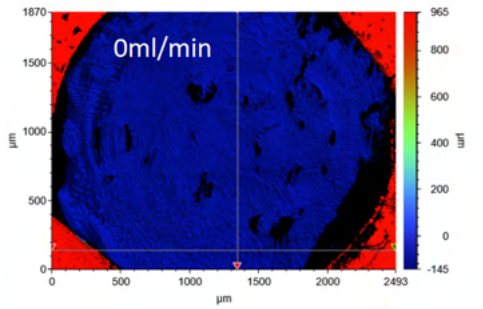
0ml/min

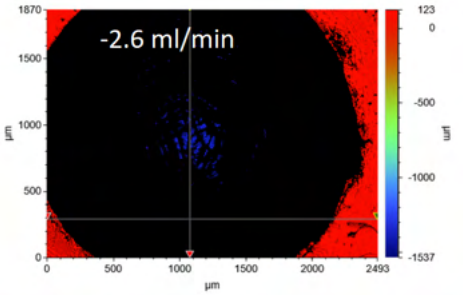
-2.6 ml/min

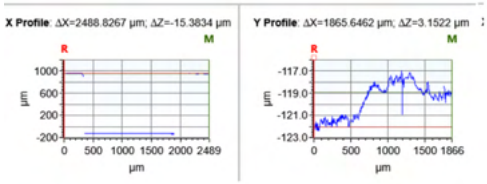
X Profile: ΔX=2488.8267 µm; ΔZ=-15.3834 µm
Y Profile: ΔX=1865.6462 µm; ΔZ=3.1522 µm

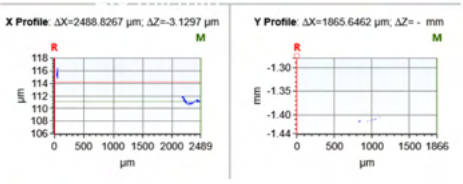
X Profile: ΔX=2488.8267 µm; ΔZ=-3.1297 µm
Y Profile: ΔX=1865.6462 µm; ΔZ= - mm

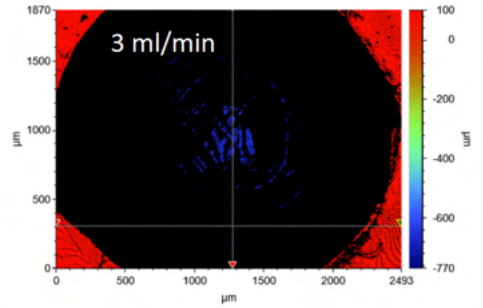
3 ml/min

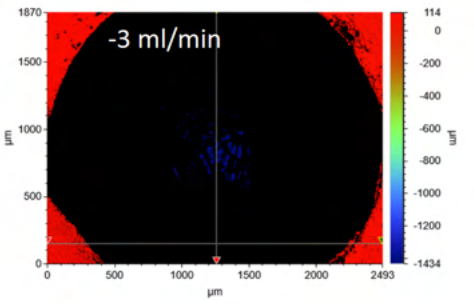
-3 ml/min

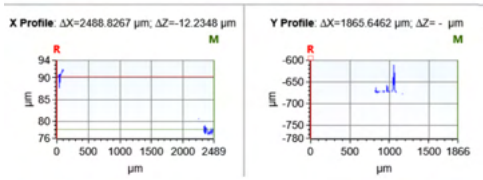
X Profile: ΔX=2488.8267 µm; ΔZ=-12.2348 µm
Y Profile: ΔX=1865.6462 µm; ΔZ= - µm

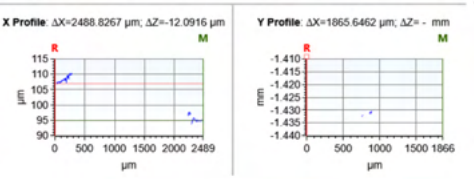
X Profile: ΔX=2488.8267 µm; ΔZ=-12.0916 µm
Y Profile: ΔX=1865.6462 µm; ΔZ= - mm

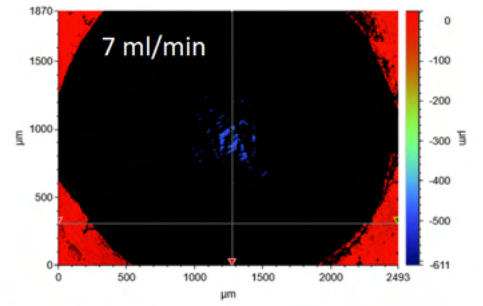
7 ml/min

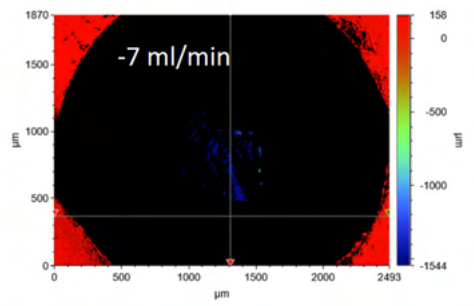
-7 ml/min

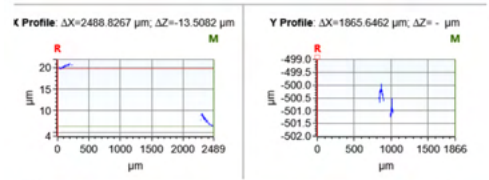
X Profile: ΔX=2488.8267 µm; ΔZ=-13.5082 µm
Y Profile: ΔX=1865.6462 µm; ΔZ= - µm

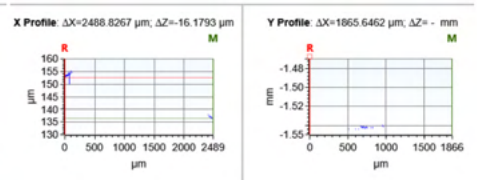
X Profile: ΔX=2488.8267 µm; ΔZ=-16.1793 µm
Y Profile: ΔX=1865.6462 µm; ΔZ= - mm

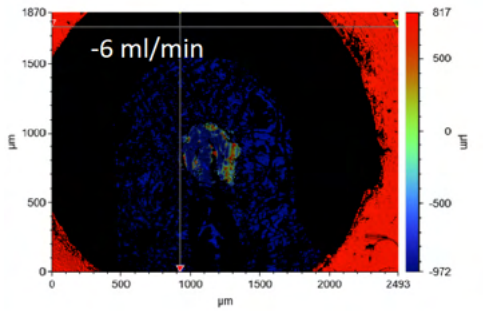
-6 ml/min

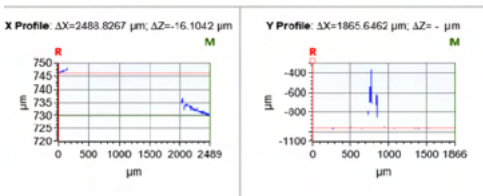
X Profile: ΔX=2488.8267 µm; ΔZ=-16.1042 µm
Y Profile: ΔX=1865.6462 µm; ΔZ= - µm

J

Failure Modes

The device can fail to function as desired due to several reasons based on manufacturing, material properties and user handling. Some of the anticipated failure modes are as follows:

1. Leakage in the channels due to failure of the bond between glass layer 2 and actuator half layer or glass layer 3 and actuator half layer. The steps of the plasma bonding process, such as, keeping the layers in contact under pressure for the required duration after plasma bonding or removing particles from the surfaces before carrying out the bonding procedure, not being carried out correctly can be the reason for this.
2. Leakage in the channels due to cracks in glass layer 1 or glass layer 4 due to user handling. The top and bottom glass layers are made of a thin glass coverslip which becomes even more prone to breakage after the holes are laser cut into it. Thus, not applying excessive force to bond the coverslips to seal the channels is recommended.
3. Bubbles leaking into the culture media channel due to improper sealing of connections and tubing. To prevents this, ensure that all tubing is fitted properly to the connectors and seal the connections with Parafilm if the problem persists.
4. Leakage of culture media into the vacuum channel due to failure of the bond between actuator half layers and the porous membrane. To prevent this, before curing the thin PDMS layers for bonding the actuator half layers to the membrane, it must be ensured that the layers are well aligned and the uncured PDMS for bonding is in contact with both the surfaces.
5. Detachment of the coverslips. This can lead to disruption of flow in culture media channel and ultimately lead to cell death due to lack of availability of culture media. Using a glue to bond the coverslip on, after the cells have been seeded, or using an external holder to hold the coverslips against the device glass surface is recommended.
6. Piercing the cell culture membrane while pipetting liquids for surface treatment or cells onto it. To prevent this, contact of the membrane with the pipette tip must be avoided while using the device.
7. Blockage of channels due to debris getting stuck in the channel, in the volume between the glass layers, before it is sealed by a coverslip. This will cause the flow in the channel to vary from the desired flow. The debris must be flushed out before sealing the channel.

Bibliography

[1] Lab equipment and lab supplies, fisher scientific. URL https://www.fishersci.com/us/en/browse/90111011/cell-culture-dishes.

[2] Nanoscribe photoresins specifically designed for two-photon polymerization. URL https://www.nanoscribe.com/en/products/ip-resins.

[3] Phalloidin. URL https://www.thermofisher.com/order/catalog/product/P3457#/P3457.

[4] Pluronic® f-127 powder, bioreagent, suitable for cell culture: Sigma-aldrich. URL https://www.sigmaaldrich.com/NL/en/product/sigma/p2443.

[5] Pulmonary alveolus, wikipedia. URL https://en.wikipedia.org/wiki/Pulmonary_alveolus.

[6] Organs-on-chips with integrated electrodes for trans-epithelial electrical resistance (TEER) measurements of human epithelial barrier function. *Lab on a Chip*, 17(13):2264–2271, 2017. ISSN 14730189. doi: 10.1039/c7lc00155j.

[7] A durable and biocompatible ascorbic acid-based covalent coating method of polydimethylsiloxane for dynamic cell culture. 14(132), 2017.

[8] Fluid recirculation for cell perfusion with reduced shear stress, Jan 2019. URL https://www.fluigent.com/applications/fluid-recirculation-for-cell-perfusion-with-reduced-shear-stress/.

[9] Human organs-on-chips, wyss institute, Retrieved May 2020. URL https://wyss.harvard.edu/technology/human-organs-on-chips/.

[10] Bi/ond, empowering biological innovation by engineering microchips through nourishing, stimulating and monitoring cells., Apr 2021. URL https://www.gobiond.com/.

[11] Flexdym starter pack - alternative to pdms, Jul 2021. URL https://eden-microfluidics.com/eden-materials/flexdym-pack-alternative-to-pdms/.

[12] Ob1 mk3+ microfluidic flow controller, Feb 2021. URL https://www.elveflow.com/microfluidic-products/microfluidics-flow-control-systems/ob1-pressure-controller/.

[13] New pressure controller: Lineup series, Feb 2021. URL https://www.fluigent.com/product/microfluidic-components-3/lineup-series-push-pull/.

[14] Cell culture plastics: Thermo fisher scientific - us, accessed October 23, 2020. URL https://www.thermofisher.com/nl/en/home/life-science/cell-culture/cell-culture-plastics.html.

[15] Sensor integration, Retrieved 29-10-2020. URL https://www.micronit.com/technologies/functionalities/sensor-integration.

[16] Lung-on-chip system, alveolix, Retrieved 4-11-2020. URL https://www.alveolix.com/our-products/.

[17] Membrane chips, microfluidic-chipshop, Retrieved 4-11-2020. URL https://www.microfluidic-chipshop.com/catalogue/microfluidic-chips/polymer-chips/membrane-chips/.

[18] Organ-on-chip, aline inc., Retrieved 4-11-2020. URL https://alineinc.com/our-products/organ-on-chip/.

[19] Lung-chip, emulate, Retrieved 4-11-2020. URL https://www.emulatebio.com/lung-chip.

[20] µ-slide membrane ibipore flow, Retrieved 4-11-2020. URL https://ibidi.com/channel-slides/247--slide-membrane-ibipore-flow.html.

[21] Organ-on-a-chip systems, micronit technologies, Retrieved 4-11-2020. URL https://www.micronit.com/microfluidics/sensorised-ooc.

[22] Organoplate®-3-lane, mimetas, Retrieved 4-11-2020. URL https://mimetas.com/page/organoplate®-3-lane.

[23] Synali lung model – air liquid interface-based lung model, synvivo, Retrieved 4-11-2020. URL https://www.synvivobio.com/synali-lung-model/.

[24] Humimic chips – superpowers for superb insights, Retrieved 4-11-2020. URL https://www.tissuse.com/en/humimic/chips/.

[25] Microfluidics, topas advanced polymers/polyplastics, Retrieved 4-11-2020. URL https://topas.com/markets/diagnostics/microfluidics.

[26] Sarah Aalbers. Low-cost benchtop equipment and procedures for organ-on-chip prototyping. Master's thesis, TU Delft, 2021. URL http://resolver.tudelft.nl/uuid:b5dbf40f-e405-4aa4-9d74-e320c43681b1.

[27] Jason Adamson, Linsey E Haswell, Gary Phillips, and Marianna D Gaça. In vitro models of chronic obstructive pulmonary disease (copd). In Ignacio Martin-Loeches, editor, *Bronchitis*, chapter 3. IntechOpen, Rijeka, 2011. doi: 10.5772/18247. URL https://doi.org/10.5772/18247.

[28] Fahima Akther, Shazwani Binte Yakob, Nam Trung Nguyen, and Hang T. Ta. Surface Modification Techniques for Endothelial Cell Seeding in PDMS Microfluidic Devices. *Biosensors*, 10(11), 2020. ISSN 20796374. doi: 10.3390/bios10110182.

[29] Joji Ando and Kimiko Yamamoto. Effects of shear stress and stretch on endothelial function. *Antioxidants and Redox Signaling*, 15(5):1389–1403, 2011. ISSN 15230864. doi: 10.1089/ars.2010.3361.

[30] Christelle ANGELY. Comparing the accuracy of syringe pumps, peristaltic pumps and pressure controllers, Apr 2021. URL https://darwin-microfluidics.com/blogs/reviews/comparing-the-accuracy-of-syringe-pumps-peristaltic-pumps-and-pressure-controllers.

[31] Bavani Balakrisnan, Sheetal Patil, and Elisabeth Smela. Patterning pdms using a combination of wet and dry etching. *J. Micromech. Microeng*, 3532:203–47002, 07 2009. doi: 10.1088/0960-1317/19/4/047002.

[32] Layla J. Barkal, Clare L. Procknow, Yasmín R. Álvarez-Garciá, Mengyao Niu, José A. Jiménez-Torres, Rebecca A. Brockman-Schneider, James E. Gern, Loren C. Denlinger, Ashleigh B. Theberge, Nancy P. Keller, Erwin Berthier, and David J. Beebe. Microbial volatile communication in human organotypic lung models. *Nature Communications*, 8(1), 2017. ISSN 20411723. doi: 10.1038/s41467-017-01985-4. URL http://dx.doi.org/10.1038/s41467-017-01985-4.

[33] Layla J. Barkal, Clare L. Procknow, Yasmín R. Álvarez-Garciá, Mengyao Niu, José A. Jiménez-Torres, Rebecca A. Brockman-Schneider, James E. Gern, Loren C. Denlinger, Ashleigh B. Theberge, Nancy P. Keller, Erwin Berthier, and David J. Beebe. Microbial volatile communication in human organotypic lung models. *Nature Communications*, 8(1), 2017. ISSN 20411723. doi: 10.1038/s41467-017-01985-4.

[34] Kambez H. Benam, Richard Novak, Janna Nawroth, Mariko Hirano-Kobayashi, Thomas C. Ferrante, Youngjae Choe, Rachelle Prantil-Baun, James C. Weaver, Anthony Bahinski, Kevin K. Parker, and Donald E. Ingber. Matched-Comparative Modeling of Normal and Diseased Human Airway Responses Using a Microengineered Breathing Lung Chip. *Cell Systems*, 3(5):456–466.e4, 2016. ISSN 24054720. doi: 10.1016/j.cels.2016.10.003. URL http://dx.doi.org/10.1016/j.cels.2016.10.003.

[35] Kambez H. Benam, Remi Villenave, Carolina Lucchesi, Antonio Varone, Cedric Hubeau, Hyun Hee Lee, Stephen E. Alves, Michael Salmon, Thomas C. Ferrante, James C. Weaver, Anthony Bahinski, Geraldine A. Hamilton, and Donald E. Ingber. Small airway-on-a-chip enables analysis of human lung inflammation and drug responses in vitro. *Nature Methods*, 13(2):151–157, 2016. ISSN 15487105. doi: 10.1038/nmeth.3697.

[36] Kambez H. Benam, Remi Villenave, Carolina Lucchesi, Antonio Varone, Cedric Hubeau, Hyun Hee Lee, Stephen E. Alves, Michael Salmon, Thomas C. Ferrante, James C. Weaver, Anthony Bahinski, Geraldine A. Hamilton, and Donald E. Ingber. Small airway-on-a-chip enables analysis of human lung inflammation and drug responses in vitro. *Nature Methods*, 13(2):151–157, 2016. ISSN 15487105. doi: 10.1038/nmeth.3697.

[37] Cornelia Blume, Riccardo Reale, Marie Held, Timothy M. Millar, Jane E. Collins, Donna E. Davies, Hywel Morgan, and Emily J. Swindle. Temporal monitoring of differentiated human airway epithelial cells using microfluidics. *PLOS ONE*, 10(10):1–13, 10 2015. doi: 10.1371/journal.pone.0139872. URL https://doi.org/10.1371/journal.pone.0139872.

[38] Chantal Broek, Rolf Pullens, Ole Frøbert, Marcel Rutten, Wilfred Hartog, and Frans van de Vosse. Medium with blood-analog mechanical properties for cardiovascular tissue culturing. *Biorheology*, 45:651–61, 02 2008. doi: 10.3233/BIR-2008-0513.

[39] Henrik Bruus. *Theoretical Microfluidics*. Oxford University Press, Oxford, 2008.

[40] Marc Antoine Campeau, Audrey Lortie, Pierrick Tremblay, Marc Olivier Béliveau, Dominic Dubé, Ève Langelier, and Léonie Rouleau. Effect of manufacturing and experimental conditions on the mechanical and surface properties of silicone elastomer scaffolds used in endothelial mechanobiological studies. *BioMedical Engineering Online*, 16(1):1–23, 2017. ISSN 1475925X. doi: 10.1186/s12938-017-0380-5.

[41] Sébastien Cargou. Pdms membrane: thickness of a spin coated pdms layer, Dec 2020. URL https://www.elveflow.com/microfluidic-reviews/soft-lithography-microfabrication/pdms-membrane-thickness-of-a-spin-coated-pdms-layer/.

[42] Michael Chappell and Stephen Payne. *The Respiratory System*, pages 125–139. Springer International Publishing, Cham, 2020. ISBN 978-3-030-39705-0. doi: 10.1007/978-3-030-39705-0_9. URL https://doi.org/10.1007/978-3-030-39705-0_9.

[43] Barbara Cortese, Matthew Mowlem, and Morgan. Characterisation of an irreversible bonding process for coc-coc and coc-pdms-coc sandwich structures and application to microvalves. *Sensors and Actuators B Chemical*, 160, 12 2011. doi: 10.1016/j.snb.2011.07.040.

[44] P. F. Davies. Flow-mediated endothelial mechanotransduction. *Physiological Reviews*, 75(3):519–560, 1995. doi: 10.1152/physrev.1995.75.3.519. URL https://doi.org/10.1152/physrev.1995.75.3.519. PMID: 7624393.

[45] Stefanie Deinhardt-Emmer, Knut Rennert, Elisabeth Schicke, Zoltán Cseresnyés, Maximilian Windolph, Sandor Nietzsche, Regine Heller, Fatina Siwczak, Karoline Haupt, Swen Carlstedt, Michael Schacke, Marc Figge, Christina Ehrhardt, Bettina Löffler, and Alexander Mosig. Co-infection with staphylococcus aureus after primary influenza virus infection leads to damage of the endothelium in a human alveolus-on-a-chip model. *Biofabrication*, 12, 01 2020. doi: 10.1088/1758-5090/ab7073.

[46] Karel Domansky, Josiah D. Sliz, Norman Wen, Christopher Hinojosa, Guy Thompson, Jacob P. Fraser, Tiama Hamkins-Indik, Geraldine A. Hamilton, Daniel Levner, and Donald E. Ingber. SEBS elastomers for fabrication of microfluidic devices with reduced drug absorption by injection molding and extrusion. *Microfluidics and Nanofluidics*, 21(6):1–12, 2017. ISSN 16134990. doi: 10.1007/s10404-017-1941-4.

[47] Dongeun Huh, Benjamin D. Matthews, Akiko Mammoto, Martín Montoya-Zavala, Hong Yuan Hsin, Donald E. Ingber. Reconstituting Organ-Level Lung. *Science*, (June):1662–1668, 2010. doi: 10.1126/science.1188302.

[48] Ali Doryab, Ghassem Amoabediny, and Amir Salehi-Najafabadi. Advances in pulmonary therapy and drug development: Lung tissue engineering to lung-on-a-chip. *Biotechnology Advances*, 34(5):588–596, 2016. ISSN 07349750. doi: 10.1016/j.biotechadv.2016.02.006. URL http://dx.doi.org/10.1016/j.biotechadv.2016.02.006.

[49] Nicholas J. Douville, Yi Chung Tung, Ran Li, Jack D. Wang, Mohamed E.H. El-Sayed, and Shuiohi Takayama. Fabrication of two-layered channel system with embedded electrodes to measure resistance across epithelial and endothelial barriers. *Analytical Chemistry*, 82(6):2505–2511, 2010. ISSN 00032700. doi: 10.1021/ac9029345.

[50] Nicholas J. Douville, Parsa Zamankhan, Yi Chung Tung, Ran Li, Benjamin L. Vaughan, Cheng Feng Tai, Joshua White, Paul J. Christensen, James B. Grotberg, and Shuichi Takayama. Combination of fluid and solid mechanical stresses contribute to cell death and detachment in a microfluidic alveolar model. *Lab on a Chip*, 11(4):609–619, 2011. ISSN 14730189. doi: 10.1039/c0lc00251h.

[51] Mark Eddings, Michael Johnson, and Bruce Gale. Note: Determining the optimal pdms pdms bonding technique for microfluidic devices. *Journal of Micromechanics and Microengineering - J MICROMECHANIC MICROENGINEER*, 18, 06 2008. doi: 10.1088/0960-1317/18/6/067001.

[52] Marcel Felder, Bettina Trueeb, Andreas Stucki, Sarah Borcard, Janick Stucki, Bruno Schnyder, Thomas Geiser, and Olivier Guenat. Impaired wound healing of alveolar lung epithelial cells in a breathing lung-on-a-chip. *Frontiers in Bioengineering and Biotechnology*, 7, 01 2019. doi: 10.3389/fbioe.2019.00003.

[53] Nuris Figueroa-Morales, Gastón Miño, Aramis Rivera, Rogelio Caballero, E. Clément, Ernesto Altshuler, and Anke Lindner. Living on the edge: Transfer and traffic of e. coli in a confined flow. *Soft Matter*, 11, 04 2015. doi: 10.1039/C5SM00939A.

[54] Rami Fishler, Molly K. Mulligan, and Josué Sznitman. Acinus-on-a-chip: A microfluidic platform for pulmonary acinar flows. *Journal of Biomechanics*, 46(16):2817–2823, 2013. ISSN 00219290. doi: 10.1016/j.jbiomech.2013.08.020.

[55] Rami Fishler, Philipp Hofemeier, Yael Etzion, Yael Dubowski, and Josué Sznitman. Particle dynamics and deposition in true-scale pulmonary acinar models. *Scientific Reports*, 5:1–11, 2015. ISSN 20452322. doi: 10.1038/srep14071.

[56] Redrawn from Weibel ER. Morphometry of the Human Lung . Berlin: Springer Verlag; 1963. Data from Bouhuys A. The Physiology of Breathing . New York: Grune Stratton; 1977. Overview of the respiratory system: Function and structure, Retrieved Oct 2019. URL https://thoracickey.com/overview-of-the-respiratory-system-function-and-structure/.

[57] J. Garra, T. Long, J. Currie, T. Schneider, R. White, and M. Paranjape. Dry etching of polydimethylsiloxane for microfluidic systems. *Journal of Vacuum Science & Technology A: Vacuum, Surfaces, and Films*, 20(3):975–982, may 2002. ISSN 0734-2101. doi: 10.1116/1.1460896. URL http://avs.scitation.org/doi/10.1116/1.1460896.

[58] Mahboobe Ghaedi, Elizabeth A. Calle, Julio J. Mendez, Ashley L. Gard, Jenna Balestrini, Adam Booth, Peter F. Bove, Liqiong Gui, Eric S. White, and Laura E. Niklason. Human ips cell–derived alveolar epithelium repopulates lung extracellular matrix. *The Journal of Clinical Investigation*, 123(11):4950–4962, 11 2013. doi: 10.1172/JCI68793. URL https://www.jci.org/articles/view/68793.

[59] J. Gil, H. Bachofen, P. Gehr, and E. R. Weibel. Alveolar volume-surface area relation in air- and saline-filled lungs fixed by vascular perfusion. *Journal of Applied Physiology*, 47(5):990–1001, 1979. doi: 10.1152/jappl.1979.47.5.990. URL https://doi.org/10.1152/jappl.1979.47.5.990. PMID: 511725.

[60] PreSens Precision Sensing GmbH. URL https://www.presens.de/fileadmin/user_upload/brochures/190731_cawe_Presens_O2_Broschuere_07-19_dv3_web.pdf.

[61] Ray Greek and Andre Menache. Systematic reviews of animal models: Methodology versus epistemology. *International Journal of Medical Sciences*, 10(3):206–221, 2013. ISSN 14491907. doi: 10.7150/ijms.5529.

[62] Olivier T. Guenat and François Berthiaume. Incorporating mechanical strain in organs-on-a-chip: Lung and skin. *Biomicrofluidics*, 12(4), 2018. ISSN 19321058. doi: 10.1063/1.5024895.

[63] Bryan A. Hassell, Girija Goyal, Esak Lee, Alexandra Sontheimer-Phelps, Oren Levy, Christopher S. Chen, and Donald E. Ingber. Human Organ Chip Models Recapitulate Orthotopic Lung Cancer Growth, Therapeutic Responses, and Tumor Dormancy In Vitro. *Cell Reports*, 21(2):508–516, 2017. ISSN 22111247. doi: 10.1016/j.celrep.2017.09.043. URL https://doi.org/10.1016/j.celrep.2017.09.043.

[64] Irving P. Herman. *Lungs and Breathing*, pages 623–655. Springer International Publishing, Cham, 2016. ISBN 978-3-319-23932-3. doi: 10.1007/978-3-319-23932-3_9. URL https://doi.org/10.1007/978-3-319-23932-3_9.

[65] Iris Hermanns, Ronald Unger, Kai Kehe, Kirsten Peters, and Charles Kirkpatrick. Lung epithelial cell lines in coculture with human pulmonary microvascular endothelial cells: Development of an alveolo-capillary barrier in vitro. *Laboratory investigation; a journal of technical methods and pathology*, 84:736–52, 07 2004. doi: 10.1038/labinvest.3700081.

[66] Wei Hou, Siyi Hu, Ken tye Yong, Jie Zhang, and Hanbin Ma. Cigarette smoke-induced malignant transformation via STAT3 signalling in pulmonary epithelial cells in a lung-on-a-chip model. *Bio-Design and Manufacturing*, pages 383–395, 2020. ISSN 25228552. doi: 10.1007/s42242-020-00092-6.

[67] Dongeun Huh. A human breathing lung-on-a-chip. *Annals of the American Thoracic Society*, 12(March):S42–S44, 2015. ISSN 23256621. doi: 10.1513/AnnalsATS.201410-442MG.

[68] Dongeun Huh, Hideki Fujioka, Yi Chung Tung, Nobuyuki Futai, Robert Paine, James B. Grotberg, and Shuichi Takayama. Acoustically detectable cellular-level lung injury induced by fluid mechanical stresses in microfluidic airway systems. *Proceedings of the National Academy of Sciences of the United States of America*, 104(48):18886–18891, 2007. ISSN 00278424. doi: 10.1073/pnas.0610868104.

[69] Mouhita Humayun, Chung Wai Chow, and Edmond W.K. Young. Microfluidic lung airway-on-a-chip with arrayable suspended gels for studying epithelial and smooth muscle cell interactions. *Lab on a Chip*, 18(9):1298–1309, 2018. ISSN 14730189. doi: 10.1039/c7lc01357d.

[70] Mouhita Humayun, Chung Wai Chow, and Edmond W.K. Young. Microfluidic lung airway-on-a-chip with arrayable suspended gels for studying epithelial and smooth muscle cell interactions. *Lab on a Chip*, 18(9):1298–1309, 2018. ISSN 14730189. doi: 10.1039/c7lc01357d.

[71] Muhammad Asad Ullah Khalid, Young Soo Kim, Muhsin Ali, Byung Gul Lee, Young Jae Cho, and Kyung Hyun Choi. A lung cancer-on-chip platform with integrated biosensors for physiological monitoring and toxicity assessment. *Biochemical Engineering Journal*, 155(December 2019), 2020. ISSN 1873295X. doi: 10.1016/j.bej.2019.107469.

[72] K. Khanafer, A. Duprey, M. Schlicht, and R. Berguer. Effects of strain rate, mixing ratio, and stress–strain definition on the mechanical behavior of the polydimethylsiloxane (pdms) material as related to its biological applications. *Biomedical Microdevices*, 11:503–508, 2009.

[73] Tae Kyung Kim, Jeong Koo Kim, and Ok Chan Jeong. Measurement of nonlinear mechanical properties of PDMS elastomer. *Microelectronic Engineering*, 88(8):1982–1985, 2011. ISSN 01679317. doi: 10.1016/j.mee.2010.12.108. URL http://dx.doi.org/10.1016/j.mee.2010.12.108.

[74] Lars Knudsen and Matthias Ochs. The micromechanics of lung alveoli: structure and function of surfactant and tissue components. *Histochemistry and Cell Biology*, 150(6):661–676, 2018. ISSN 1432119X. doi: 10.1007/s00418-018-1747-9. URL http://dx.doi.org/10.1007/s00418-018-1747-9.

[75] Aristotle G. Koutsiaris, Sophia V. Tachmitzi, Nick Batis, Maria G. Kotoula, Constantinos H. Karabatsas, Evagelia Tsironi, and Dimitrios Z. Chatzoulis. Volume flow and wall shear stress quantification in the human conjunctival capillaries and post-capillary venules in vivo. *Biorheology*, 44(5-6):375–386, 2007. ISSN 0006355X.

[76] Sriram Krishnan. On the manufacture of very thin elastomeric films by spin-coating. 09 2008.

[77] Shreyas Kuddannaya, Yon Jin Chuah, Min Hui Adeline Lee, Nishanth V. Menon, Yuejun Kang, and Yilei Zhang. Surface chemical modification of poly(dimethylsiloxane) for the enhanced adhesion and proliferation of mesenchymal stem cells. *ACS Applied Materials and Interfaces*, 5(19):9777–9784, 2013. ISSN 19448252. doi: 10.1021/am402903e.

[78] Alexandra [Sasha] LANIECE. *Alveoli-on-a-chip*. Theses, Université Paris-Diderot ; Ecole Normale Supérieure de Paris, October 2018. URL https://hal.archives-ouvertes.fr/tel-02050336.

[79] Hai Le-The, Martijn Tibbe, Joshua Loessberg-Zahl, Marciano Palma do Carmo, Marinke van der Helm, Johan Bomer, Albert van den Berg, Anne Leferink, Loes Segerink, and Jan Eijkel. Large-scale fabrication of free-standing and sub-µm pdms through-hole membranes. *Nanoscale*, 10:7711–7718, 2018. doi: 10.1039/C7NR09658E. URL http://dx.doi.org/10.1039/C7NR09658E.

[80] Miao Liu, Jianren Sun, Ying Sun, Christopher Bock, and Quanfang Chen. Thickness-dependent mechanical properties of polydimethylsiloxane membranes. *Journal of Micromechanics and Microengineering*, 19:035028, 02 2009. doi: 10.1088/0960-1317/19/3/035028.

[81] M. Looman. Membrane fouling: Study on fouling inside an organ on a chip. Master's thesis, TU Delft, 2018. URL http://resolver.tudelft.nl/uuid:a6e555ea-0655-4fdd-87aa-f802a0bf1b08.

[82] Isabella W.Y. Mak, Nathan Evaniew, and Michelle Ghert. Lost in translation: Animal models and clinical trials in cancer treatment. *American Journal of Translational Research*, 6(2):114–118, 2014. ISSN 19438141.

[83] Julian R. Marchesi, Stephanie May, Samantha Evans, and Lee Parry. Organoids, organs-on-chips and other systems, and microbiota. *Emerging Topics in Life Sciences*, 1(4):385–400, 11 2017. ISSN 2397-8554. doi: 10.1042/ETLS20170047. URL https://doi.org/10.1042/ETLS20170047.

[84] Alvaro Mata, Aaron J. Fleischman, and Shuvo Roy. Characterization of Polydimethylsiloxane (PDMS) Properties for Biomedical Micro/Nanosystems. *Biomedical Microdevices*, 7(4):281–293, 2005. ISSN 15728781. doi: 10.1007/s10544-005-6070-2.

[85] Mark J. Mondrinos, Yoon-Suk Yi, Nan-Kun Wu, Xueting Ding, and Dongeun Huh. Native extracellular matrix-derived semipermeable, optically transparent, and inexpensive membrane inserts for microfluidic cell culture. *Lab Chip*, 17:3146–3158, 2017. doi: 10.1039/C7LC00317J. URL http://dx.doi.org/10.1039/C7LC00317J.

[86] Divya D. Nalayanda, Christopher Puleo, William B. Fulton, Leilani M. Sharpe, Tza Huei Wang, and Fizan Abdullah. An open-access microfluidic model for lung-specific functional studies at an air-liquid interface. *Biomedical Microdevices*, 11(5):1081–1089, 2009. ISSN 13872176. doi: 10.1007/s10544-009-9325-5.

[87] Michael R Nelson and Krishnendu Roy. A 96-well format microvascularized human lung- on-a-chip platform for microphysiological modeling of fibrotic diseases. 4, 2020. doi: 10.1039/d0lc00644k.

[88] Steve Paxton, Michelle Peckham, and Adele Knibbs. The leeds histology guide, Jan 1970. URL https://www.histology.leeds.ac.uk/blood/blood_wbc.php.

[89] Christine Poon. Measuring the density and viscosity of culture media for optimized computational fluid dynamics analysis of in vitro devices. *bioRxiv*, 2020. doi: 10.1101/2020.08.25.266221.

[90] Firdaus Prabowo, Adrian Law, and Hayley Shen. Effect of curing temperature and cross-linker to pre-polymer ratio on the viscoelastic properties of a pdms elastomer. *Advanced Materials Research*, 1112, 07 2015. doi: 10.4028/www.scientific.net/AMR.1112.410.

[91] Tushar H. Punde, Wen Hao Wu, Pei Chun Lien, Ya Ling Chang, Ping Hsueh Kuo, Margaret Dah Tsyr Chang, Kang Yun Lee, Chien Da Huang, Han Pin Kuo, Yao Fei Chan, Po Chen Shih, and Cheng Hsien Liu. A biologically inspired lung-on-a-chip device for the study of protein-induced lung inflammation. *Integrative Biology (United Kingdom)*, 7(2):162–169, 2015. ISSN 17579708. doi: 10.1039/c4ib00239c.

[92] Zichen Qian, David Ross, Wenkai Jia, Qi Xing, and Feng Zhao. Bioactive polydimethylsiloxane surface for optimal human mesenchymal stem cell sheet culture. *Bioactive Materials*, 3(2):167–173, 2018. ISSN 2452199X. doi: 10.1016/j.bioactmat.2018.01.005. URL https://doi.org/10.1016/j.bioactmat.2018.01.005.

[93] William Quiros-Solano, Nikolas Gaio, Oscar Stassen, Yusuf Arik, Cinzia Silvestri, Nicole van Engeland, Andries van der Meer, Robert Passier, Cecilia Sahlgren, Carlijn Bouten, Albert Van den Berg, R. Dekker, and P.M. Sarro. Microfabricated tuneable and transferable porous pdms membranes for organs-on-chips. *Scientific Reports*, 8, 09 2018. doi: 10.1038/s41598-018-31912-6.

[94] Esra Roan and Christopher M. Waters. What do we know about mechanical strain in lung alveoli? *American Journal of Physiology - Lung Cellular and Molecular Physiology*, 301(5):625–635, 2011. ISSN 10400605. doi: 10.1152/ajplung.00105.2011.

[95] Barbara Rothen-Rutishauser, Loretta Müller, Fabian Blank, Christina Brandenberger, Christian Mühlfeld, and Peter Gehr. A newly developed in vitro model of the human epithelial airway barrier to study the toxic potential of nanoparticles. *ALTEX*, 25:191–6, 02 2008. doi: 10.14573/altex.2008.3.191.

[96] Leonie Rouleau, Joanna Rossi, and Richard Leask. Concentration and time effects of dextran exposure on endothelial cell viability, attachment, and inflammatory marker expression in vitro. *Annals of biomedical engineering*, 38:1451–62, 04 2010. doi: 10.1007/s10439-010-9934-4.

[97] Corning Incorporated Life Sciences. *Corning Cell Culture Product Selection Guide*.

[98] Veronika Sedláková, Michaela Kloučková, Zuzana Garlíková, Kateřina Vašíčková, Josef Jaroš, Mário Kandra, Hana Kotasová, and Aleš Hampl. Options for modeling the respiratory system: inserts, scaffolds and microfluidic chips. *Drug Discovery Today*, 24(4):971–982, 2019. ISSN 18785832. doi: 10.1016/j.drudis.2019.03.006.

[99] Katelyn L. Sellgren, Elizabeth J. Butala, Brian P. Gilmour, Scott H. Randell, and Sonia Grego. A biomimetic multicellular model of the airways using primary human cells. *Lab on a Chip*, 14(17):3349–3358, 2014. ISSN 14730189. doi: 10.1039/c4lc00552j.

[100] Seyed Ali Mousavi Shaegh, Fabio De Ferrari, Yu Shrike Zhang, Mahboubeh Nabavinia, Niema Binth Mohammad, John Ryan, Adel Pourmand, Eleanor Laukaitis, Ramin Banan Sadeghian, Akhtar Nadhman, Su Ryon Shin, Amir Sanati Nezhad, Ali Khademhosseini, and Mehmet Remzi Dokmeci. A microfluidic optical platform for real-time monitoring of pH and oxygen in microfluidic bioreactors and organ-on-chip devices. *Biomicrofluidics*, 10(4):1–14, 2016. ISSN 19321058. doi: 10.1063/1.4955155. URL http://dx.doi.org/10.1063/1.4955155.

[101] Jesus Shrestha, Maliheh Ghadiri, Melane Shanmugavel, Sajad Razavi Bazaz, Steven Vasilescu, Lin Ding, and Majid Ebrahimi Warkiani. A rapidly prototyped lung-on-a-chip model using 3D-printed molds. *Organs-on-a-Chip*, 1(November 2019):100001, 2019. ISSN 26661020. doi: 10.1016/j.ooc.2020.100001. URL https://doi.org/10.1016/j.ooc.2020.100001.

[102] Jesus Shrestha, Maliheh Ghadiri, Melane Shanmugavel, Sajad Razavi Bazaz, Steven Vasilescu, Lin Ding, and Majid Ebrahimi Warkiani. A rapidly prototyped lung-on-a-chip model using 3D-printed molds. *Organs-on-a-Chip*, 1(January): 100001, 2019. ISSN 26661020. doi: 10.1016/j.ooc.2020.100001.

[103] Jesus Shrestha, Sajad Razavi Bazaz, Hamidreza Aboulkheyr Es, Dania Yaghobian Azari, Benjamin Thierry, Majid Ebrahimi Warkiani, and Maliheh Ghadiri. Lung-on-a-chip: the future of respiratory disease models and pharmacological studies. *Critical Reviews in Biotechnology*, 40(2):213–230, 2020. ISSN 15497801. doi: 10.1080/07388551.2019.1710458.

[104] Utku M. Sonmez, Ya-Wen Cheng, Simon C. Watkins, Beth L. Roman, and Lance A. Davidson. Endothelial cell polarization and orientation to flow in a novel microfluidic multimodal shear stress generator. *Lab Chip*, 20:4373–4390, 2020. doi: 10.1039/D0LC00738B. URL http://dx.doi.org/10.1039/D0LC00738B.

[105] S. Soons. Photo-patterned, ph-responsive hydrogel membranes for integrated fluid control. Master's thesis, TU Delft, 2018. URL http://resolver.tudelft.nl/uuid:dacc2ce3-99e5-46dd-ac9e-1aec82e447cb.

[106] W. Sripumkhai, A. Lekwichai, W. Bunjongpru, S. Porntheeraphat, B. Tunhoo, E. Ratanaudomphisut, T. Kamsri, C. Hruanun, A. Poyai, and J. Nukeaw. On-chip platinum micro-heater with platinum temperature sensor for a fully integrated disposable PCR module. *Advanced Materials Research*, 93-94(January):129–132, 2010. ISSN 10226680. doi: 10.4028/www.scientific.net/AMR.93-94.129.

[107] Andreas O. Stucki, Janick D. Stucki, Sean R.R. Hall, Marcel Felder, Yves Mermoud, Ralph A. Schmid, Thomas Geiser, and Olivier T. Guenat. A lung-on-a-chip array with an integrated bio-inspired respiration mechanism. *Lab on a Chip*, 15 (5):1302–1310, 2015. ISSN 14730189. doi: 10.1039/c4lc01252f.

[108] Janick D. Stucki, Nina Hobi, Artur Galimov, Andreas O. Stucki, Nicole Schneider-Daum, Claus Michael Lehr, Hanno Huwer, Manfred Frick, Manuela Funke-Chambour, Thomas Geiser, and Olivier T. Guenat. Medium throughput breathing human primary cell alveolus-on-chip model. *Scientific Reports*, 8(1):1–13, 2018. ISSN 20452322. doi: 10.1038/s41598-018-32523-x.

[109] Synvivo. *SynALI 3D Lung Model Using Idealized Microvascular Network*. Synvivo, accessed November 5, 2020.

[110] Janna Tenenbaum-Katan, Rami Fishler, Barbara Rothen-Rutishauser, and Josué Sznitman. Microfluidic in vitro platforms of pulmonary alveolar physiology. In Igor Lacković and Darko Vasic, editors, *6th European Conference of the International Federation for Medical and Biological Engineering*, pages 777–780, Cham, 2015. Springer International Publishing. ISBN 978-3-319-11128-5.

[111] Janna Tenenbaum-Katan, Arbel Artzy-Schnirman, Rami Fishler, Netanel Korin, and Josue Sznitman. Biomimetics of the pulmonary environment in vitro: A microfluidics perspective. *Biomicrofluidics*, 12(4), 2018. ISSN 19321058. doi: 10.1063/1.5023034.

[112] Jean-Yves Tinevez, Nick Perry, Johannes Schindelin, Genevieve M. Hoopes, Gregory D. Reynolds, Emmanuel Laplantine, Sebastian Y. Bednarek, Spencer L. Shorte, and Kevin W. Eliceiri. Trackmate: An open and extensible platform for single-particle tracking. *Methods*, 115:80–90, 2017. ISSN 1046-2023. doi: https://doi.org/10.1016/j.ymeth.2016.09.016. URL https://www.sciencedirect.com/science/article/pii/S1046202316303346. Image Processing for Biologists.

[113] Michael Toepke and David Beebe. Pdms absorption of small molecules and consequences in microfluidic applications. *Lab on a chip*, 6:1484–6, 01 2007. doi: 10.1039/b612140c.

[114] Berend Van Meer, H. Vries, Karl Firth, Jasper Weerd, L.G.J. Tertoolen, H.B.J. Karperien, Pascal Jonkheijm, Chris Denning, A.P. IJzerman, and C.L. Mummery. Small molecule absorption by pdms in the context of drug response bioassays. *Biochemical and Biophysical Research Communications*, 482, 11 2016. doi: 10.1016/j.bbrc.2016.11.062.

[115] B.J. van Meer, H. de Vries, K.S.A. Firth, Jasper van Weerd, L.G.J. Tertoolen, H.B.J. Karperien, Pascal Jonkheijm, C. Denning, A.P. IJzerman, and C.L. Mummery. Small molecule absorption by pdms in the context of drug response bioassays. *Biochemical and biophysical research communications*, 482(2):323–328, 2017. ISSN 0006-291X. doi: 10.1016/j.bbrc.2016.11.062.

[116] Christopher M. Waters, Esra Roan, and Daniel Navajas. Mechanobiology in lung epithelial cells: Measurements, perturbations, and responses. *Comprehensive Physiology*, 2(1):1–29, 2012. ISSN 20404603. doi: 10.1002/cphy.c100090.

[117] E. R. Weibel. How to make an alveolus. *European Respiratory Journal*, 31(3):483–485, 2008. ISSN 09031936. doi: 10.1183/09031936.00003308.

[118] Ewald R. Weibel. Lung morphometry: the link between structure and function. *Cell and Tissue Research*, 367(3):413–426, 2017. ISSN 14320878. doi: 10.1007/s00441-016-2541-4.

[119] Ewald R. Weibel, Bernard Sapoval, and Marcel Filoche. Design of peripheral airways for efficient gas exchange. *Respiratory Physiology Neurobiology*, 148(1):3 – 21, 2005. ISSN 1569-9048. doi: https://doi.org/10.1016/j.resp.2005.03.005. URL http://www.sciencedirect.com/science/article/pii/S1569904805000935. Structure and Function in the Periphery of the Lung.

[120] Steven E. Weinberger, Barbara A. Cockrill, and Jess Mandel. Chapter 1 - pulmonary anatomy and physiology—the basics. In Steven E. Weinberger, Barbara A. Cockrill, and Jess Mandel, editors, *Principles of Pulmonary Medicine (Fifth Edition)*, pages 1 – 18. W.B. Saunders, Philadelphia, fifth edition edition, 2008. ISBN 978-1-4160-5034-6. doi: https://doi.org/10.1016/B978-1-4160-5034-6.50004-X. URL http://www.sciencedirect.com/science/article/pii/B978141605034650004X.

[121] Cong Xu, Min Zhang, Wenwen Chen, Lei Jiang, Chunying Chen, and Jianhua Qin. Assessment of Air Pollutant PM2.5 Pulmonary Exposure Using a 3D Lung-on-Chip Model. *ACS Biomaterials Science & Engineering*, 6(5):3081–3090, 2020. ISSN 2373-9878. doi: 10.1021/acsbiomaterials.0c00221.

[122] Xingyuan Yang, Kaiyan Li, Xu Zhang, Chang Liu, Bingkun Guo, Weijia Wen, and Xinghua Gao. Nanofiber membrane supported lung-on-a-chip microdevice for anti-cancer drug testing. *Lab on a Chip*, 18(3):486–495, 2018. ISSN 14730189. doi: 10.1039/c7lc01224a.

[123] Pauline Zamprogno, Simon Wüthrich, Sven Achenbach, Janick Stucki, Nina Hobi, Nicole Schneider-Daum, Claus-Michael Lehr, Hanno Huwer, Thomas Geiser, Ralph Schmid, and Olivier Guenat. Second-generation lung-on-a-chip array with a stretchable biological membrane. *bioRxiv*, page 608919, 2019. doi: 10.1101/608919.

[124] Min Zhang, Cong Xu, Lei Jiang, and Jianhua Qin. A 3D human lung-on-a-chip model for nanotoxicity testing. *Toxicology Research*, 7(6):1048–1060, 2018. ISSN 20454538. doi: 10.1039/c8tx00156a.

[125] Helene Zirath, Mario Rothbauer, Sarah Spitz, Barbara Bachmann, Christian Jordan, Bernhard Müller, Josef Ehgartner, Eleni Priglinger, Severin Mühleder, Heinz Redl, Wolfgang Holnthoner, Michael Harasek, Torsten Mayr, and Peter Ertl. Every breath you take: Non-invasive real-time oxygen biosensing in two- and three-dimensional microfluidic cell models. *Frontiers in Physiology*, 9(JUL):1–12, 2018. ISSN 1664042X. doi: 10.3389/fphys.2018.00815.

[126] Agnieszka Zuchowska, Piotr Kwiatkowski, Elzbieta Jastrzebska, Michal Chudy, Artur Dybko, and Zbigniew Brzozka. Adhesion of MRC-5 and A549 cells on poly(dimethylsiloxane) surface modified by proteins. *Electrophoresis*, 37(3):536–544, 2016. ISSN 15222683. doi: 10.1002/elps.201500250.